Numerical Combustion of Aviation Fuel Part I
A Cross-Model Comparison of n-Heptane Premixed Flame

Hongzhi R. Zhang and Adel F. Sarofim
Department of Chemical and Fuel Engineering
University of Utah
Salt Lake City, Utah, USA 84112
Corresponding Author: hongzhi@crsim.utah.edu

Abstract
Four different n-heptane mechanisms were used to simulate a fuel rich n-heptane premixed flame and their results were compared with experimental measurements. In addition to discussion of the numerical performance of each mechanism, flux analysis coupled with the atomic distribution technique was used to find the major reaction pathways for fuel consumption, product formation, and the evolution of olefins and other intermediates. Hydrogen abstraction followed by β scission is the major fuel consumption route overtaken by unimolecular decomposition only at 1400-1500K. At that high temperature, however, not much fuel remains so that unimolecular decomposition reactions contribute insignificantly toward the overall fuel decomposition process. Low temperature chemistry of peroxy radicals forms a minor fuel consumption route in this premixed flame. Olefins are formed by β scission and consumed by direct decomposition, radical addition, and hydrogen abstraction reactions. The techniques and pitfalls of flux analysis were also discussed in order to map out a methodology that can be used to identify the true nature of the combustion chemistry. The results obtained from this study for n-heptane is critical to build practical combustion mechanisms for large paraffins, which are major components of liquid aviation transportation fuels. It should be recognized that the conclusions derived here are for premixed flames, and may not apply to diffusion flames.

Introduction
The combustion phenomena of aviation fuels have generated tremendous interests in both experimental and numerical combustion communities recently. Experimental evidences indicate that most common aviation fuels, such as JP8 used by US military to power their fighter engines and combat vehicles, are composed of normal paraffins, iso paraffins, cyclo paraffins and aromatics[1-3]. The chemical nature of normal paraffins can be the most important factor in studying the combustion process of aviation fuels since as much as 79% of the fuel in Doute et al.'s kerosene flames was found as normal alkanes[4]. Thus a complete knowledge of carbon flow through the major reaction pathways of normal alkane combustion is a critical piece of information to understand the combustion nature of aviation fuels.
Among normal alkanes used for commercial fuels, n-heptane is probably the best studied as one of the indication fuels for gasoline octane rating and a popular surrogate fuel for diesel and kerosene. Like any other fuels, the combustion of n-heptane is believed to include both a low temperature region, where the peroxy chemistry dominates, and a high temperature region, where pyrolysis and oxidation reactions generates fast consumed intermediates through C_2, C_3, C_4 reactions. Dagaut et al. put this temperature division line at 750K from their high-pressure perfectly stirred reactor experiments of n-heptane oxidation[5], where 50 species were quantitatively analyzed. In another n-heptane oxidation experiment, Simon et al. identified 16 products in a jet-stirred reactor at 923K[6]. Autoignition is also a popular topic studied by Minetti et al. in a rapid compression machine[7] and by Seiser and coworkers in a counter-flowing non-premixed system[8]. The ignition delay time is another popular interest studied by Colket and Spadaccini[9], and by Burcat and coworkers[10].
There are also many experimental data of n-heptane premixed flames. El Bakali et al. measured the structure of a rich laminar premixed n-heptane/O_2/N_2 flame with an equivalence ratio of 1.9[11]. Detailed concentration profiles of more than two-dozen intermediates and major products were reported to shed light into the reaction kinetics of n-heptane decomposition, formation and consumption of olefins, formation of major products and the chemistry of C_2, C_3, and C4 species. The same Orleans group also studied four low-pressure premixed flames with a wide spectrum of equivalence ratio from lean (0.7) to rich (2.0)[12]. Later they extended the n-heptane combustion experiments to atmospheric pressure in a similar study with three equivalence ratios at 1.0, 1.5[13] and 1.9[14]. Gas chromatography was used to identify isomers that could not be distinguished in earlier experiments using mass spectrometer[11] and gave more insights in how olefins are formed and consumed.
Besides experimental combustion studies, literature in numerical combustion of n-heptane is also abundant. Pitsch and coworkers proposed a 77-reaction mechanism to study the pollutant-relevant intermediate species using a counter-flow diffusion flame and discussed qualitatively the contribution of different class of reactions in the process of fuel consumption[15]. They found about 30% of the fuel was consumed by the unimolecular

decomposition by direct rupture of one carbon-carbon sigma bond. Voevlle and coworkers validated a detailed mechanism[16] against the experimental data of four low-pressure n-heptane premixed flames, and later the mechanism was modified to fit a new atmospheric n-heptane flame[14]. A Milan group proposed a complete mechanism for n-heptane combustion with both low and high temperature reactions. This large mechanism with almost 7000 reactions allows each individual reaction to have fractional coefficients and unlimited number of reactants and products and was verified for n-heptane, iso-octane[17] and kerosene[18] flames. Lawrence Livermore National Laboratory published their detailed n-heptane mechanism[19] and was validated against results from numerous experiments including ignition behind reflected shock waves, a rapid compression machine, a continuously stirred reactor and a high-pressure turbulent flow reactor.

The comparison of the performance of different mechanisms is also found abundant in literature. Davis and Law compared three n-heptane mechanisms with their laminar flame speed experimental data[20] and found Held et al.'s mechanism[21] was the best one for the range of C/O ratios they studied. Held et al.'s mechanism was also the winner out of three mechanisms in Davidson et al.'s performance test[22] for ignition delay times at reflected shock waves. However in another reflected shock wave test[23] of the OH concentration time histories during the ignition of stoichiometric n-heptane/oxygen mixture diluted in argon, none of the three mechanisms described the phenomena accurately.

The abundance in literature of heptane combustion chemistry and comparisons between different models laid the foundation for model building of higher hydrocarbon fuels such as decane, dodecane and cetane found in commercial fuels. One way to build mechanisms for large paraffins is through automatic reaction generation by identifying all relevant reaction classes and assigning the rate of the similar reactions from existing heptane kinetics. Usually a reaction set with a formidable size will be obtained using automatic generation mechanism and it is proved impossible to build any practical models under current computing technology. Thus a methodology to build effective models for higher hydrocarbon compounds is desperately needed. A flux analysis of numerical combustion results can bring the true nature of chemistry according to their importance to our current understanding of the combustion phenomena. As one of the best-studied fuels in laboratories and on computers, heptane is probably the best choice to start with for flux analysis to discover the most important reaction pathways for fuel decomposition, formation and consumption of olefins, evolution of intermediates and formation of major products. This study will investigate the major reaction pathways of the heptane consumption and the pathways channeling carbon atoms from fuel to the products and aromatics in numerical combustion and validate the findings with experimental evidence. The difference among existing mechanisms will be discussed and a philosophy of how large paraffin fuels are burned will be established. The knowledge of heptane combustion chemistry is critical to build future effective mechanism with manageable size for higher hydrocarbon fuels, aviation fuels in particular.

Table 1. Specifications of four n-heptane mechanisms

Model	Species	Reactions	Run Time	Temp. Range	Ref.
Pitsch	44	112	2-3 min	Low and High	26
Utah-Gas2	187	932	1 hour	High Only	
LLNL	650	2500	5 hours	Low and High	25
Milan	260	6950×5*	3 days	Low and High	24
* Each individual reaction in the Milan mechanism can be rewritten into as many as a dozen elementary steps in CHEMKIN format.					

Experimental Data and Numerical Models

Table 1 gives specifications of four mechanisms chosen in this study for the major reaction pathways Analysis of n-heptane combustion. Milan mechanism[24] (referred as Milan in this paper) published by Ranzi and coworkers is a complete heptane mechanism including 260 species and almost 7000 reactions. This mechanism allows individual reaction to have fractional coefficients and unlimited number of reactants and products in a way that each reaction can be rewritten as many as a dozen elementary steps. Therefore the number of equivalent elementary reactions in CHEMKIN format that Milan mechanism supports maybe reach 30 thousands. Milan mechanism includes both low and high temperature chemistry and was tested against data from n-heptane, iso-octane, methyl cyclohexane and kerosene experiments in laminar premixed condition or plug flow reactor configuration[17, 18]. Another detailed heptane mechanism[25] is reduced from a complete set proposed by Westbrook and coworkers[19] (referred as LLNL in this paper) and was validated using data from experiments of reflected shock waves, a rapid compression machine, a continuously stirred reactor and a high-pressure turbulent flow reactor. It includes 650 species and 2500 reactions including both low and high temperature chemistry. Besides the two larger mechanisms, also chosen is a smaller Pitsch n-heptane model[26] (referred as Pitsch in this paper) extended from

an earlier publication[15] with both high temperature oxidation and low temperature peroxy radical reactions. This remarkably efficient model with only 112 reactions and 44 species requires much less computing power and time to run than the two larger mechanisms. Also included is a relatively small mechanism compiled at University of Utah (referred as Utah-Gas2 in this paper) with 187 species and 1000 reactions based on sub modules of a) Miller and Melius benzene formation submechanism[27]; b) Tsang's propane and propene chemical kinetics[28, 29]; c) Pitz and Westbrook's n-butane submechanism[30]; d) Emdee-Brezinsky-Glassman's toluene and benzene oxidation submechanism[31]; e) Marinov and Malte's ethylene oxidation submeehanism[32]; f) Marinov-Westbrook-Pitz's hydrogen model[33]; g) Wang and Frenklaeh's acetylene reaction set with vinylie and aromatic radicals[34]; h) Hwang[35], Miller et al.'s[36], and Westbrook's acetylene oxidation models[37]; i) Vovelle and eoworkers' n-heptane decomposition model[16]; j) Pitseh et al.'s iso-octane decomposition model[38]. UTAH-GAS2 is the core mechanism that will be used to build up a new aviation fuel capability, namely JP8, in the future. The specifications of these four mechanisms are summarized in Table 1 as well as the requirement of computing resources.

These four mechanisms were tested against the experimental data of a laminar premixed n-heptane flame at atmospheric pressure with an equivalence ratio of 1.9[14]. The simulator used for this study is CHEMKIN III[39] and the thermodynamics data were obtained from CHEMKIN thermodynamic database[40] or estimated by THERGAS[41] employing Benson's additivity theory. The transport properties of species are obtained from CHEMKIN transport database[42] or estimated from the transport properties of similar species.

Comparison of Numerical Combustion with Experimental Data

The numerical combustion results of a rich n-heptane premixed flame using four mechanisms listed in Table 1 were compared to the experimental measurements.

Probe Effects Probe effect is one kind of difficulties that may prevent the simulation efforts from getting accurate results. Bittner and Howard suggested a shift of 2mm and lowering by 100K in most fuel-rich combustion simulations[43]. However, it was suggested by Hartlieb et al., who documented the probe effects in a flat premixed fuel-rich propene/oxygen/argon flame at 50 mbar, that the effects are rather arbitrary for different species[44].

In this study, the probe effects were corrected by an optimal temperature profile sought out to fit the oxygen concentration profile. This technique is based on the chemical nature of the large paraffin decomposition reactions. At high temperature two kinds of decomposition reactions are identified in literature that are responsible for the consumption of n-heptane. The first class is the unimolecular decomposition reaction that breaks one carbon-carbon sigma bond to form two alkyl radicals; the other is through the hydrogen abstraction followed by the β scission reaction to form one alkyl radical and one olefin. The β scission reaction requires a set of active radicals as abstractors under aerobic environment, while the unimolecular decomposition does not need involvement of oxygen. If both anaerobic and aerobic decomposition reactions in a mechanism are with reasonable accuracy, the temperature profile in the real flame should bring a correct consumption rate of the oxygen. The reverse may not be true. If the mechanism is correct, however, a fit of the oxygen concentration should give a hint of the temperature profile in reality, and if either class of reactions is not correct, the mechanism should give runaway results using optimal temperature profile.

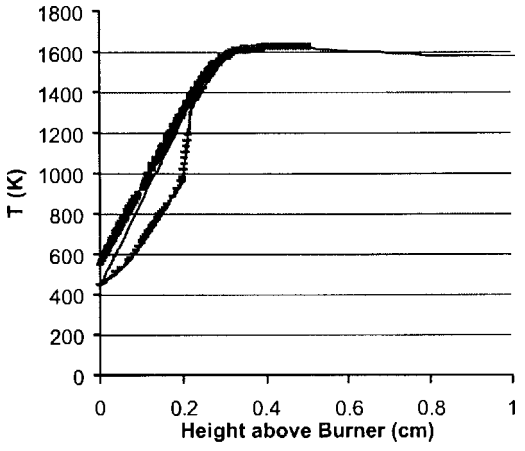

Figure 1. Optimal temperature profiles used for simulation. Heavy line for Milan mechanism; Light line for Utah-Gas2 and Pitsch mechanism; Line with symbol for LLNL reduced mechanism.

Optimal temperature profile for every mechanism was found and plotted in Figure 1 hopefully to catch the true nature of the flame structure. All mechanisms except LLNL model succeed to fit the oxygen concentration profile after the experimental temperature peak is shifted away from the burner surface by 0.05cm. The UTAH-GAS2 and Pitseh mechanism use the same temperature profile compared to that of Milan mechanism with a slightly higher cold gas temperature. The exception of LLNL model that lowers the temperature profile in the reaction zone brings changes, such as a better fit of oxygen profile and closer peak positions to the experimental measurements for most species. Several other shifting schemes of temperature profile were also tried for LLNL mechanism and the optimal temperature

profile using oxygen as reference was found to give the most accurate flame structure.

Fuel, oxidant and major products The concentration profiles for the fuel, oxygen and major products are shown in Figure 2. Since the oxygen profile is used as a reference to adjust the temperature history used for individual mechanism, the simulation result of every mechanism matches the experimental oxygen concentration pretty well.

It will be quite surprising, however, if the success of

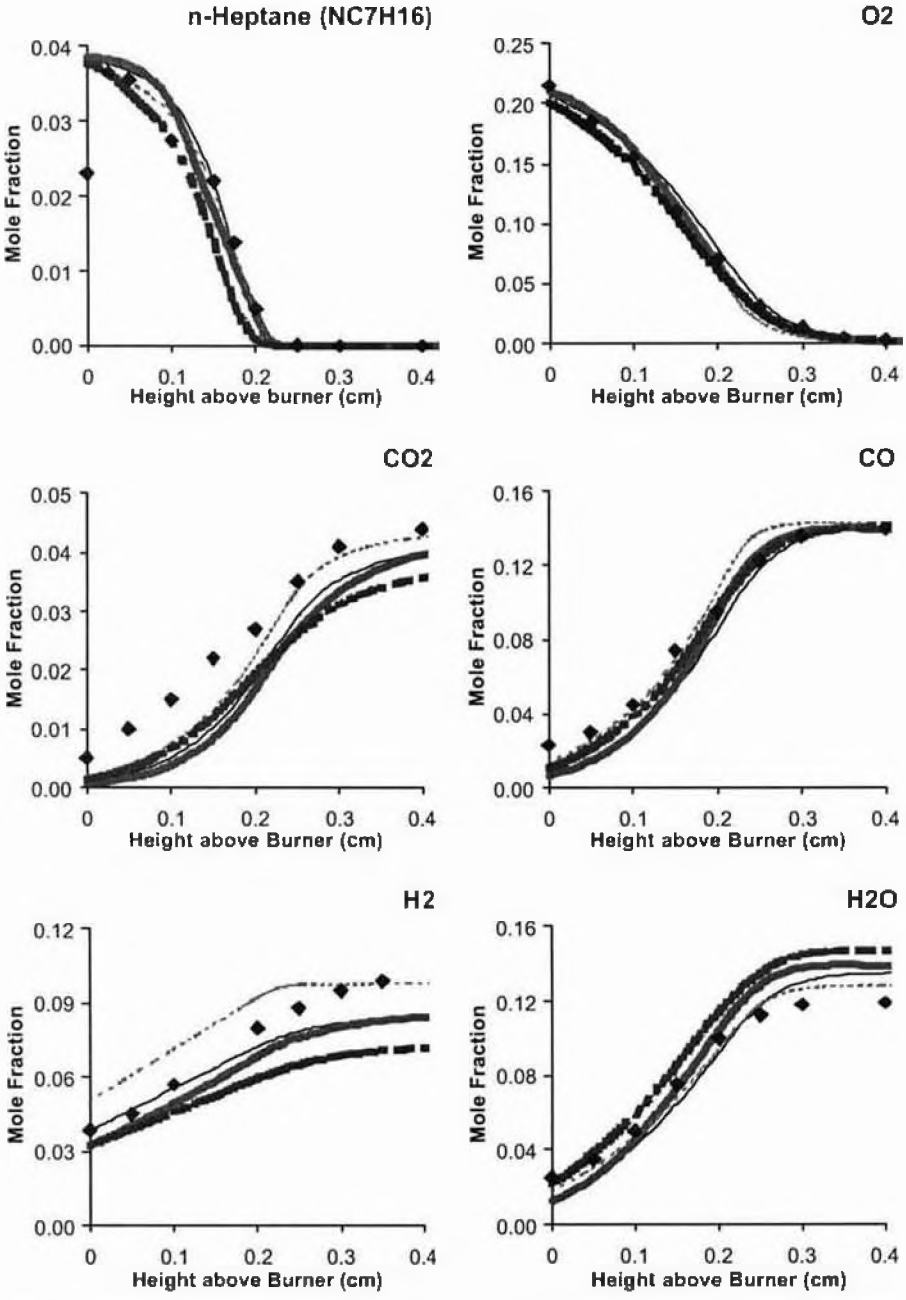

Figure 2. Comparison between numerical combustion results and experimental data for fuel, oxidant, and major products. Heavy line for LLNL reduced mechanism; Light line for Utah-Gas2; Heavy dot line for Milan mechanism; Light dot line for Pitsch mechanism.

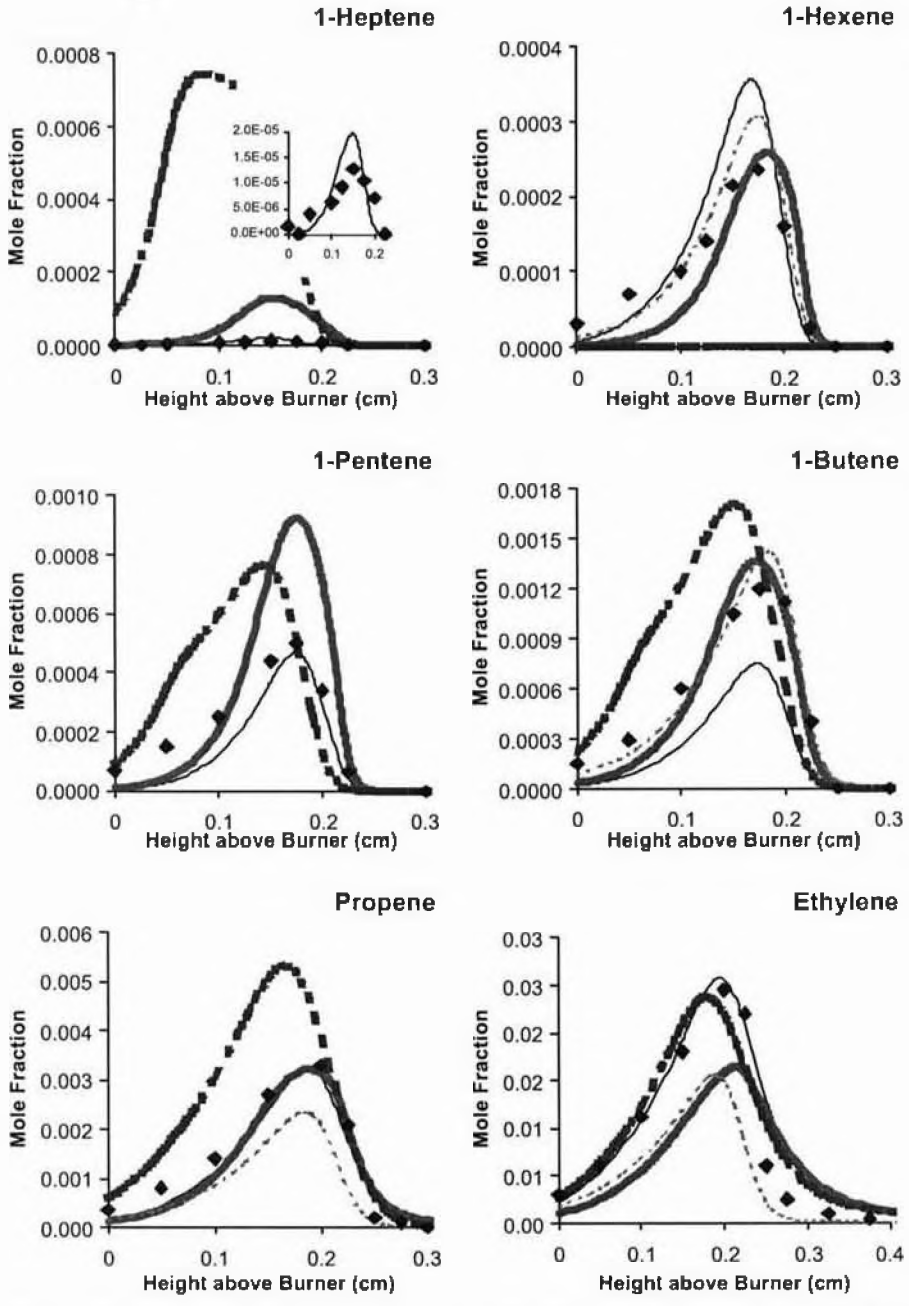

Figure 3. Comparison between numerical combustion results and experimental data for olefins. Heavy line for LLNL reduced mechanism; Light line for Utah-Gas2; Heavy dot line for Milan mechanism; Light dot line for Pitsch mechanism.

oxygen will be extended to the concentration profiles of n-heptane since each mechanism employs different rates for fuel consumption reactions. The numerical results using UTAH-GAS2 and Pitsch model are the better ones to capture the fuel consumption rate within 5% deviation from the experimental data. The LLNL mechanism is able to match most of the n-heptane profile except in the low temperature chemistry range between 0.1cm to 0.2cm above the burner surface, where it under-predicts the concentration by about 20%. Milan mechanism, in general, under-predicts the fuel concentration profile by almost 40% and its fuel consumption rate is systematically faster than what is suggested by the experimental measurement. Considering the accuracy

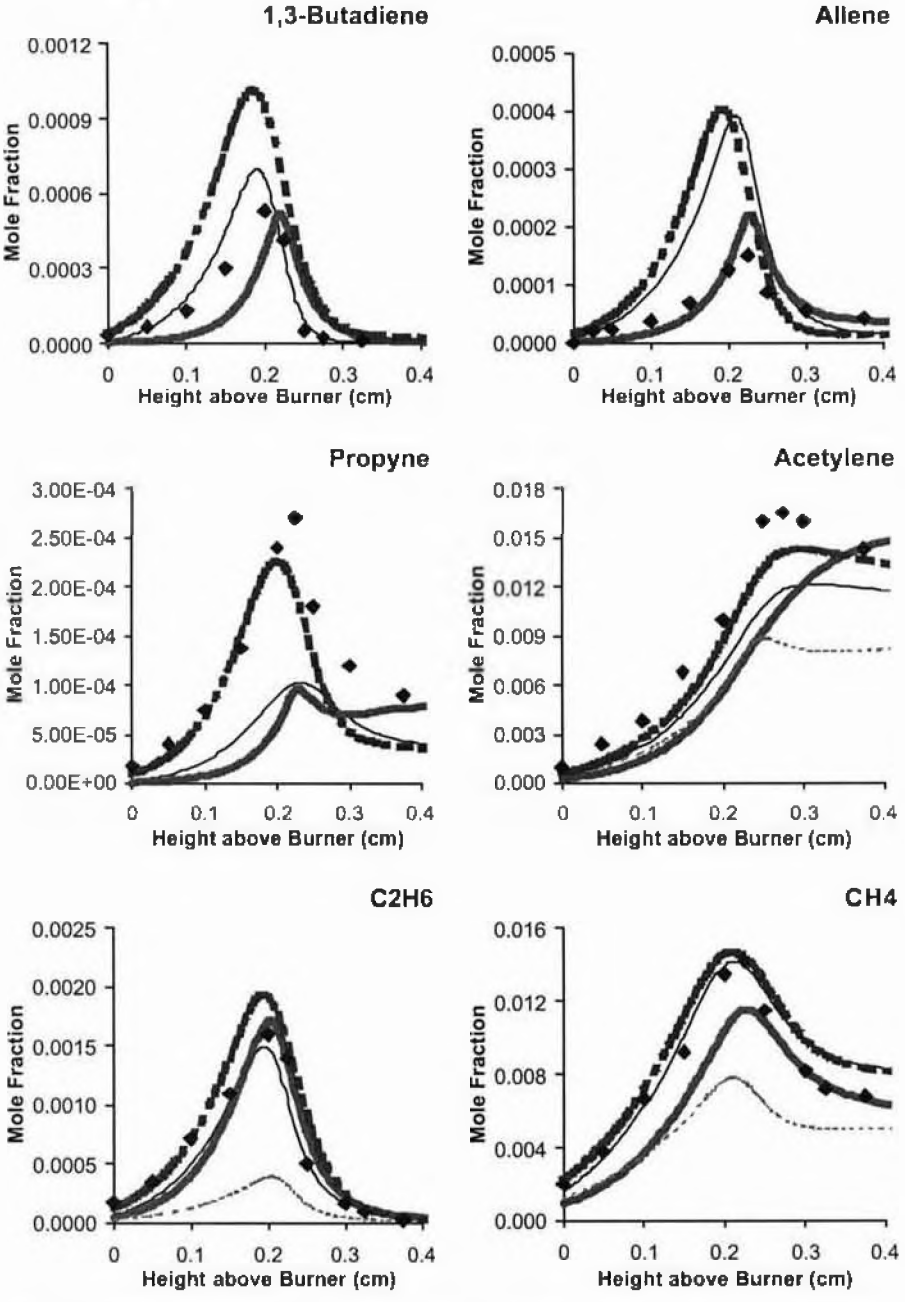

Figure 4. Comparison between numerical combustion results and experimental data for dienes, alkynes and paraffins. Heavy line for LLNL reduced mechanism; Light line for Utah-Gas2; Heavy dot line for Milan mechanism; Light dot line for Pitsch mechanism.

Milan mechanism gives in the oxygen concentration profile, its unimolecular decomposition reactions maybe too fast, plus other reasons that lead to an overall faster fuel consumption rate. Table 2 summarized the deviation of numerical simulation results from the experimental data for fuel, major products, olefins, dienes, alkynes, and other important intermediates. Besides the numerical deviation data, Table 2 also lists the best performer(s) among these four mechanisms for each individual species. Oxygen is not included in Table 2 because it is the reference compound for this study. The smaller deviation may not indicate better performance since the shape of

Table 2: The Deviation of Simulation Results from Experimental Data

Model	C_7H_{16}*	H_2O	H_2	CO_2	CO	C_2H_6	CH_4
Pitsch	-3%**	8	31	-4	11	-75	-42
Utah-Gas2	4	13	-15	-10	3	-7	-1
LLNL	-18	17	-16	-10	0	8	-18
Milan	-37	19	-28	-19	0	20	4
Best	P, U#	P	U, P	P	M	U, L	U, M
Model	**C_7H_{14}-1**	**C_7H_{14}-2**	**C_7H_{14}-3**	**C_6H_{12}**	**C_5H_{10}**	**C_4H_8**	**C_3H_6**
Pitsch				30		16	-35
Utah-Gas2	53	83	95	51	-7	-38	-6
LLNL	×10	×12	×19	10	85	13	-5
Milan	×15***	×15	×15	-×325	53	43	61
Best	U	U	U	P, U	U	P, L	L, U
Model	**C_2H_4**	**$13C_4H_6$**	**AC_3H_4**	**PC_3H_4**	**C_4H_4**	**C_2H_2**	**C_6H_6**
Pitsch	-38					-49	
Utah-Gas2	4	28	×2.6	-62	-36	-27	150
LLNL	-34	6	46	-64		-34	
Milan	-4	×2	×2.7	-19	×2	-13	55
Best	U	U	L	M	U	M	M

* The species shown in this table are n-heptane, H_2O, H_2, CO_2, CO, C_2H_6, CH_4, 1-heptene, 2-heptene, 3-heptene, 1-hexene, 1-pentene, 1-butene, propene, ethylene, 1,3-butadiene, allene, propyne, 1-buten-3-yne, acetylene, benzene

** The deviation is in percentage away from the experimental data. A blank box indicates the mechanism does not include such species; × indicates the multiples of the simulation results deviating from experiments; + is for over-prediction; - is for under-prediction

*** The three isomers of heptene are not distinguished in the Milan model, so the concentration of heptene is equally divided into three isomers to calculate the deviation

P stands for Pitsch; U for Utah-Gas2; L for LLNL; M for Milan

concentration profile and the position of maximum concentration are also important factors to judge the strength of a mechanism. Therefore, to get correct interpretation, the actual shape of concentration profiles plotted in Figure 24 should be overweighed than the percentage of deviation.

The two smaller mechanisms give not only a better fuel consumption rate, but also better profiles for major products. The only exception is carbon monoxide, which is best predicted by Milan mechanism in both reaction zone and post-flame zone. Pitsch mechanism is the closest to the experimental CO data in reaction zone but over-predicts it in post-flame zone by 11%. The Utah-Gas2 and LLNL mechanism under-predict the CO concentration in reaction zone but the deviation is reduced when the distance from the burner surface increases. The deviation in post-flame zone using Utah-Gas2 and LLNL mechanism is within 2-3% of the experimental data. Although all four mechanisms under-predict the concentration of carbon dioxide in reaction zone, the best performer Pitsch mechanism is able to predict the concentration profile of CO_2 within 4% in the post-flame zone. The Utah-Gas2 and LLNL mechanisms give similar results of 10% under-prediction of CO_2 concentration compared to the worst 20% deviation using Milan mechanism. Again the smaller mechanisms perform better in water vapor prediction. Pitsch mechanism is the best one about 8% higher than the experimental data and Utah-Gas2 is 13% over. LLNL and Milan mechanisms give nearly 20% over-prediction. No mechanisms are able to catch the concentration profile of H_2 in both reaction and post-flame zones. Utah-Gas2 and Pitsch mechanisms are better than their larger counterparts that Utah-Gas2 matches the concentration in reaction zone and Pitsch mechanism catches the trend in post-flame zone.

The four major combustion products are correlated through the water-gas shift equilibrium, $H_2O + CO = CO_2 + H_2$, well known as a checkpoint for both the experimental and numerical combustions. It is evident that water-gas shift equilibrium is directing the concentration distribution of the major products in this study. Milan mechanism gives the highest concentration for water vapor followed in order by LLNL, Utah-Gas2 and Pitsch mechanisms. The trend for H_2 concentration profiles is reversed favoring the Pitsch mechanism. The CO and CO_2 concentration profiles also assert the water-gas shift equilibrium except for the results using Pitsch mechanism, which gives highest concentration for both oxides. The simplicity of Pitsch mechanism is suspected to be responsible for this exception. It would be quite surprising if Pitsch mechanism did not predict higher concentration of carbon oxides because more carbon atoms are stored into intermediates in bigger mechanisms lowering the carbon flux into major products.

Olefins There are quite a few olefins formed during the combustion of n-heptane, but only olefins with their double bond at the end of the carbon chain will be considered since other isomers are much lower in concentration. The three isomers of heptenes are exceptions since their evolution history offers crucial information for fuel decomposition process. In general, Utah-Gas2 is the best performer among the four mechanisms for almost every olefin from C_2 to C_7 as seen in Table 2 and Figure 3. The deviation of the numerical results from the experimental data is getting worse when the number of carbon atoms in olefin increases. Also it is interesting to notice that olefins with even number of carbon atoms are better predicted than their counterparts with odd number of carbon atoms.

Although only results for 1-heptene are plotted in Figure 3, the numerical deviation of two other heptene isomers is listed in Table 2 except for Pitsch mechanism, which does not support any heptene isomers. Milan mechanism does not distinguish heptene isomers, and only the lumped concentration profile of all three isomers is available from numerical combustion. Thus the deviation of numerical result for each individual isomer is obtained by equally distributing the lumped concentration among the three isomers. Both Milan and LLNL mechanisms over-predict the heptene concentration by one order of magnitude. Utah-Gas2 gives remarkable results for heptenes that all three isomers are predicted within a factor of 2, especially for the prediction of 1-heptene illustrated in the imbedded graph with only 50% over-prediction. The concentration profile of 1-hexene is predicted well by almost every mechanism except for Milan model, which under-predicts it by two orders of magnitude. Among the other three mechanisms, Pitsch mechanism is the best one with a 30% deviation and Utah-Gas2 is only slightly worse. Although LLNL mechanism only over-predicts the maximum concentration of 1-hexene by 10%, the shape of the concentration profile is systematically shifted away from the burner surface by a small distance compared to the experimental data. Despite the shift that is common for quite a few LLNL concentration profiles, the overall performance of LLNL mechanism for 1-hexene is with reasonable accuracy.

While once again Pitsch mechanism does not participate the competition for 1-pentene for its goal of simplicity, Utah-Gas2 is no doubt the best mechanism for this olefin. It is almost a perfect match with an under-prediction for only 7% comparing to the over-prediction of 85% by LLNL model and 53% by Milan mechanism. Besides the large discrepancy, Milan mechanism predicts the maximum concentration too early by 0.3 mm. Milan mechanism continues to predict the maximum concentration of 1-butene 0.25 mm earlier than experimental measurement. Both Pitsch and LLNL mechanism are able to predict the 1-butene concentration profile within 15% of the experimental data comparing to the prediction of 38% lower for Utah-Gas2 and 43% higher using Milan model.

Propene and ethylene are very important species in combustion because of their roles in the C_2-C_3 chemistry. Besides the earlier concentration peak, the Milan mechanism also over-predicts the propene by 61%. It is obvious that Utah-Gas2 and LLNL mechanism outperform the other two models with a deviation of only 5-6%. Pitsch mechanism is able to predict position of the maximum propene concentration but the value is predicted 35% lower. Again Utah-Gas2 best predicts the ethylene concentration with a deviation of 4% only comparing to the 35% under-prediction by Pitsch and LLNL mechanisms. The Milan mechanism predicts the concentration peak slightly earlier but with only 4% deviation. Overall performance of Milan model is better than LLNL and Pitsch mechanisms for ethylene.

The systematical shift of concentration profiles using Milan mechanism toward burner surface comparing with experimental evidence is probably because the temperature profile used is not best for that mechanism. The numerical combustion results are very likely to be improved if the temperature profile is shifted more distant from the burner surface although at the cost of oxygen profile. However, the horizontal shift of temperature profile usually does not affect the concentration profiles vertically. It seems that Milan mechanism intends to produce too much olefin compounds except for 1-hexene under-predicted by two orders of magnitude and for ethylene for which Milan mechanism is among the best performers. Despite the incomplete family of olefins in Pitsch mechanism, the smallest model is able to show its competitiveness in 1-hexene and 1-butene predictions and gives reasonable results for propene and ethylene. LLNL mechanism shows strength in 1-butene and propene results and puts up reasonable predictions for other olefins except for heptenes. Utah-Gas2 is the best mechanism for

olefin formation and consumption chemistry. The most remarkable strength of Utah-Gas2 is its ability to predict the first olefin compounds – heptene isomers – directly formed from the decomposition of heptane fuel. The mechanism is able to catch the trend of experimental concentration profiles and the position of the maximum concentration for all three heptene isomers. It predicts the value of the maximum concentration for heptenes within a factor of 2.

Dienes, Alkynes and Paraffins There is no single mechanism that is best for all species in Figure 4, which are smaller dienes, alkynes and paraffins most with 3 carbon atoms or less. From the analysis of olefins, Pitsch mechanism is found never among the best ones to predict smaller species in addition to its incomplete set of larger compounds, a casualty of the pursuit of simplicity. Among the species in Figure 4, Pitsch mechanism does not include 1,3-butadiene, not even the smaller propyne and allene. It does offer predictions for C_1-C_2 species but with less accuracy than other mechanisms. Pitsch mechanism is able to catch the trend of acetylene concentration profile but under-predicts the peak value by 49%. Similar performance is given to the two smallest paraffins as the concentration of ethane is under-predicted by 75%, and that of methane by 42%.

LLNL mechanism is not able to reproduce the trend of concentration profile for the two alkynes. The shapes of both propyne and acetylene profiles are not even close to the experimental measurements. Except the failure in alkynes, LLNL mechanism gives some remarkable performance in dienes and paraffins. The mechanism is the best performer to predict the concentration of allene – an important compound related to the propargyl radical – with a deviation of 46% over-prediction, and that of ethane – related to the important intermediate methyl radical – with only 8% higher than the experimental data. LLNL mechanism also gives reasonable results for methane that is under-predicted by 18% and for 1,3-butadiene that is under-predicted by 6%. The concentration profiles for these two compounds are also slightly later than the experimental measurement.

Like its larger companion, Milan model also shows its strength in olefins as a detailed combustion mechanism. Its performance in the prediction of alkynes meets no competition from other mechanisms. Milan mechanism predicts the concentration profile of propyne within 20% comparing to the second best model Utah-Gas2's 62%. It under-predicts the concentration of acetylene by 13% considering the 27% under-prediction using Utah-Gas2. It is also among the best performer for methane prediction with a small deviation of 4%. It gives a reasonable result for ethane with a 20% deviation and overshoots the two dienes by a factor of 2 or 3.

Utah-Gas2 is detailed enough to match the experimental data for almost every species in Figure 4. It gives unquestionably good results for paraffins and slightly under-predicts ethane by 7% and methane by 1% only. It is the best performer for 1,3-butadiene with a discrepancy of 28% but more accurate profile shape and position of maximum concentration compared to the slightly shifted profile using LLNL mechanism. It is the second best performer for acetylene shadowed only by Milan mechanism. It catches the trend for the concentration profile of propyne with an under-prediction of 62%. It over-predicts the concentration of allene by a factor of 3.

As a casualty of simplicity, Pitsch mechanism fails in the prediction of smaller paraffins and alkynes in addition to missing larger alkyne and diene species. The other three mechanisms are detailed enough to predict the concentration of these compounds well and each has its unique strength. For instance, LLNL mechanism is superior for dienes; Utah-Gas2 is best for paraffins; and Milan model has no competitors for alkynes.

Aromatics The formation of the first aromatic ring is only entertained by Utah-Gas2 and Milan mechanism (Figure 5). Milan mechanism is the better one to predict the benzene concentration only 55% higher than the experimental data compared to 150% over-prediction using Utha-Gas2. Both mechanisms are able to catch the trend of the concentration profile but only Utah-Gas2 is able to predict the correct peak position.

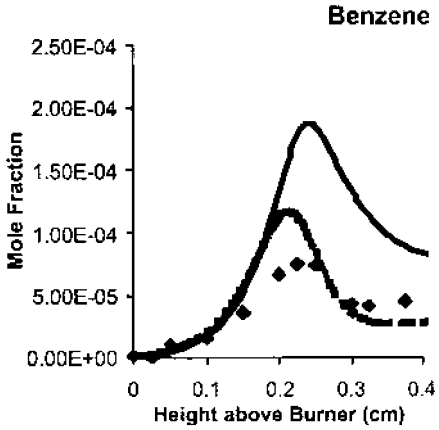

Figure 5. Comparison between numerical combustion results and experimental data for benzene. Solid line for Utah-Gas2; Dot line for Milan mechanism.

Summary The strength of each mechanism is examined and illustrated in Figure 6. Pitsch mechanism catches the fuel consumption rate nicely and is able to predict the concentration of the major products, including the major radiating agents CO_2 and H_2O, with remarkable accuracy considering its simplicity with only 112 reactions. Except its strength in the fuel consumption and product formation, Pitsch mechanism is unable to predict correctly the concentration profiles of smaller species with 3 carbon atoms or less. Those species include stable

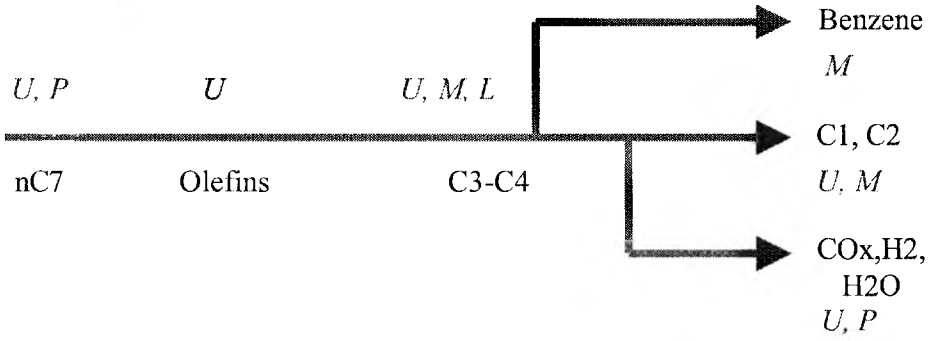

Figure 6. Strength of each n-heptane mechanism. U for Utah-Gas2; P for Pitsch mechanism; L for LLNL reduced mechanism; M for Milan mechanism.

paraffins with one or two carbon atoms, as well as important combustion intermediates with high hydrogen deficiency that are very reactive and critical for the formation of the first aromatics rings. Also concerned is its incomplete set of species in olefins and dienes – another casualty of simplicity. Despite the weakness for intermediate species, Pitsch mechanism is a highly useful tool. Its remarkably small size makes it converge in 2-3 minutes on a PII chip. Pitsch mechanism should also be considered as a primitive run to offer first estimation of concentration profiles for many species, especially for major products, if a larger, detailed, slower, and hard to converge mechanism is intended later on.

The two largest mechanisms – the Milan and LLNL models – show their strength in the smaller compounds that Pitsch mechanism is unable to predict correctly. LLNL mechanism scores in the prediction of small paraffins, plus small olefins and dienes that are critical for the formation of the first aromatics. However the mechanism is unable to do the same for the large olefins as well as the alkynes – an important building block for the polycyclic aromatic hydrocarbons. Milan mechanism has similar weakness when its usefulness for the larger olefins is examined. However, unlike the LLNL mechanism, it fairs remarkably well when alkynes are of the major concern, as well as for the smallest olefin – ethylene. It also gives reasonable results for dienes that makes it one of the best choices for alkynes and small alkenes. No doubt Milan mechanism is the best performer to predict the concentration profile of the first aromatic ring.

Utah-Gas2 is a complete and cost-effective mechanism. It finishes most premixed flame runs in about an hour comparing to the one to five work days usually required when LLNL and Milan mechanisms are used. Even with this cost-effective emphasis, Utah-Gas2 does not compromise the details necessary to catch the true nature of combustion phenomena. It includes all the important species of C2-C4 chemistry and it is one of the best mechanisms to use for paraffins, olefins, dienes and alkynes. Those species are critical to the formation of the first aromatics. The mechanism over-predicts the concentration of benzene by only a factor of 2. The most remarkable achievement for Utah-Gas2 is its ability to predict correctly the concentration of almost every olefins detectable in a n-heptane flame, especially large olefins with 5 to 7 carbon atoms that are over-predicted by one to two orders of magnitude using LLNL or Milan mechanisms. As will be discussed later, olefins are very important intermediates directly related to fuel consumption through β scission reactions. Its strength for the concentration of olefins makes Utha-Gas2 one of the best mechanisms to catch the rate of fuel consumption with a deviation of only 4%. In addition to the superior performance for the chemistry of fuel and many intermediates, Utah-Gas2 is joining the Pitsch mechanism to beat down larger models in the prediction of major products. Thus the mechanism is a very good choice for many scenarios and simulation goals, for instance, when the fuel consumption rate, or the radiation from the combustion, or the formation of pollutants such as carbon oxides and aromatics are concerned.

Flux Analysis Techniques, Pitfalls and Scenarios

Flux analysis is used to find the flow of atoms, usually carbon, within a network of species connected by reactions. The flux of a reaction is defined as $AT^n e^{\frac{-E}{RT}} \prod_{i=1}^{n} [C_i]$, where $AT^n e^{\frac{-E}{RT}}$ is the Arhenius form of reaction rate and $[C_i]$ is the concentration of the reactants. The Arhenius parameters can be found in the kinetic model used for simulation and the temperature profile is evolved from the experimental data. Simulation results give concentration profiles needed in flux analysis. Then calculated fluxes between species can be elaborated by a flow chart such as that in Figure 7 for fuel consumption fluxes at a position 0.2 cm above the burner surface using Utah-Gas2 mechanism.

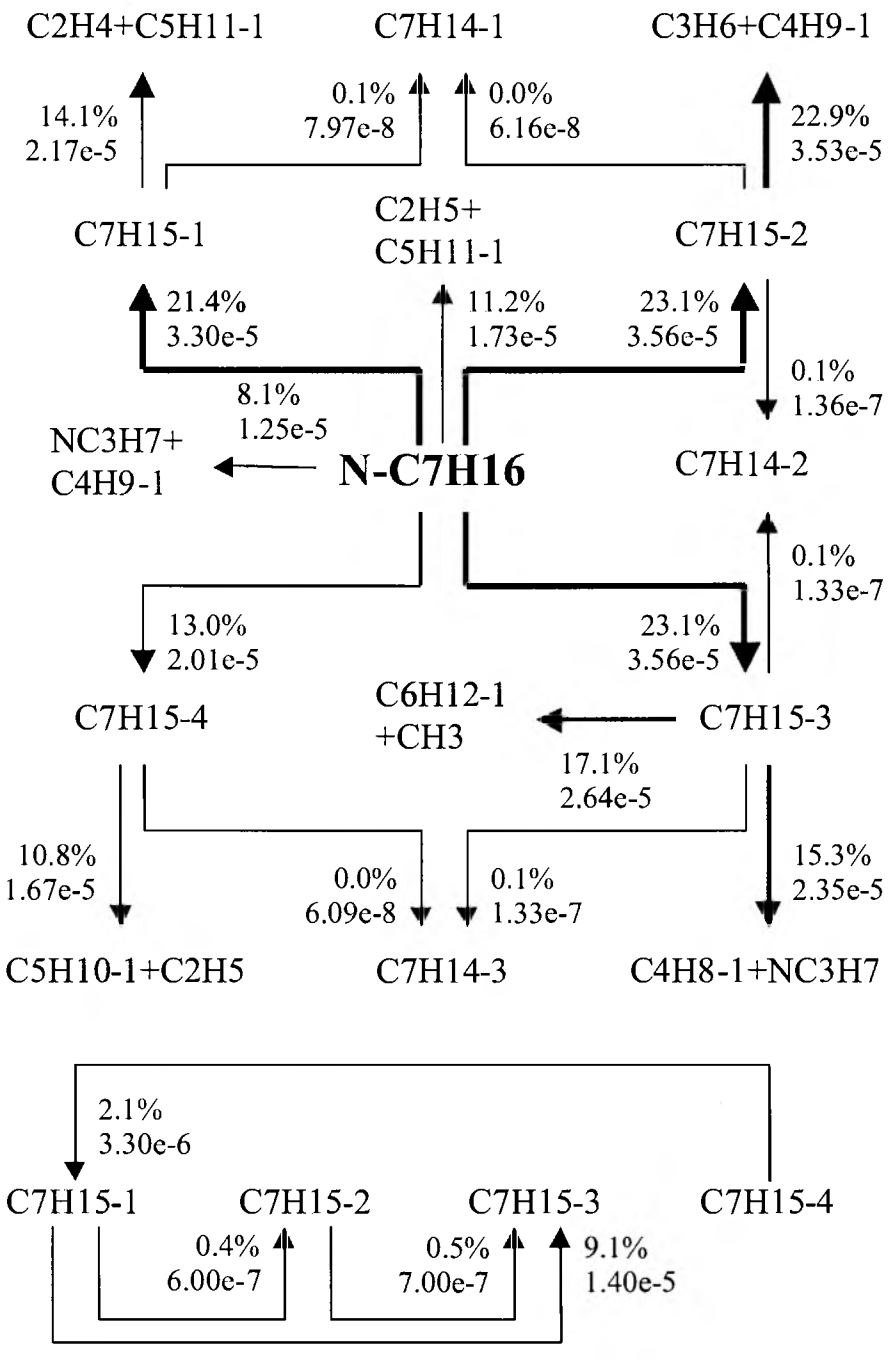

Figure 7. Flux analysis flow chart for fuel consumption at a position 0.2 cm above the burner surface using Utah-Gas2 mechanism. Unit in mole/cm^3 s.

There are two values associated with each flux in Figure 7. One is the molar flux (mole/cm^3 s) in the direction indicated by the arrow; the other gives the percentage of the carbon atoms released from fuel consumption at that position that is flowing through the associated flux. The weight of the arrow is proportional to the value of the flux thus the relative importance of each pathway can be easily observed. All the fluxes into carbon sinks through decomposition reactions, such as C_7H_{14}-x or C_3H_6+C_4H_9-1, are usually added up to 100%, which is always checked in this study to assert the self-consistency of the system.

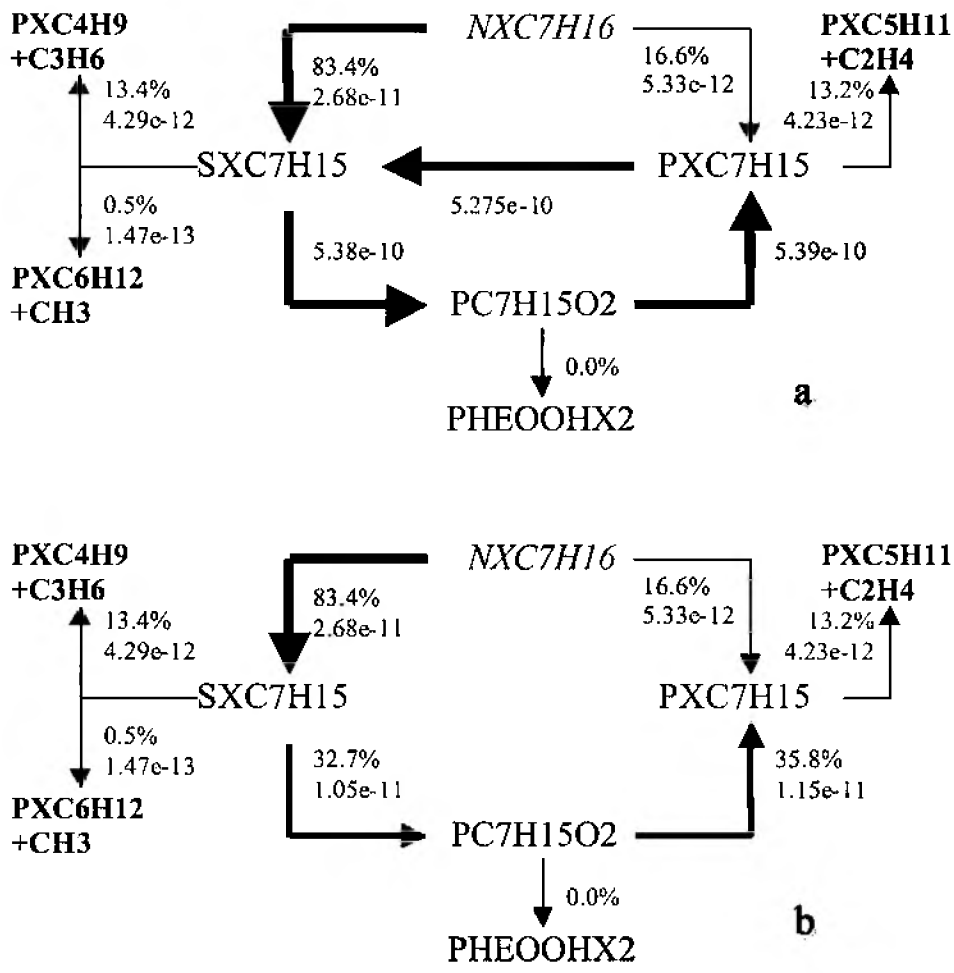

Figure 8. a) Cycling and b) decycling.

The **self-consistency** assertion is to guarantee that pseudo steady state around important intermediates holds without significant transport phenomena so that results obtained from flux analysis are valid without concerns of contamination from component convection and diffusion. The contamination from convection and diffusion will degrade the credibility of flux analysis by adding extra inlet or outlet sources. For example, if there is a net flow out, a reaction pathway not at current location will be benefited from the mass transfer and may invalidate the conclusion of the major reaction pathways identified from flux analysis in current environment if the mass transfer is large enough. There are only two occasions in this study that self-consistency assertion fails. One is the hoarding scenario near the burner surface; the other is the low temperature chemistry region for LLNL mechanism. Both occasions are taken care of with extra cautions.

Another scenario of flux analysis worthy of attention is **decycling** – a procedure to screen out repeatedly counted fluxes due to cycles inside the carbon flow chart such as the one shown in Figure 8a for the fuel decomposition analysis at a position 0.025 cm above the burner surface using Pitsch mechanism. Carbon atoms released from fuel molecules flow into either primary or secondary heptyl radicals then into smaller hydrocarbon fragments via β scission reactions. Unimolecular decomposition reactions are not significant at this point since the temperature is low around 550K only. Besides the role in low temperature chemistry, peroxy radicals in Pitsch mechanism are also used to construct a second isomerization route between primary and secondary heptyl radicals. It is an indirect isomerization route in addition to the normal direct isomerization reaction from primary toward more stable secondary radical. Thus there is a cycle from PXC7H15 (primary heptyl radical) to

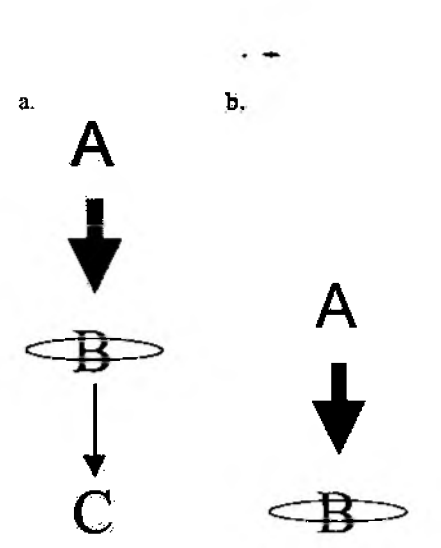

Figure 9. a) Funneling and b) hoarding.

SXC7H15 (secondary heptyl radical) to PC7H15O2 (peroxy alkyl radical) to PXC7H15. Since isomerization reactions are faster than decomposition reactions, carbon atoms may circle many times during the same time interval. The result is a much larger flow inside the cycle than the carbon flow actually released from fuel molecules. A black box approach is much helpful by treating the cycle as a single unit that only inflow and outflow of carbon atoms are important. In this case, only the net isomerization flux between primary and secondary radicals is concerned. In Figure 8b, the flow graph is decycled by removing repeatedly counted fluxes. It gives a much smaller isomerization flux in the direction from secondary toward primary radical representing 30-35% of the total carbon atoms released from the fuel molecules. The kinetic advantage of secondary heptyl radical formation at low temperature is clearly illustrated after decycling.

The decycling technique brings another concern in flux analysis for **missing reactions scenarios** due to mechanism simplification. Missing reactions sometimes make analysis more difficult, especially when they are coupled with cycling problem. Figure 8 also gives a good example of the negative effects from kinetic over-simplification. The cycle discussed earlier can be avoided if the isomers of heptyl peroxy radical can be distinguished. The formation of peroxy radical from secondary heptyl radical might not lead to a fast isomerization toward primary heptyl radical if a peroxy radical isomerization from more stable primary position to less stable secondary position is required. The pitfall of missing reactions is often found in simplified mechanisms since a few species, not always convertible quickly from each other, may be lumped into one species to assume different roles in reactions. Very likely misinterpretation follows.

In contrast to the fast carbon flow in cycling, **funneling** allows only very small flux going through. In Figure 9a, a funneling scenario occurs when the large flux from species *A* to species *B* is funneling through *B* in trivial flux since the reaction from *B* to *C* is the controlling step. The worst case for funneling is **hoarding** scenario when the carbon flow is nearly blocked, such as the case in Figure 9b. When funneling and hoarding occurs, species *B* will hold up large amount of carbon atoms and the mechanism will not reflect the nature of combustion. For example, in an effort here at University of Utah to build a model for dodecane, the reaction outlet of 1-hexyl radical was accidentally omitted. When the mechanism was tested against some experimental data, the concentration profile of CO was found much lower than the concentration profile of CO_2. However the experimental data suggested that the reverse was true since it was a fuel rich flame. Finally the hoarding scenario of hexyl radical was found by flux analysis and surprisingly the radical was found holding up 22% of the total carbon. No wonder the numerical combustion was more like a fuel lean flame. Funneling also cause stiffness of mechanism that greatly hikes the efforts to get the simulation converged and makes that mechanism unattractive.

It is not an easy task, however, to prevent the funneling and hoarding scenarios. Very often hundreds of species are used in numerical combustion and there are even more fluxes since several fluxes can connect any pair of species. To monitor every flux in the simulation is indeed impossible. However, a simple **atomic distribution analysis** for every species in the system is very effective to find these pitfalls. The carbon atomic distribution in numerical combustion using Pitsch, Utah-Gas2 and LLNL reduced mechanisms is listed in Appendix 1, 2, 3. The set of most important carbon-containing species is same for all three mechanisms and these species are shown in Figure 10. Heptane fuel contains majority of the carbon in reaction zone and carbon oxides dominate the post-flame zone. Ethylene is also a very important species since its formation root in β scission reactions. Ethylene holds up to 12-13% of carbon atoms in simulation results using Pitsch and LLNL mechanisms, and up to 21% when Utah-Gas2 is used. Experimental evidence suggests that both LLNL and Pitsch mechanisms under-predicts the concentration of ethylene and Utah-Gas2 gives almost a perfect match. The other important species is acetylene, which controls 7-11% of the carbon atoms. Species containing significant portion of total carbon, such as ethylene and acetylene, should be given more respect when the strength of a mechanism is examined. The missing carbon atoms in ethylene concentration alone in LLNL and Pitsch mechanisms are equal to almost 10% of total carbon in the system. The missing carbon atoms must be distributed into other species to reduce the numerical combustion accuracy and cause negative cascading impacts. From this aspect, Utah-Gas2 is proved

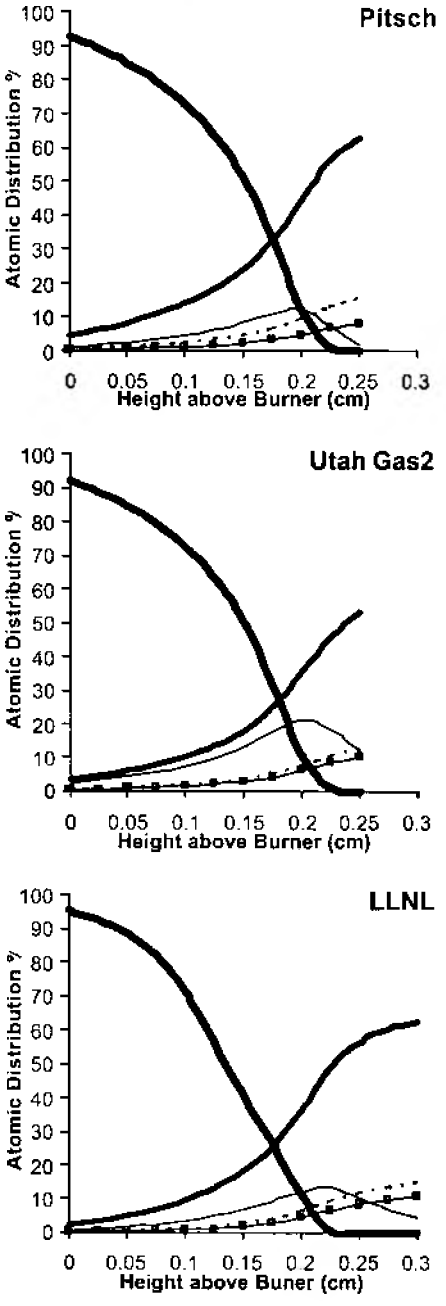

Figure 10. Carbon atomic distribution. Heavy line for n-C_7H_{16}; Medium line for CO; Light line for C_2H_4; Dot line for CO_2; Line with symbol for C_2H_2.

once again as a more reliable model than Pitsch and LLNL mechanisms.

The complexity of mechanism also influences the total percentage of carbon accountable in major species – at least holding 1% of the carbon atoms. A set of 13 major species from the simplest Pitsch model holds almost every carbon atom in the system such that at most 0.5% of the carbon distributed in other 31 species (Appendix 1). This is not true for Utah-Gas2 and LLNL mechanisms. Up to 2.5% of carbon atoms are not accountable in a set of 16 major species when Utah-Gas2 is used (Appendix 2). The percentage of carbon atoms not in the major set increases at higher temperature region where aromatic compounds are forming, growing, and coagulating. Since LLNL reduced mechanism does not include a sub-mechanism of aromatics, the missing carbon scenario is different from that of Utah-Gas2. LLNL mechanism is able to include the majority of the carbon atoms at high temperature region using a major set of 33 species but leaves out up to 2.2% of carbon atoms in low temperature region (Appendix 3). Thus the complexity of chemistry in C2-C4 compounds and peroxy radicals is probably the major reason for the carbon atoms not in the major set of LLNL mechanism.

Atomic distribution technique can detect the sudden or unusual concentration growth for some species so that funneling and hoarding scenarios can be easily monitored. Atomic distribution technique is also a very important tool to confirm the flux analysis results. The importance of major reaction pathways from flux analysis sometimes needs to be checked with atomic distribution technique to make sure that enough reactants are still available. One example will be discussed later for fuel consumption.

Cross-Model Flux Analysis

In this study, only three of the four mechanisms used in earlier sections will be selected to do the flux analysis. Milan mechanism is the victim for following reasons. First Milan mechanism is not able to catch the fuel consumption rate. The simulation results may be improved by finding a better temperature profile at the cost of oxygen profile. However, the task is not easy to be accomplished with a reasonable investment in time and computing power because of the formidable size of that mechanism. Second, the philosophy behind the Milan mechanism such as lumped technique got some serious attention when LLNL mechanism was built. Thus LLNL mechanism may provide some similarities and insights into Milan mechanism.

Fuel Consumption via Hydrogen Abstraction Chemical bond needs to be broken for fuel molecules to decompose in any combustion phenomena. There are two types of reaction class responsible for the decomposition of hydrocarbon fuels since there are only two kinds of bond. One is called the unimolecular decomposition – the direct rupture of a carbon-carbon sigma bond to form two alkyl radicals; the other one is the break of a carbon-hydrogen bond by an abstractor from a pool of radicals to form one alkyl radical. No matter which formation pathway an individual alkyl radical may go through, it

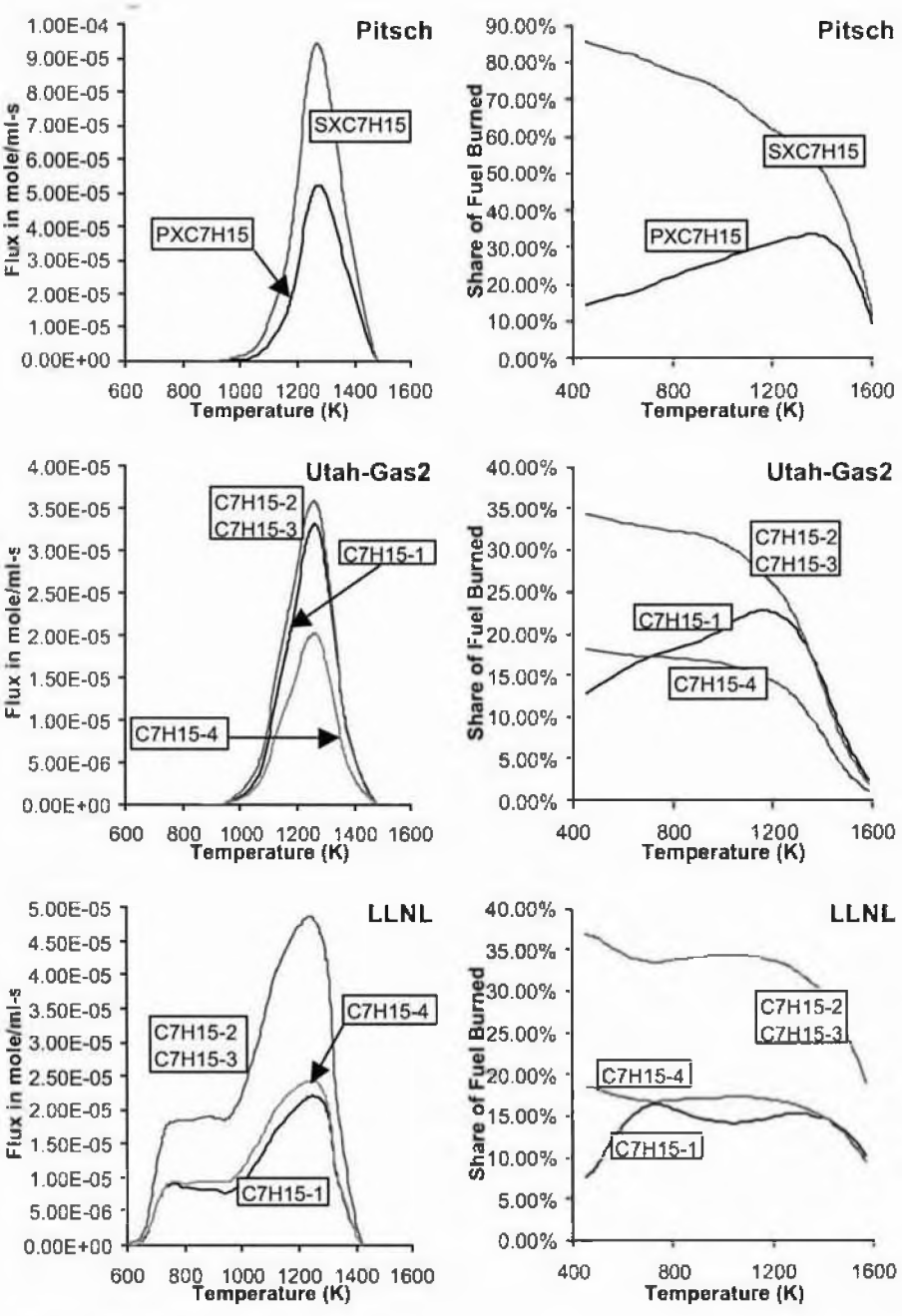

Figure 11. Hydrogen abstraction fluxes.

decomposes by β scission to form one smaller alkyl radical plus one olefin.

Unimolecular: $C_nH_{2n-2} = C_mH_{2m-1} + C_{n-m}H_{2n-2m+1}$

H Abstraction: $C_nH_{2n+2} + A = C_nH_{2n+1} + AH$

β Scission: $C_nH_{2n-1} = C_mH_{2m+1} + C_{n-m}H_{2n-2m}$

Flux analysis was carried out for the n-heptane premixed flame tested in earlier sections for selected mechanisms and numerical results were documented in Appendix 1, 2, 3. Those appendices serve as the database in this study.

The magnitude of each hydrogen abstraction flux has been illustrated in Figure 11, as well as the percentage of carbon atoms released from fuel molecules that flow through each individual flux. Pitsch mechanism supports only two n-heptyl radical isomers, one primary radical and one secondary radical denoted by PXC7H15 and SXC7H15 respectively. The more detailed mechanisms, LLNL and Utah-Gas2, are able to distinguish all four possible n-heptyl radical isomers denoted by C7H15-1,

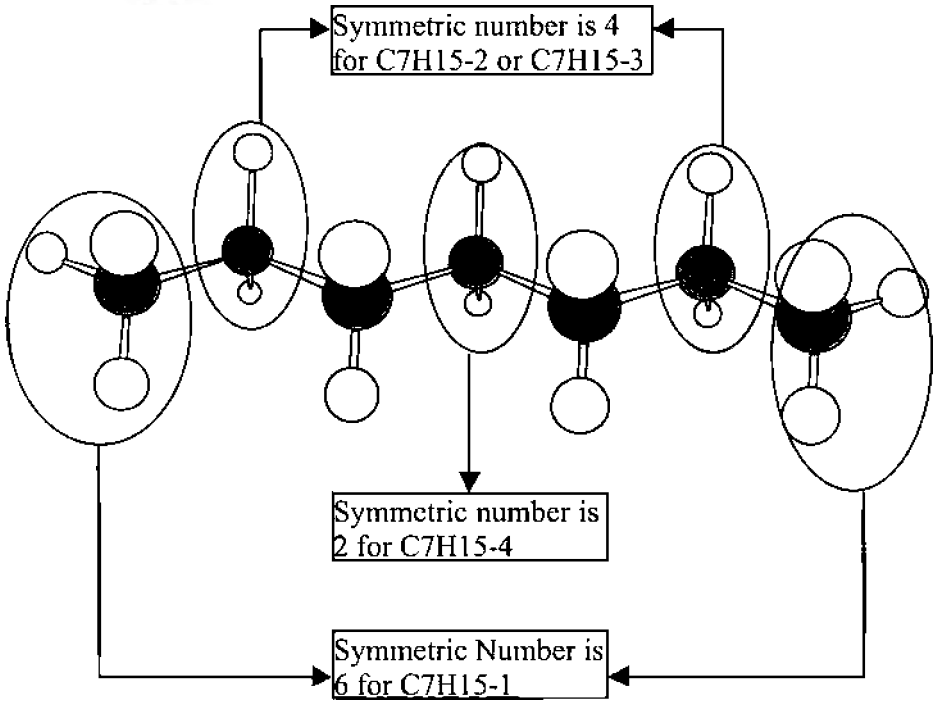

Figure 12. Symmetric number for hydrogen abstraction reactions.

C7H15-2, C7H15-3, and C7H15-4. C7H15-2 and C7H15-3 are produced faster than the other two isomers. The favor of C7H15-2 and C7H15-3 over C7H15-1 is due to less stable chemical nature of C7H15-1 than its secondary competitors. Symmetric number also plays an important role in formation reactions as illustrated in Figure 12. For the reactions to form C7H15-1 the symmetric number is 6 since there are three hydrogen atoms on each end of the molecule; the symmetric number for the formation of either C7H15-2 or C7H15-3 is 4 because of only 2 hydrogen atoms on each abstracted carbon atom. It is not surprised that the formation of C7H15-4 is always slower than that of C7H15-2 or C7H15-3 because the symmetric number for C7H15-4 production is 2 only – the lowest one among all four isomers. When enough heat is available, the reaction barrier for primary radical is easier to overcome and the formation rate of primary radical gets closer to that of secondary radicals. At very high temperature the symmetric number becomes the most important factor to determine product distribution among different isomers, and C7H15-1 formation benefited from the higher symmetric number will eventually become dominant.

Figure 11 shows some similarities between Pitsch and Utah-Gas2 mechanisms for hydrogen abstraction reactions. Abstraction reactions accelerate at around 950K and become trivial at 1475K for both mechanisms. Utah-Gas2 and Pitsch mechanisms also share similar peak position and maximum value of hydrogen abstraction fluxes. Flux profiles for both mechanisms are bell-shaped and reach maximum value around 1270K. The primary n-heptyl radical is formed by 5×10^{-5} mole/ml-s for Pitsch mechanism compared to 3.5×10^{-5} mole/ml-s for Utah-Gas2. The secondary radical formation fluxes are even closer by 9.4×10^{-5} mole/ml-s for Pitsch mechanism and 9.1×10^{-5} mole/ml-s for Utah-Gas2. In term of percentage of carbon atoms released from fuel into each flux, the secondary radical fluxes dominate at very low temperature and continue to be the major fuel consumption pathways through the acceleration stage for the hydrogen abstraction reactions. The primary radical formation fluxes pick up the stream at higher temperature. The gap with the secondary radical formation rate narrows down and finally the formation of primary radical exceeds. However, the increasing importance of primary radical formation should not upset the overall leading position of secondary radical fluxes since the high temperature required for primary radical domination also inhibits its fast production in favor of direct rupture of carbon-carbon sigma bond, another competing fuel consumption pathway. For Utah-Gas2, the formation rate of C7H15-1 surpasses that of C7H15-4 at 700K and outpaces those of C7H15-2 and C7H15-3 at 1350K. Because of the lowest symmetric number, the formation flux toward C7H15-4 radical in Utah-Gas2 is the slowest

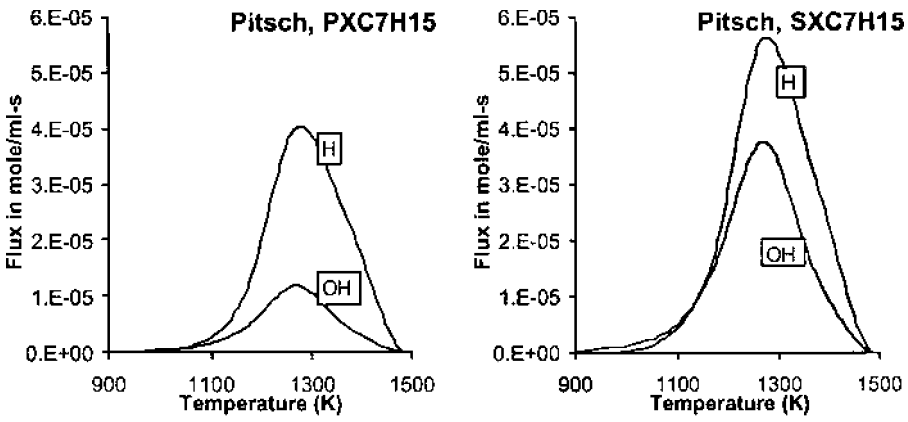

Figure 13. Hydrogen abstraction fluxes in Pitsch mechanism.

among all its isomers, except at locations very near burner surface.

The LLNL mechanism gives a totally different picture for hydrogen abstraction reactions. Abstraction reactions accelerate at a lower temperature around 600K and diminish at 1420K. Both acceleration and deceleration of abstraction fluxes have deeper slopes than those from the two smaller mechanisms. Besides the earlier startup of abstraction, LLNL mechanism gives unique bimodal flux profiles with one peak at 700K and another at 1275K. Unlike Utah-Gas2, formation of C7H15-1 is the slowest in LLNL mechanism, only surpassing that of C7H15-4 at 1410K. Although the difference between C7H15-1 formation and those of C7H15-2 and C7H15-3 is reduced gradually, C7H15-1 formation never dominates.

Each mechanism employs a different set of radicals for hydrogen abstraction reactions. Among the four radicals used in Pitsch mechanism, H and OH are the two dominant ones reacting two to four orders of magnitude faster than the other two radicals, HO_2 and O_2, except at temperature range lower than 900K where HO_2 hydrogen abstraction reactions are the fastest. Under any circumstances, O_2 is never comparable with other radicals in abstracting a hydrogen atom from the fuel molecule. In Figure 13, the hydrogen abstraction fluxes with two most active radicals for Pitsch mechanism are plotted. The hydroxyl radical is the faster abstractor at lower temperature overtaken by the hydrogen radical when temperature is higher than 1100K. Hydroxyl radical abstracts a secondary hydrogen 3 times faster than a primary one. The energy barrier is the dominant factor to determine the product distribution for abstraction reactions with hydroxyl radical. If hydrogen is the abstractor, a secondary hydrogen is abstracted 30% faster than a primary one. Thus the symmetric number is important for this class of reaction and likely the steric hindrance of the secondary positions is also considered.

There are also four radicals involved in the hydrogen abstraction reactions using Utah-Gas2 plotted in Figure 14. Hydrogen radical is still the most active abstractor and hydroxyl, oxygen and methyl radicals are the minor abstractors with fluxes one order of magnitude lower than that of hydrogen radical. Unlike in Pitsch mechanism that OH radical contributes significantly to the total flux, the overall rate of hydrogen abstraction reactions in Utha-Gas2 is determined by hydrogen radical only. OH and O radicals give similar size of abstraction fluxes for all three heptyl radicals. The CH_3 abstraction reactions are less sensitive to the symmetric number since the fluxes toward C7H15-2 and C7H15-3 is twice of that toward C7H15-1 and C7H15-4. One unique characteristics of CH_3 abstraction reaction is its earlier peak position at 1170K comparing to 1270K for all other radicals in Utah-Gas2.

LLNL reduced mechanism uses 14 radicals for hydrogen abstraction reactions. The uniqueness in the size of radical pool and chemical kinetics of LLNL mechanism should take the major responsibility for its bimodal flux profiles. Figure 15 plots the three most active radicals in LLNL mechanism led again by hydrogen radical. Hydroxyl radical also contributes significantly in abstraction reactions. Oxygen radical, joined by an army of other radicals, CH3, HO2, C2H5, C3H3, CH3O, O2, CH3O2, C7H15O2-1, C7H15O2-2, C7H15O2-3, ordered with importance, contributes little toward the overall fluxes. Hydrogen abstraction reactions with hydroxyl radical give LLNL mechanism a very unique feature. These abstraction fluxes reach their maximum at very early position around 800K compared to 1270K using Utah-Gas2 or Pitsch mechanism. This early peak is also far away from its own hydrogen radical flux peak at 1340K. The abstraction reaction rate not the OH concentration profile should take the responsibility for the earlier peak since OH reaches its maximu m concentration at 1570K. Indeed hydroxyl and hydrogen radicals represent two different groups of radicals in LLNL mechanism. One set of radicals with most activities at lower temperature around 800K includes OH, CH3O, HO2, CH3O2, C2H5, C7H15O2-1, C7H15O2-2, and C7H15O2-3. H, O and

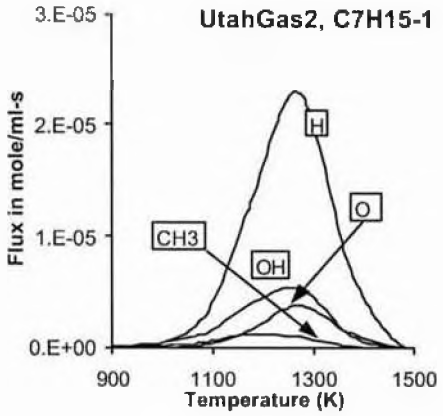

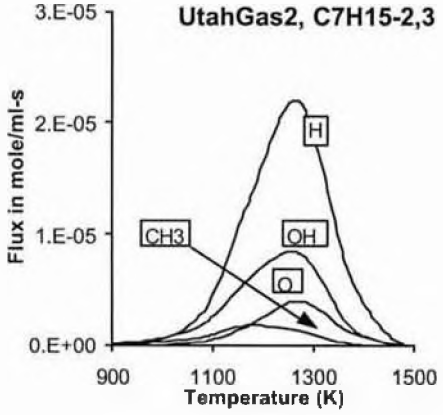

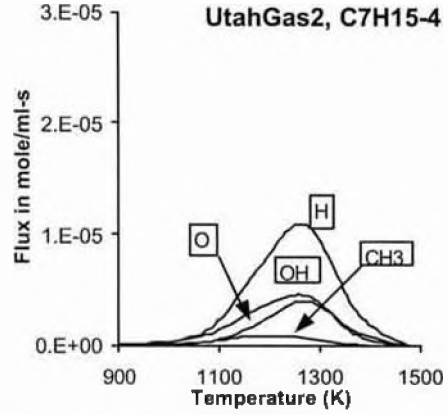

Figure 14. Hydrogen abstraction fluxes in Utah-Gas2.

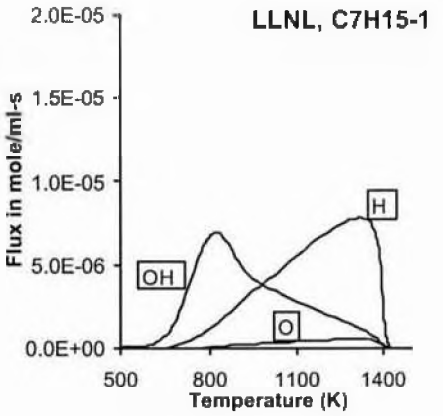

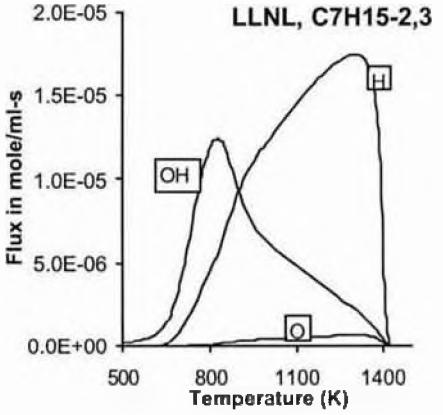

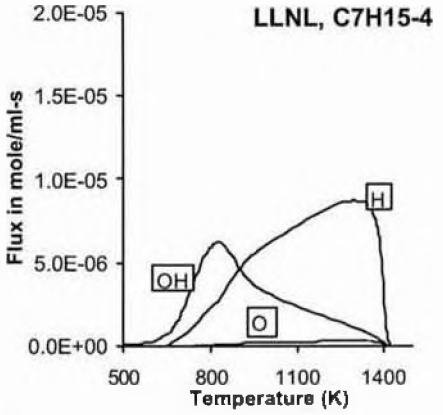

Figure 15. Hydrogen abstraction fluxes in LLNL reduced mechanism.

C2H3 radical form the second set that is most active at higher temperature around 1270K. Methyl radical is an exception since its abstraction reactions give a flat top flux curve between 965 and 1270K. Because hydrogen and hydroxyl radical have their maximum activities in different temperature regions LLNL mechanism offers the unique bimodal overall abstraction fluxes.

Each mechanism has its own philosophy of fuel combustion, even for single reaction class of hydrogen abstraction. For example, the importance of symmetric number is well supported in utah-Gas2 and its primary radical formation rate exceeds those of secondary isomers at high temperature. In contrast to Utah-Gas2, C7H15-1 formation rate in LLNL mechanism only surpasses that of

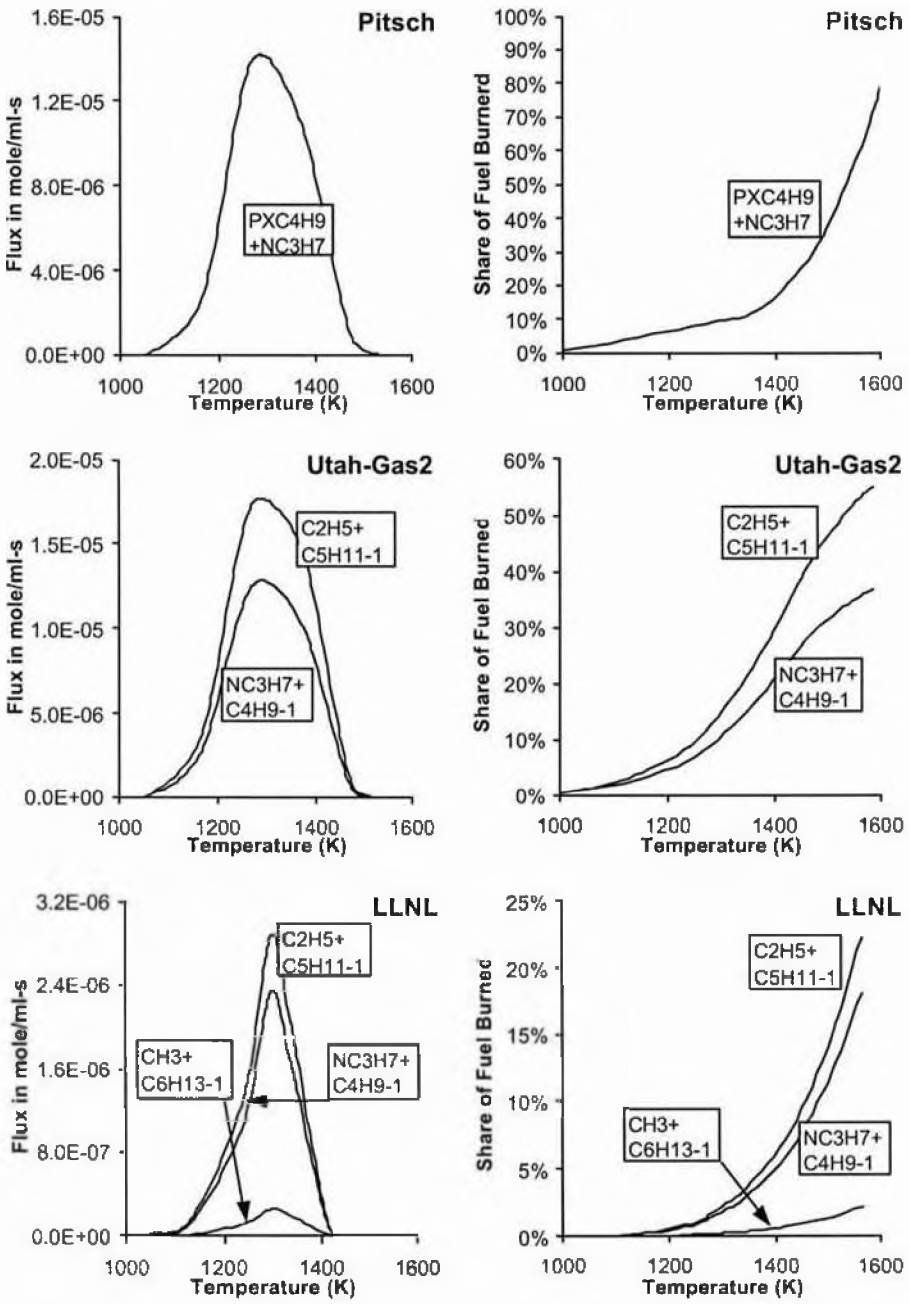

Figure 16. Unimolecular decomposition fluxes.

C7H15-4, the isomer with lowest symmetric number, at 1410K. Despite the differences in kinetics, there are also similarities among these mechanisms. The chemical nature for C7H15-4 is treated same as that of other secondary isomers except for the symmetric number by both Utah-Gas2 and LLNL mechanisms. The formation rate of C7H15-4 is assigned half of that toward C7H15-2. This simplification neglects the possibly larger steric hindrance for C7H15-4. It is also common for mechanisms to have two sets of abstractors active in different temperature regions. Another example is CH3 radical in Utah-Gas2. Abstraction fluxes of methyl radical reach maximum about 100K earlier than other abstraction fluxes. Nonetheless Utah-Gas2 does not give a bimodal

shape since the earlier peak is not comparable in strength with major peaks.

Fuel Consumption via Unimolecular Decomposition Besides hydrogen abstraction, unimolecular decomposition is another important fuel consumption route reported for diffusion flames in literature[15]. Unimolecular decomposition fluxes for the premixed flame in this study are plotted in Figure 16 as well as the percentage of carbon atoms released from fuel molecules that flow through each flux. Pitsch mechanism supports only one unimolecular decomposition reaction to form one butyl plus one propyl radical. The reaction starts at 1050K very much synchronized with hydrogen abstraction reactions but with a peak of only 9% in magnitude. It becomes the leading fuel consumption pathway at 1500K after a steep percentage gain starting from 1350K. However at the same temperature, the reaction becomes trivial, about 50K later than the abstraction reactions.

The shape of decomposition fluxes using Utah-Gas2 is very similar to that of Pitsch mechanism with important points at almost same temperatures. There are differences too. Besides the butyl plus propyl decomposition, another reaction to form ethyl plus pentyl radical is also responsible for fuel consumption with an even higher flux. The new reaction is responsible for the faster unimolecular decomposition in Utha-Gas2, twice as fast as that in Pitsch mechanism. The decomposition fluxes start a steep percentage increase at 1350K, 100K earlier than that in Pitsch mechanism. Decomposition fluxes start to exceed hydrogen abstraction reactions at 1300-1350K and account for half of the fuel consumption at 1400K.

Decomposition fluxes in LLNL mechanism reach their maximum around 1300K, very close to Utah-Gas2 and Pitsch mechanisms' 1270K. LLNL model also accelerates its decomposition reactions at 1050K and those reactions become trivial at 1425K about 75K earlier than the other two mechanisms. LLNL mechanism shows a fast percentage gain after 1400K similar to Pitsch mechanism. Decomposition reactions are never dominant until 1600K, at which temperature decomposition fluxes account for 50% of total fuel consumption. The reactions to ethyl plus pentyl radicals and to propyl plus butyl radicals are still the most important ones. The reaction toward C2+C5 is about 11% higher than that toward C3+C4, a gap much smaller than Utah-Gas2's 38%. A new reaction to form methyl plus hexyl radicals is added but contributes only 5% toward the overall decomposition because of the unstable methyl radical. LLNL model gives a much smaller total decomposition flux only one sixth in strength compared to Utah-Gas2, or 40% compared to Pitsch mechanism.

Utah-Gas2 has the most active unimolecular decomposition reactions followed by Pitsch mechanism. Decomposition fluxes become the major fuel consumption routes at 1400K using Utah-Gas2 compared to 1500K for Pitsch and 1600K for LLNL mechanisms. However, at that high temperature, less than 1% of n-heptane fuel left in the combustion system as seen in Table 3. Thus the unimolecular decomposition reactions never contribute significantly toward the overall fuel consumption process.

Table 3. Carbon Atoms Remained in Fuel Molecules

HAB (cm)	T (K)	Pitsch	Utah-Gas2	T (K)	LLNL
0.000	450.0	92.74%	92.33%	450.0	95.43%
0.025	552.4	89.42	88.91	491.1	92.73
0.050	654.8	85.16	84.65	532.1	88.59
0.075	757.2	79.77	79.36	580.4	82.16
0.100	859.6	72.88	72.61	657.3	71.88
0.125	962.0	63.73	63.53	734.2	56.65
0.150	1064.4	51.05	50.54	811.2	41.11
0.175	1167.0	33.26	31.53	888.1	26.71
0.200	1269.0	12.20	10.51	965.0	11.33
0.225	1372.0	1.00	0.91	1337.5	0.48
0.250	1474.0	0.01	0.01	1420.0	0.00
0.275				1498.8	0.00
0.300				1565.0	0.00

β scission Despite the differences in chemical nature and reaction rate, both unimolecular decomposition and hydrogen abstraction reactions have a same class of

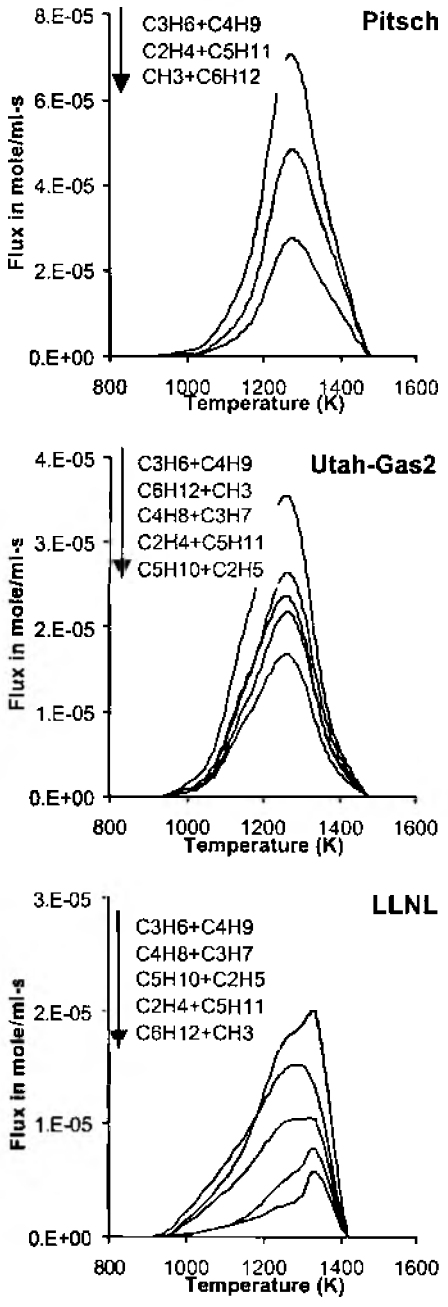

Figure 17. β scission fluxes. Arrow indicates the direction of decreasing fluxes.

product – alkyl radicals. All alkyl radicals decompose via β scission reactions into one smaller alkyl radical and one olefin usually by breaking a C-C bond. With appropriate kinetic parameters, the whole fuel consumption process can be explained in a cascading alkyl radical decomposition plus olefin chemistry. One exception of this decomposition cascade is that in some reactions a hydrogen radical is formed instead of a smaller alkyl radical. These reactions are extremely unfavorable never significant for fuel consumption since about 100 kJ/mol extra energy needed to break a C-H bond than a C-C bond at 25°C[45]. On the other hand, hydrogen radical can be considered as the smallest member in the homologous series of radicals H, CH_3, C_2H_5, ..., and can be treated as a special case for the cascading alkyl radical decomposition.

There are at most two possible β scission reactions for each alkyl radical isomer. For example, following are all possible β scission reactions for n-heptyl radical.

$$CH_3CH_2CH_2CH_2CH_2CH_2CH_2\bullet \rightarrow C_2H_4 + CH_3CH_2CH_2CH_2CH_2\bullet \quad (1)$$

$$CH_3CH_2CH_2CH_2CH_2CH\bullet CH_3 \rightarrow CH_3CH_2CH_2CH_2CH_2CH{=}CH_2 + H \quad (2)$$

$$CH_3CH_2CH_2CH_2CH_2CH\bullet CH_3 \rightarrow CH_2{=}CHCH_3 + CH_3CH_2CH_2CH_2\bullet \quad (3)$$

$$CH_3CH_2CH_2CH_2CH\bullet CH_2CH_3 \rightarrow CH_2{=}CHCH_2CH_3 + CH_3CH_2CH_2\bullet \quad (4)$$

$$CH_3CH_2CH_2CH_2CH\bullet CH_2CH_3 \rightarrow CH_3CH_2CH_2CH_2CH{=}CH_2 + CH_3 \quad (5)$$

$$CH_3CH_2CH_2CH\bullet CH_2CH_2CH_3 \rightarrow CH_3CH_2CH_2CH{=}CH_2 + CH_3CH_2 \quad (6)$$

Primary heptyl radical is formed much slower than its secondary isomers except at very high temperature, thus the flux of primary radical β scission reaction (1) is ranked as the second slowest flux for all three mechanisms in Figure 17. Similarly, it is no surprise that reaction (3) is the most active flux for all three mechanisms since the secondary radical C7H15-2 or C7H15-3 forms faster than other isomers and reaction (3) is the only significant consumption route for C7H15-2. Reaction (2) also with C7H15-2 as reactant is too slow to have any impacts on the total fuel consumption process. The symmetric heptyl isomer C7H15-4 is formed slower because of the low symmetric number as discussed earlier, thus reaction (6) is never among the most active ones. Reaction (6) is ranked the slowest in Utah-Gas2 and third out of five in LLNL reduced mechanism. Reaction (6) is faster than reaction (1) in LLNL reduced mechanism since C7H15-4 is produced faster than C7H15-1 as discussed earlier. However, the over-prediction of 1-pentene in Figure 3 by LLNL model suggests that C7H15-4 is overproduced. Reaction (5) gives contradictory results. Methyl radical is the least stable among alkyl radicals. According to the Hammond-Leffler Postulate[46], the higher energy of products suggests a higher energy barrier for reaction (5) that undermines the advantage from abundance of C7H15-3 reactant. These two opposite forces competing with each other and should be evaluated carefully. For both Pitsch and LLNL reduced mechanism the energy barrier are taken more serious, and reaction (5) is the slowest among all decomposition fluxes. The Vovelle heptane

decomposition sub-model in Utah-Gas2 probably overvalues the forward rate of reaction (5) since the reaction is even faster than reaction (4), which has the same reactant C7H15-3 but more stable products. The faster rate of reaction (5) is the major reason for the overestimation of 1-hexene in Figure 3 by Utah-Gas2. Enhanced reaction (5) also slows down reaction (4) so that 1-butene was under-predicted by 38% using Utah-Gas2 in Figure 3.

β scission is the dominant decomposition route of alkyl radicals formed from hydrogen abstraction or unimolecular decomposition of fuel molecules. A buildup process is also at work parallel to β scission to consume some of the alkyl radicals formed from fuel cracking. The scale of buildup process is listed in Appendix 1, 2, 3 for all three mechanisms. It is obvious that buildup process is only significant at locations very close to the burner surface before the pseudo steady state of heptyl radicals is reached. For example, 39.2% of the carbon atoms released from fuel consumption are stored in primary heptyl radical at 0.025 cm above the burner surface using Pitsch mechanism and the numerical combustion reaches pseudo steady state for heptyl radicals at 0.05 cm above the burner surface. The other two mechanisms give similar results that hoarding phenomena are only observable at very close region near the burner surface usually less than half of a millimeter.

Hydrogen abstraction or unimolecular decomposition followed by β scission is the fundamental chemistry of combustion phenomena. β scission, which leads to one olefin and one smaller alkyl radical, is the power engine to push combustion process forward by cracking larger hydrocarbon fragments down into smaller ones. Thus correct chemistry for β scission reactions is critical not only for fuel consumption process, but also for olefin formation, C2-C4 chemistry, and most likely the whole combustion phenomena.

Isomerization Isomerization reactions have very important impacts on the chemistry of fuel consumption and olefin formation. Most isomerization reactions are facilitated via a transient ring with 5-7 members. Isomerization from C7H15-1 to C7H15-3 should be the fastest reaction since it forms a most stable 6-member transition state and this is suggested by Utah-Gas2 mechanism.

Since Pitsch mechanism does not distinguish secondary

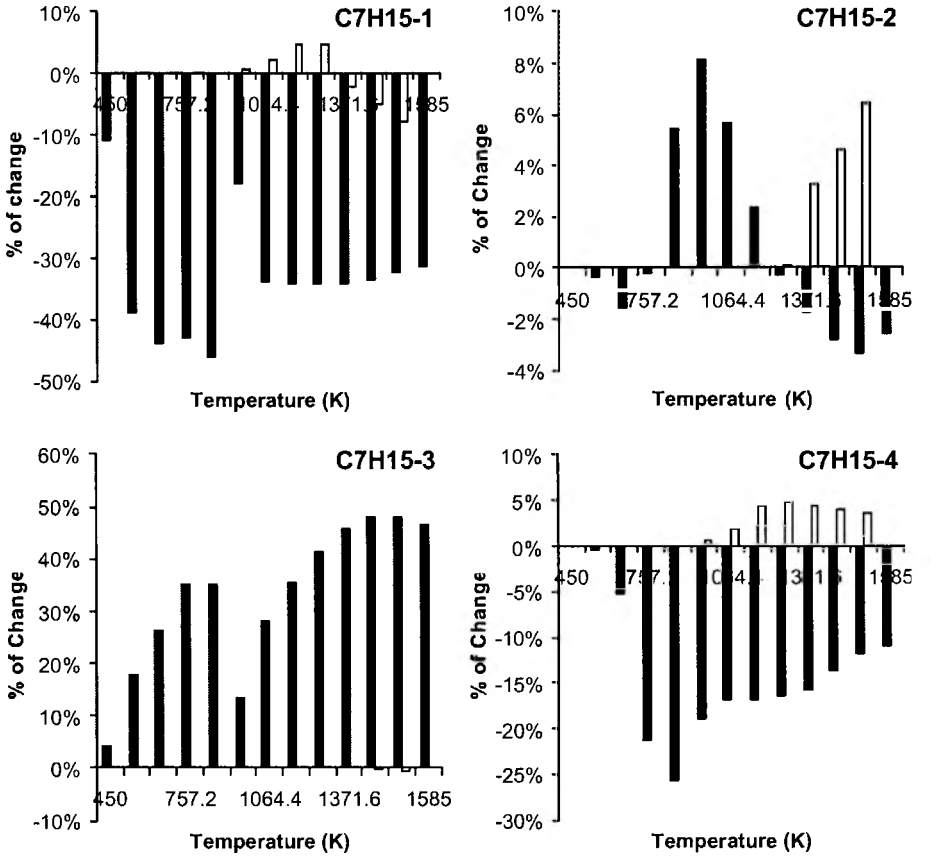

Figure 18. Percentage change of heptyl radical formation with isomerization included.

heptyl radical isomers, there is only one isomerization reaction between primary and lumped secondary radicals. This isomerization reaction is contaminated with a peroxy radical cycle discussed earlier (Figure 8). With the decycling technique, the direction of the isomerization reaction is made clear (Appendix 1). At low temperature, unimolecular decomposition reactions consume only a trivial portion of the fuel and majority of the carbon atoms are converted into heptyl radicals. The ratio of secondary over primary radical is at least 3 to 1 if temperature is lower than 1000K. Thus the abundance of secondary heptyl radical isomer is the dominant force to push the isomerization process in Pitsch mechanism. The isomerization scenario has a direction switch at higher temperature since the formation rate of primary radical gradually catches up that of secondary radical. The abundance of reactant surrenders to the activation energy of isomerization reactions. According to the Hammond-Leffler Postulate, the isomerization reaction from primary toward secondary radical should proceed faster than the reverse reaction benefited from a lower energy barrier since primary radical is higher in energy than secondary ones. The Hammond-Leffler Postulate is followed religiously at temperature higher than 1000K to switch the net isomerization flow from primary toward secondary radical.

Utah-Gas2 and LLNL mechanisms feature four isomerization reactions for their distinguished heptyl radicals (Appendix 2, 3). Because the formation of C7H15-2 and C7H15-3 is almost at the same pace from hydrogen abstraction reactions, the isomerization direction between C7H15-2 and C7H15-3 depends heavily on other isomerization reactions that will change concentration of these chemically similar radicals. Both Utah-Gas2 and LLNL mechanisms give some direction switching scenes for C7H15-2 and C7H15-3 isomerization. The isomerization between primary heptyl radical and other isomers follows the Hammond-Leffler Postulate such that primary toward secondary radical isomerization is always favorable than the reverse reaction. There are two exceptions, however. At very low temperature, the combustion chemistry may favor the abundance of reactant over the lower energy barrier. This reversion is obvious in Pitsch mechanism but barely observable only at very low temperature region (< 650K) for C7H15-1 and C7H15-2 isomerization in Utah-Gas2. The second exception is the reaction between C7H15-1 and the symmetric species C7H15-4. The isomerization from C7H15-4 toward C7H15-1 has a symmetric number of 6 since all six hydrogen atoms at both end of the molecule can migrate compared to a symmetric number of 2 for the reverse reaction. The higher symmetric number competes with the lower energy barrier for the net isomerization direction. LLNL reduced mechanism favors the lower energy barrier while Utah-Gas2 considers the higher symmetric number more significant. Two opposite directions are assigned to this isomerization reaction by Utah-Gas2 and LLNL mechanisms that may influence concentration profiles of some larger olefins significantly. As shown in Figure 18, the formation rate of C7H15-4 decreases by as much as 25% in Utah-Gas2 compared to a moderate 5% gain for C7H15-4 formation in LLNL model. This reduction of C7H15-4 formation may help Utah-Gas2 to lower the 1-pentene prediction to fit the experiment data with a 7% deviation in figure 3. The favorable position in isomerization, a too active formation reaction, and maybe a too fast decomposition rate of C7H15-4 are probably adequate to explain the 85% over-prediction of 1-pentene using LLNL mechanism. In general, Utah-Gas2 supports some very active isomerization reactions. As shown in Figure 18, the change of heptyl isomer formation rate due to isomerization is at least a factor of 5 higher using Utah-Gas2 than that using LLNL mechanism except for the least active C7H15-2. C7H15-3 is another heptyl radical isomer that should be paid attention to. LLNL mechanism shows almost no obvious isomerization effects while Utah-Gas2 suggests an increase of C7H15-3 formation by as much as 50%. This increase may be responsible for the Utah-Gas2's 50% overestimation of 1-hexene in Figure 3 in addition to a too fast decomposition rate as discussed earlier. The majority gain of C7H15-3 is at the cost of C7H15-1, whose formation rate is slowed down by 30-40%. However, the impacts of this reduction are hardly identified from experimental data since the decomposition of C7H15-1 into C2H4+C5H9-1 is not the major formation route for detectable ethylene.

Evolution of Olefins Olefins are important fuel components since they present in many commercial fuels such as gasoline from thermo cracking process. Olefins are also very important combustion products since they are always produced in earlier stage of combustion process than alkynes, paraffins, dienes, and other intermediates by hydrogen abstraction and β scission reactions. Therefore, the evolution of olefins provides vital information for the combustion nature of large hydrocarbon fuels.

Among the three mechanisms, Pitsch heptane model provides the smallest olefin reaction set involving only 1-hexene, 1-butene, propene and ethylene. Both Utah-Gas2 and LLNL mechanisms give a full set of olefin species from C2 to C7 including all three n-heptene isomers. Utah-Gas2 has the most complete set that also includes all three butene isomers, C_4H_8-1, C_4H_8-2 and iso-butene. Major olefin formation and consumption reactions and their peak temperatures and maximum fluxes are listed in Table 4.

Olefin chemistry is very different from model to model as illustrated in Figure 19-20 for heptene isomers using Utah-Gas2 and LLNL reduced mechanism. Hydrogen abstraction by oxygen molecules is the most important

Table 4. Olefin Formation and Consumption

	Formation						Consumption					
	Pitsch Mechanism											
	Type	Peak T(K)	Max Flux*	Type	Peak T(K)	Max Flux	Type	Peak T(K)	Max Flux	Type	Peak T(K)	Max Flux
C_6H_{12}	D^{1}	1269	2.74×10^{-5}				D^{2}	1269	2.54×10^{-5}	HA^{3}	1269	1.83×10^{-6}
C_4H_8	C^{4}	1269	2.19×10^{-5}				D^{5}	1372	2.76×10^{-5}	AD^{6}	1372	2.18×10^{-6}
C_3H_6	D^{7}	1269	7.08×10^{-5}	C^{8}	1372	1.82×10^{-5}	A^{9}	1372	5.70×10^{-5}	HA^{10}	1372	2.87×10^{-5}
C_2H_4	D^{11}	1371	1.15×10^{-4}	D^{12}	1269	8.61×10^{-5}	HA^{13}	1372	4.15×10^{-4}	D^{14}	1474	1.81×10^{-7}
	Utah-Gas2											
$1C_7H_{14}$	HA^{15}	1167	2.88×10^{-7}				D^{16}	1269	1.78×10^{-7}	D^{17}	1269	1.62×10^{-7}
$2C_7H_{14}$	HA^{18}	1167	5.68×10^{-7}				D^{19}	1269	7.95×10^{-7}	HA^{20}	1167	7.39×10^{-8}
$3C_7H_{14}$	HA^{21}	1167	4.04×10^{-7}				D^{22}	1269	6.09×10^{-7}	HA^{23}	1167	7.63×10^{-9}
C_6H_{12}	D^{24}	1269	2.64×10^{-5}				D^{25}	1269	2.08×10^{-5}	HA^{26}	1269	5.72×10^{-6}
C_5H_{10}	D^{27}	1269	1.67×10^{-5}				D^{28}	1372	5.58×10^{-6}	AD^{29}	1269	6.90×10^{-6}
C_4H_8	D^{30}	1269	2.35×10^{-5}	D^{31}	1269	3.86×10^{-6}	HA^{32}	1269	1.34×10^{-5}	AD^{33}	1269	1.63×10^{-5}
C_3H_6	A^{34}	1372	4.43×10^{-5}	D^{35}	1269	3.53×10^{-5}	HA^{36}	1372	5.70×10^{-5}	AD^{37}	1372	4.20×10^{-5}
C_2H_4	D^{38}	1269	1.10×10^{-4}	D^{39}	1269	9.10×10^{-5}	HA^{40}	1474	1.86×10^{-4}	AD^{41}	1474	7.35×10^{-5}
	LLNL Reduced Mechanism											
$1C_7H_{14}$	D^{42}	811	1.21×10^{-6}	D^{43}	1338	8.41×10^{-7}	D^{44}	1338	1.90×10^{-6}	HA^{45}	1338	6.63×10^{-7}
$2C_7H_{14}$	D^{46}	811	2.74×10^{-6}	D^{47}	1338	6.01×10^{-7}	D^{48}	1338	2.49×10^{-6}	HA^{49}	1338	8.69×10^{-7}
$3C_7H_{14}$	D^{50}	811	2.60×10^{-6}	D^{51}	1338	4.73×10^{-7}	D^{52}	1338	2.36×10^{-6}	HA^{53}	965	8.30×10^{-7}
C_6H_{12}	D^{54}	1338	5.63×10^{-6}	HA^{55}	1338	6.81×10^{-7}	D^{56}	1338	1.09×10^{-5}	HA^{57}	1338	3.69×10^{-6}
C_5H_{10}	D^{58}	965	1.04×10^{-5}	C^{59}	965	2.62×10^{-6}	D^{60}	1338	2.05×10^{-5}	A^{61}	1338	5.13×10^{-6}
C_4H_8	D^{62}	965	1.52×10^{-5}	A^{63}	1338	3.44×10^{-6}	HA^{64}	1338	2.37×10^{-5}	D^{65}	1338	7.80×10^{-6}
C_3H_6	D^{66}	1338	1.03×10^{-4}	A^{67}	1338	6.27×10^{-5}	HA^{69}	1338	1.04×10^{-4}	$??^{68}$	1338	9.03×10^{-5}
C_2H_4	D^{70}	1338	1.46×10^{-4}	D^{71}	1338	8.75×10^{-5}	HA^{72}	1499	1.66×10^{-4}			

* Maximum flux in unit mole/cm^3-s

Table 4 (continues)

D = Decomposition;
A = Addition;

1. SXC7H15 => PXC6H12 + CH3;
4. C3H5 + CH3 ⇔ PXC4H8;
7. SXC7H15 => PXC4H9 + C3H6;
10. C3H6 + A ⇔ C3H5 + AH;
13. C2H4 + H ⇔ C2H3 + H2;
16. C7H14-1 => CH3 + C4H6-13 + C2H5;
19. C7H15-2 => NC3H7 + NC4H7;
22. C7H15-3 => C2H5 + C5H9;
25. C6H12-1 => NC3H7 + AC3H5;
28. C5H10-1 => AC3H5 + C2H5;
31. C6H11-1 ⇔ C4H8-1 + C2H3;
34. AC3H5 + H ⇔ C3H6;
37. C3H6 + A ⇔ products;
40. C2H4 + A ⇔ C2H3 + AH;
43. C7H15-1(2) ⇔ C7H14-1 + H;
46. C7H14OOH2-3(3-2) ⇔ C7H14-2 + HO
48. C7H14-2 ⇔ NC3H7 + C4H7;
51. C7H15-3(4) ⇔ C7H14-3 + H;
54. C7H15-3 ⇔ C6H12-1 + CH3;
56. C6H12-1 ⇔ NC3H7 + C3H5-A;
59. C2H5 + C3H5-A ⇔ C5H10-1;
62. C7H15-3 ⇔ C4H8-1 + NC3H7;
65. C4H8-1 ⇔ C3H5-A + CH3;
68. C3H6 + H2 ⇔ IC3H7 + H;
71. NC3H7 ⇔ C2H4 + CH3;

C = Combination; HA = Hydrogen Abstraction;
AD = Addition Followed by Decomposition

2. PXC6H12 => NXC3H7 + C3H5;
3. PXC6H12 + A=>C6H11 + AH;
5. PXC4H8 ⇔ C3H5 + CH3;
6. PXC4H8 + OH ⇔ NXC3H7 + CH2O;
8. C2H3 + CH3 ⇔ C3H6;
9. C3H6 + H ⇔ NXC3H7;
11. NXC3H7 ⇔ CH3 + C2H4;
12. C2H5 (+M) ⇔ C2H4 + H (+M);
14. C2H4 (+M) ⇔ C2H2 + H2 + M;
15. C7H15-1(2) + O2 ⇔ C7H14-1 + HO2;
17. C7H14-1 => C4H9-1 + AC3H5;
18. C7H15-2(3) + O2 ⇔ C7H14-2 + HO2;
20. C7H14-2 + A => products + AH;
21. C7H15-3(4) + O2 ⇔ C7H14-3 + HO2;
23. C7H14-3 + A => products + AH;
24. C7H15-3 ⇔ C6H12-1 + CH3;
26. C6H12-1 + A ⇔ products + AH;
27. C7H15-4 ⇔ C5H10-1 + C2H5;
29. C5H10-1 + H ⇔ products;
30. C7H15-3 ⇔ C4H8-1 + NC3H7;
32. C4H8-1 + H ⇔ products + AH;
33. C4H8-1 + A ⇔ products;
35. C7H15-2 ⇔ C3H6 + C4H9-1;
36. C3H6 + A ⇔ products + AH;
38. C2H5 (+M) ⇔ C2H4 + H (+M);
39. NC3H7 ⇔ CH3 + C2H4;
41. C2H4 + A = products;
42. C7H14OOH1-2 ⇔ C7H14-1 + HO2;
44. C7H14-1 ⇔ PC4H9+C3H5-A;
45. C7H15-1 + A => C7H13 + AH;
2;
47. C7H15-2(3) ⇔ C7H14-2 + H;
49. C7H14-2 + A => C7H13 + AH;
50. C7H14OOH3-4(4-3)⇔C7H14-3+HO2;
52. C7H14-3 ⇔ NC3H7 + C4H7;
53. C7H14-3 + A => C7H13 + AH;
55. C7H14O1-3 + OH ⇔ C6H12-1 + HCO + H2O;
57. C6H12-1 + A => C6H11 + AH;
58. C7H15-4 ⇔ C5H10-1 + C2H5;
60. C5H10-1 ⇔ C2H5 + C3H5-A;
61. C5H10-1 + H ⇔ C5H11-X;
63. C4H7 + H ⇔ C4H8-1;
64. C4H8-1 + A => C4H7 + AH;
66. IC3H7 ⇔ C3H6 + H;
67. C3H5-A + H ⇔ C3H6;
69. C3H6 + A ⇔ products + AH;
70. C2H5 (+M) ⇔ C2H4 + H (+M);
72. C2H4 + H ⇔ C2H3 + H2;

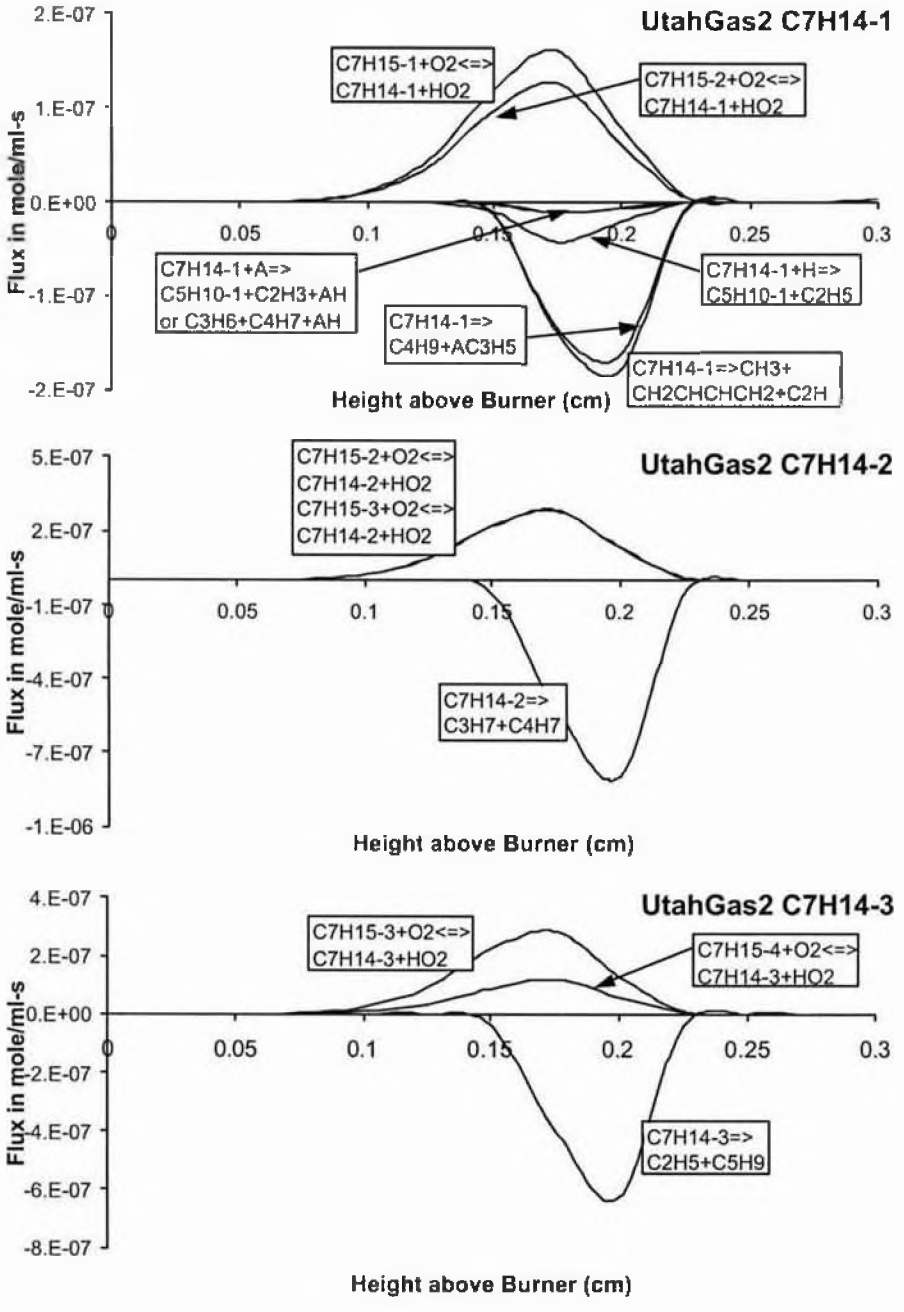

Figure 19. Olefin formation and consumption fluxes for Utah-Gas2.

heptene formation route provided by Utah-Gas2 for all three isomers.

$$C_7H_{15}\text{-}1 + O_2 \leftrightarrow C_7H_{14}\text{-}1 + HO_2$$
$$C_7H_{15}\text{-}2 + O_2 \leftrightarrow C_7H_{14}\text{-}1 + HO_2$$
$$C_7H_{15}\text{-}2 + O_2 \leftrightarrow C_7H_{14}\text{-}2 + HO_2$$
$$C_7H_{15}\text{-}3 + O_2 \leftrightarrow C_7H_{14}\text{-}2 + HO_2$$
$$C_7H_{15}\text{-}3 + O_2 \leftrightarrow C_7H_{14}\text{-}3 + HO_2$$
$$C_7H_{15}\text{-}4 + O_2 \leftrightarrow C_7H_{14}\text{-}3 + HO_2$$

These reactions become important at 850K and their fluxes reach maximum around 1170K. At about 1400K, these reactions become trivial. Utah-Gas2 supports three different major consumption routes of heptene isomers. Heptene can be consumed by unimolecular decomposition into one alkyl radical and one alkenyl radical. The

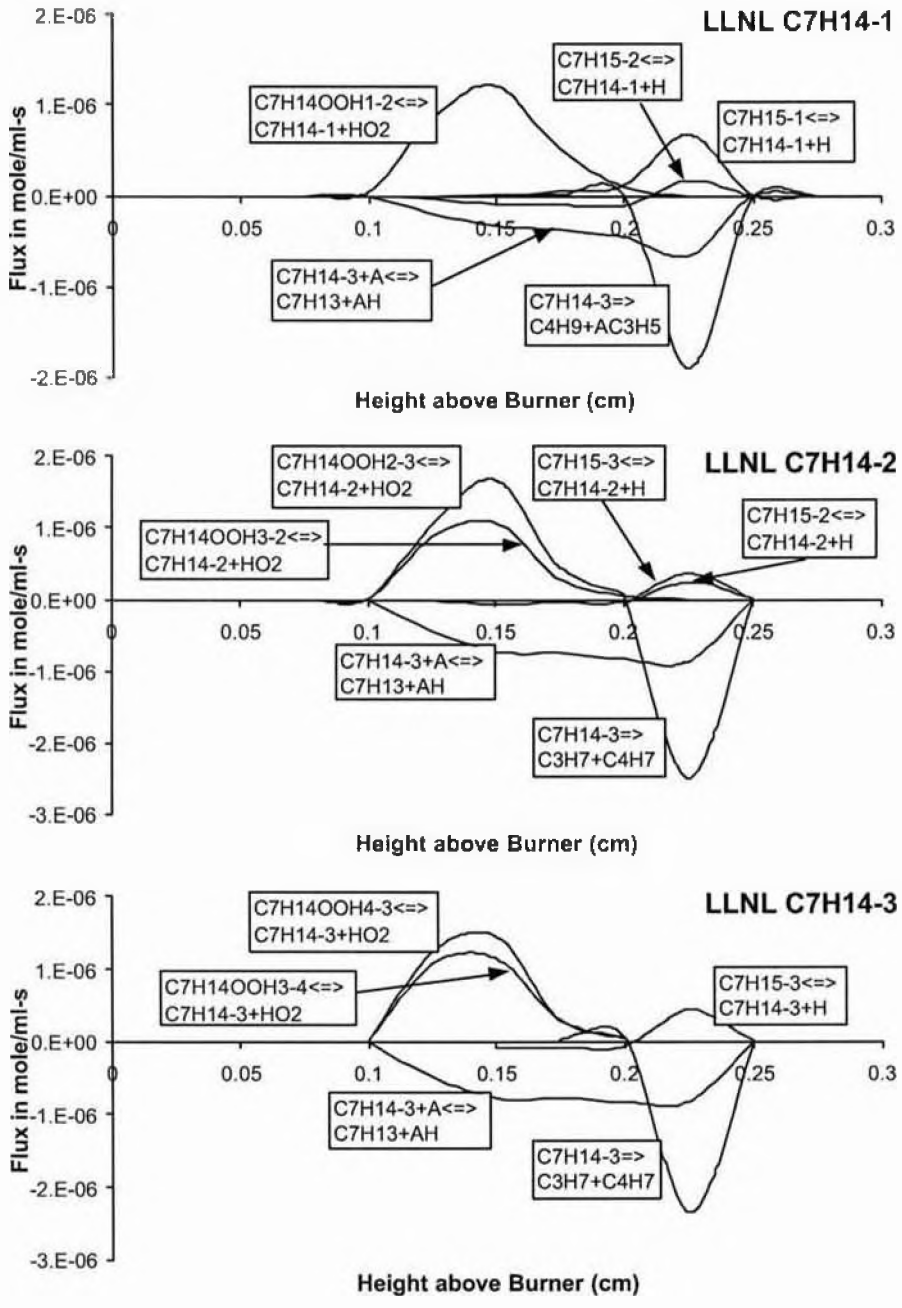

Figure 20. Olefin formation and consumption fluxes for LLNL mechanism.

breaking bond is usually the C-C sigma bond between α and β position since allylic radical is more stable among possible products. Also of importance is the formation of butadiene from 1-heptene decomposition, which is the most active consumption route for that isomer. Hydrogen addition followed by β scission represents the third most active consumption route for 1-heptene, but this reaction class is not supported for other heptene isomers. Hydrogen abstraction followed by β scission is a minor consumption route for all three isomers. Depending on the abstraction site, the alkenyl radical intermediate can be broken into C2-C5 olefins plus one smaller alkenyl radical. All consumption reactions start around 1000K and reach maximum at 1270K, very similar as

unimolecular decomposition reactions seen in earlier sections.

Since LLNL mechanism includes low temperature peroxy radical chemistry, its olefin formation has a lot of unique features (Figure 20). There are two classes of major formation reactions. For temperature lower than 900K, heptene isomers are formed exclusively from the decomposition of α-hydroperoxy heptyl radicals such as

$$CH_3 - CH(OOH) - \dot{C}H - CH_2 - CH_2 - CH_2 - CH_3 \leftrightarrow C_7H_{14} - 2 + HO_2$$

Low temperature peroxy radical chemistry dominates the formation of heptene isomers overtaken by dehydrogenation reactions of heptyl radicals only when the flame temperature reaches 1000K. Although olefin formation chemistry is very different in Utah-Gas2 and LLNL mechanisms, both mechanisms share a few common consumption reactions. For LLNL mechanism, unimolecular decomposition is also identified as the major consumption route of heptene isomers. These reactions start around 1000K and reach maximum at 1350K. Hydrogen abstraction reactions are also recognized as the minor consumption route. These reactions start early in low temperature region to consume heptene isomers formed from α-hydroperoxy heptyl radical decomposition. Fluxes of hydrogen abstraction reactions reach maximum value, however, at high temperature region almost synchronized with unimolecular decomposition reactions.

Despite the model-wise difference in heptene isomers, the chemistry of other olefins is very similar among all three mechanisms. The oxygenated compounds from low temperature chemistry only shows significance for the formation of 1-hexene in LLNL mechanism but with a magnitude one order lower than the competing β scission reaction (Table 4). β scission reaction is also the exclusive formation route of 1-hexene in Utah-Gas2 and Pitsch mechanism, and dominates 1-pentene formation using Utah-Gas2 and LLNL mechanism. LLNL model also supports a smaller combination flux of ethyl radical and allyl radical for 1-pentene formation with a 20% share.

There are quite a few disputes for the 1-butene chemistry. Combination of allyl radical and methyl radical is picked as the exclusive formation route in Pitsch mechanism while Utah-Gas2 prefers two β scission reactions of 3-heptyl radical (major) and 1-hexyl radical (minor). LLNL mechanism also supports the β scission reaction of 3-heptyl radical as the major formation route in addition to its minor butenyl radical hydrogenation route. The philosophy behind propene is also not unified. Pitsch mechanism supports a β scission reaction of secondary heptyl radical as the major formation route plus a minor addition route of methyl radical onto vinyl radical. Utah-Gas2 puts the β scission reaction of 2-heptyl radical as second most important formation reaction only surpassed by the slightly faster hydrogenation of 3-propenyl radical. The importance of allyl radical hydrogenation is also recognized by LLNL mechanism, but the reaction is 30% slower than the most active formation reaction that is given to the dehydrogenation of 2-propyl radical. There is a trend for growing diversities in major formation reactions, as olefin gets smaller. It is surprised, however, the formation of the smallest ethylene is in ubiquitous consensus. Ethylene is formed either by the decomposition of 1-propyl radical or by the dehydrogenation of ethyl radical and both pathways have almost equal importance.

No matter how much difference behind the formation chemistry, the consumption of olefin is limited within a set of few reaction classes and often all three mechanisms agree on the same reactions. For example, the direct decomposition into 1-propyl radical and allyl radical in addition to a minor route of hydrogen abstraction reaction represents the consumption chemistry of 1-hexene for all three mechanisms. 1-pentene is consumed by direct decomposition reaction plus hydrogen addition reaction for both Utah-Gas2 and LLNL mechanism. There are three consumption reaction classes assigned for 1-butene. Pitsch mechanism considers direct decomposition reaction into methyl radical and allyl radical as the major route in addition to a minor addition then decomposition reaction. Hydrogen abstraction reaction is considered the most important pathway by the other two mechanisms. The second outlet of 1-butene is assigned to addition then decomposition reaction by Utah-Gas2 or to direct decomposition reaction by LLNL mechanism. Hydrogen abstraction reaction and addition then decomposition reaction almost equally qualified for the major consumption routes of propene for all three mechanisms. Hydrogen abstraction is also the universal consumption route for ethylene. Especially for Pitsch and LLNL mechanisms, the abstraction reaction is the exclusive sink for ethylene. Utah-Gas2 suggests a competing route of hydrogen addition then decomposition about 30% of share.

Low Temperature Chemistry Although peroxy radical reactions have been long recognized as the low temperature chemistry in hydrocarbon combustion, rates of these reactions are only offered recently with reasonable accuracy from theoretical chemistry computations[47, 48]. Among the three mechanisms, Utah-Gas2 does not support low temperature chemistry. Pitsch mechanism intends to address it with a reaction route via di-peroxy radical to hydroperoxy ketone followed by decomposition to smaller alkyl radicals as shown in Figure 8. This route matches the major low temperature reactions proposed in other larger models such as LLNL mechanism, but is compromised by simplification emphasis with lumped peroxy radical as discussed earlier. This lumped peroxy radical acts as an intermediate for faster isomerization between primary and secondary

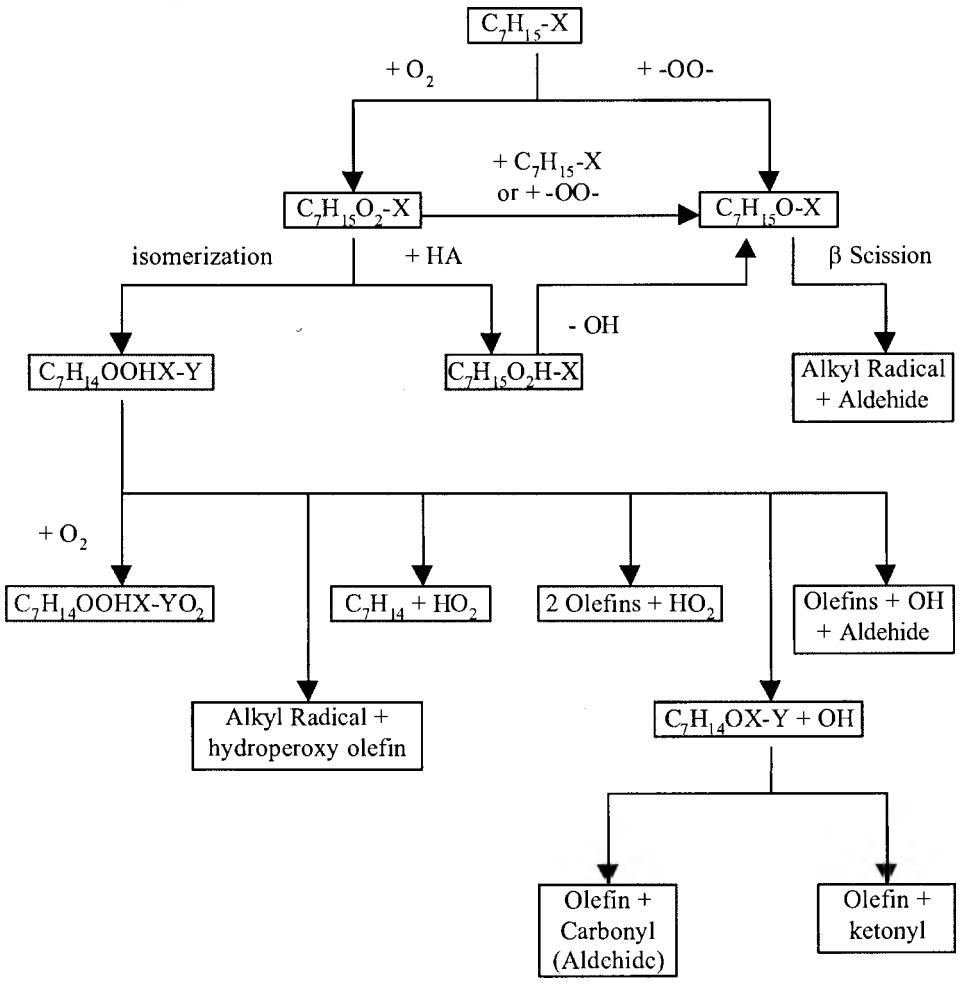

Figure 21. Low temperature reaction network in LLNL reduced mechanism.

heptyl radicals. If isomers of peroxy radicals are to be distinguished with following radical reactions,

Secondary heptyl ⇔ *secondary peroxy* ⇔ *primary peroxy* ⇔ *primary heptyl*

then the faster isomerization cycling can be greatly slowed down since the isomerization between primary and secondary peroxy radicals will be the controlling step. Without this limiting step, the fast decomposition of the lumped peroxy radical into both heptyl radicals with an equal decomposition rate facilitates the carbon flow from secondary to primary heptyl radical because secondary heptyl radical is more abundant. Thus Pitsch mechanism will not give us much useful information of low temperature chemistry since the entry species of low temperature chemistry diverts the carbon flow from peroxy radical reactions into isomerization instead.

LLNL mechanism supports very detailed peroxy chemistry. Its major species for the low temperature chemistry are listed in Appendix 4 and their reactions are illustrated in ball and stick models. Also a summary of low temperature reaction network is elaborated in Figure 21. The peroxy chemistry starts with a heptyl radical, C_7H_{15}-X, reacting with an oxygen molecule to form a peroxy radical, $C_7H_{15}O_2$-X. A peroxy radical can be transformed into a heptoxy radical, $C_7H_{15}O$-X, either by reacting with a heptyl radical or another peroxy radical, or by abstracting a hydrogen from other species then breaking the weak O-O bond. A heptoxy radical can break into one alkyl radical and one aldehyde molecule by β scission reaction. A peroxy radical can also form a hydroperoxy heptyl radical by intra-molecular reconstruction via a ring transition state including 5-8 members. This ring structure is stabilized quickly by breaking one C-H bond to form the new O-H bond.

There are many reactions involving with the consumption of hydroperoxy heptyl radical. 1) It can attach one more

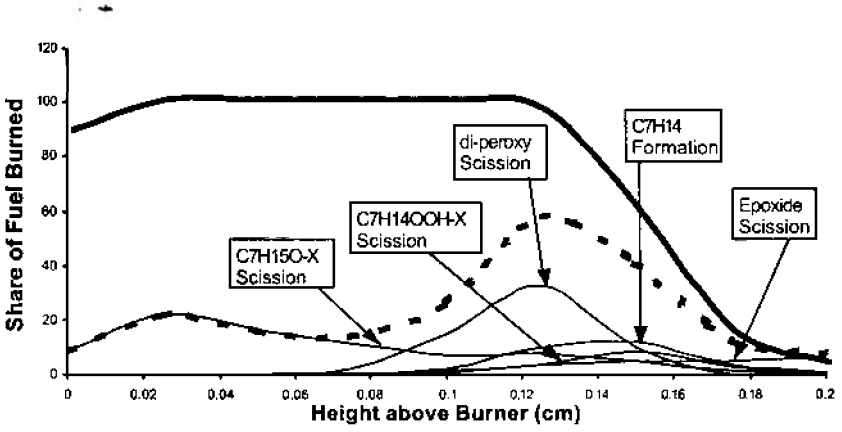

Figure 22. Low temperature fluxes in LLNL reduced mechanism. Heavy solid line for peroxy radical formation; Heavy dot line for total decomposition from low temperature chemistry.

oxygen molecule to form a di-peroxy radical. The product is not very stable since it has to dissipate the C-O bond formation energy. A di-proxy radical undergoes intra-molecular hydrogen abstraction from the carbonyl carbon via a transient ring structure, releases one hydroxyl radical to form a hydroperoxy ketone, which is also an energized molecule. The excess chemical energy quickly dissembles the hydroperoxy ketone into a hydrogenated di-carbonyl radical by losing another hydroxyl radical. LLNL mechanism suggests a further break of the di-carbonyl radical by β scission. 2) A hydroperoxy heptyl radical can also break into one alkyl radical and one hydroperoxy olefin by β scission, or 3) two olefins and one hydroperoxy radical, or 4) one olefin and one aldehyde and one hydroxyl radical. 5) α-hydroperoxy heptyl radical with the hydroperoxy site next to the radical site will become a heptene isomer by losing a hydroperoxy radical. 6) Epoxide is also a possible product from hydroperoxy heptyl radical by forming an oxygen-containing ring after losing a hydroxyl radical.

Low temperature chemistry is a very important part of the LLNL chemistry. It is evident that peroxy radical reactions dominate the fuel consumption near the burner surface where the temperature is lower than 800K (Appendix 3). As discussed earlier, self-consistency is a very important check to guarantee pseudo steady state around major intermediates without significant contamination of component convection and diffusion. Self-consistency check fails for the peroxy radical chemistry. Most peroxy radicals formed at earlier stage do not undergo decomposition directly into smaller alkyl radicals, olefins and carbonyls but are carried into higher temperature region by convection. Figure 22 shows that almost 100% of fuel molecules go form peroxy radicals via alkyl radicals before the flame reaches 700K, but only a small portion, up to 25% of the total peroxy radicals formed decompose into smaller fragments. The low reactivity of peroxy radical is overturned when the flame is hotter than 900K. In addition to direct formation from fuel consumption, peroxy radicals carried by the flow from low temperature region decompose there as well. Thus more products are released from low temperature chemistry than the locally formed peroxy radicals can supply. At 0.125 cm above the burner surface peroxy radical chemistry reaches its maximum flux that is about 30% of the total fuel consumption maximum at 0.216 cm above the burner surface.

Figure 22 also shows the most important decomposition reaction classes of low temperature chemistry. Although β scission reaction of alkanoyl radical dominates fuel consumption at very low temperature region around 500K, low fluxes at that region do not have significant impacts on total fuel consumption process. The largest sink of oxygenated compounds is the decomposition of β-dicarbonyl radical, which consumes up to one third of the total carbon released from fuel consumption at 750K. β-dicarbonyl radical is a subset of hydrogenated dicarbonyl radicals with carbonyl carbon on the β position of each other. The second largest consumer of oxygenated compounds is the formation of heptene isomers from α-hydroperoxy alkyl radical for a share of up to 12% of total fuel consumption. β scission of other hydroperoxy alkyl radicals into smaller fragments represents the next biggest outlet, and followed by decomposition reaction of epoxide.

Experimental evidence gives some suggestions how fast low temperature chemistry should be. Concentration profiles of heptene isomers reach their maximum at temperature around 800K using LLNL mechanism compared to 1075K suggested by Utah-Gas2 in Figure 23. The low temperature mark of heptene isomer formation is unique even in LLNL mechanism since other olefins reach their maximum at temperatures much higher at about 1300K. The dominant formation route for smaller

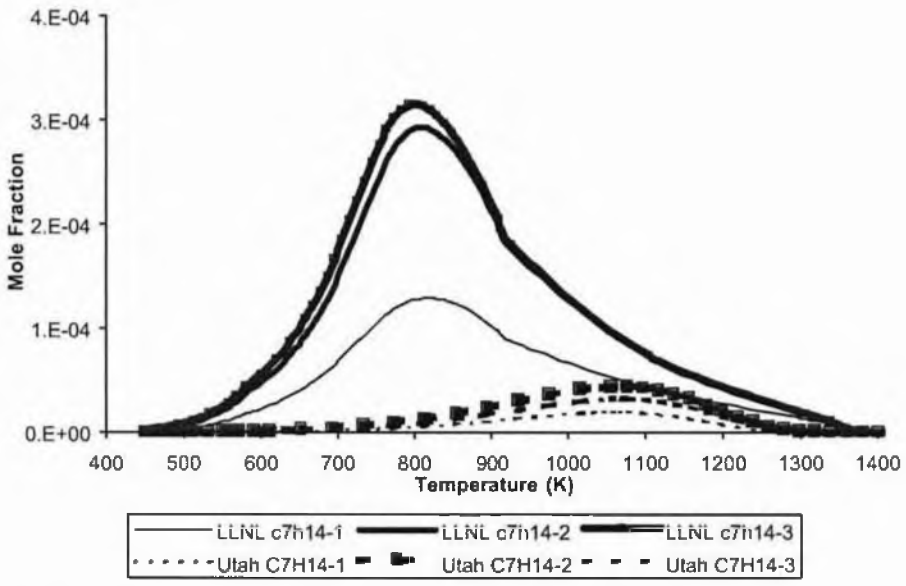

Figure 23. Heptene concentration profiles as a function of temperature.

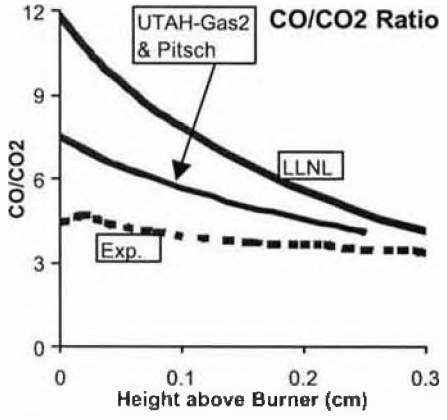

Figure 24. CO/CO2 ratio using each heptane mechanism.

olefins is often β scission of alkyl radical – a high temperature reaction class. There is no doubt that too faster low temperature decomposition of α-hydroperoxy alkyl radical should take the major responsibility for the overproduction of heptene isomers using LLNL mechanism by a factor of 10 to 20 (Table 2) with an early peak at 800K (Figure 3) since that decomposition reaction is identified in Table 4 as the dominant formation route with a share up to 85% at 800K.

The CO/CO_2 ratio also gives some hints of the overstated low temperature reaction rates in LLNL mechanism. The formation of CO_2 takes place mainly in two reactions.

$$HCCO + O_2 \Leftrightarrow HCO + CO_2$$

$$CO + OH \Leftrightarrow CO_2 + H$$

The first reaction progresses via a four-member ring transition state followed by rupturing 2 C-C bonds and one O-O bond and forming 4 C-O bonds at the same time. The forward reaction is more favorable than the reverse one and the net affect is like a one direction reaction toward the CO_2 product. The second reaction is even more important to convert CO toward CO_2, especially in post reaction zone. This reaction forms 2 C-O bonds and breaks one O-H bond and one bond in the triple bond of CO molecule. The carbon atom in CO triple bond is extremely reactive because it has a pair of lone electrons. The forward reaction is also very favorable toward CO_2 except at very high temperature where the reaction is in equilibrium. Therefore the CO/CO_2 ratio can be used to decide the richness of fuel condition. It is well known that very lean fuel intends to produce more CO_2 than CO because more oxygen is available either in molecular or radical form. On the other hand, too active low temperature chemistry will intend to tie the oxygen into peroxy, carbonyl, and other oxygenated species so that the whole combustion system will sense a slightly richer condition due to the bonded oxygen. Thus a higher CO/CO_2 ratio may suggest overheated low temperature chemistry. Figure 24 shows the CO/CO_2 ratio in numerical combustion using Utah-Gas2, Pitsch and LLNL mechanisms as well as the experimental measurements.

LLNL mechanism suggests a ratio much higher than the experimental data by almost a factor of 2 in low temperature region. Results using Utah-Gas2 and Pitsch mechanisms are higher than but closer to the experimental data. LLNL mechanism gives a CO/CO_2 ratio 30-50% higher than those of the other two mechanisms in reaction zone and 15-20% higher in post flame zone. From the carbon atom distribution data in Appendixes1, 2, 3, it is obvious that LLNL mechanism includes many low temperature chemistry species. For example, LLNL mechanism supports large amount of epoxides, whose population is about same as that of the stable propene. Also the total concentration of a set of aldehyde species is almost close to that of methane – an important combustion product. Besides these two sets of compounds, LLNL mechanism also supports other carbonyl compounds such as ketones and their radicals. Roughly, LLNL mechanism has up to 20% of carbon in compounds containing oxygen atoms, a level about one order of magnitude higher than the other two mechanisms. For example, when oxygenated compounds reach their concentration maximum at 0.175 cm above the burner surface, bonded oxygen atoms represents 3% of the total oxygen. Since major stable species H_2O, CO, CO_2, O_2 contain 93.6% of the total oxygen, these oxygenated compounds, most are low temperature species, account for a significant share of the remaining oxygen. No wonder at that position, the concentration of OH radical, critical for CO_2 formation in LLNL mechanism, is only 55% of that in Utah-Gas2. Thus the impacts of oxygen inside oxygenated compounds outweigh the 20% loss of bonded carbon.

Too active low temperature chemistry intends to give a higher CO/CO_2 ratio. However, the reverse may not be true since higher CO/CO_2 ratio may come from other reasons such as the kinetic difference in producing the radical pool, especially the OH radical. For this study, specific kinetics rate of individual reaction will not be discussed to prevent the research from the disarray of major focuses. Thus it is not absolutely sure that a higher CO/CO_2 ratio in LLNL mechanism is mainly the result of faster low temperature chemistry, although it will be surprising that large amount of oxygen hold up in oxygenated species will not make significant impacts. This challenge in chemical kinetics and reaction network will be a good research topic for future studies.

Discussion

Fuel consumption analysis is the major focus of this paper since it is the tool to discover fundamentals in building larger paraffin combustion models. There are three categories of reactions are responsible for fuel consumption. At very early stage before the flame temperature reaches 800K, low temperature chemistry featuring peroxy radical and other carbonyl compounds is the major outlet of carbon atoms in fuel molecules. Among the three mechanisms in this study, only LLNL reduced mechanism has a detailed set of low temperature chemistry. The LLNL low temperature chemistry can be further divided into two different sub temperature regions. From the burner surface up to 600K, fuel consumption is dominated by decomposition of heptyl peroxy radical into one alkyl radical and one aldehyde molecule via heptanoyl radical. This reaction class also makes minor contribution for fuel consumption at the second stage of low temperature chemistry via a slightly different route with one more intermediate, hydroperoxy alkyl radical, before heptanoyl radical. The second low temperature region includes decomposition reactions of α-hydroperoxy heptyl radical and hydrogenated β-dicarbonyl radical in a slightly higher temperature range from 600K to 800K. Although peroxy radical is the exclusive fuel carbon outlet at low temperature, a significant portion of carbonyl compounds do not decompose into smaller fragments at that temperature region but are carried into higher temperature region and decompose there. LLNL low temperature chemistry contributes significantly but not dominantly toward fuel consumption process. It transforms up to one third of fuel molecules into smaller fragments. However, the significance of LLNL low temperature chemistry is challenged by the experimental evidence of heptene isomer evolution and CO/CO_2 ratio. The concentration profiles of the largest olefins in n-heptane flame offer crucial information for fuel consumption chemistry since their similar structure of carbon backbone indicates exclusive and direct formation routes from fuel molecules. LLNL reduced mechanism supports a too fast heptene formation route via low temperature decomposition of α-hydroperoxy heptyl radical and it over-predicts the concentration profile for all three heptene isomers by a factor of 10 to 20. LLNL mechanism also sees a fuel richer environment than the other two models with the same feeds. Its OH radical concentration is much lower because a significant portion of oxygen, not in stable oxygen-containing species, is held in an array of carbonyl compounds formed at low temperature region. This chemical bonding of oxygen is probably a major reason for a CO/CO_2 ratio 100% higher than the experimental data. Therefore the importance of low temperature chemistry under premixed condition studied here may be significantly overstated.

Despite the difference in kinetics and practical perspectives among three mechanisms, a consensus is reached on the dominant fuel consumption route. The largest fuel carbon consumption reaction class is hydrogen abstraction for all three mechanisms. These abstraction reactions hold the leading position overtaken by unimolecular decomposition only at 1400-1600K. H and OH radicals are the major abstractors tailed by O and CH_3 radicals. LLNL shows an interesting bimodal shape

Table 5. Possible reasons for deviation in numerical combustion against experimental data

Species	Model	Δ	Reaction Class	Possible reasons
C_7H_{16}	LLNL	-18%	Low T	Too fast peroxy radical formation
CO/CO_2	LLNL	×2	Low T	A significant portion of oxygen held in carbonyl compounds, the system is artificially fuel richer.
C_7H_{14}-1	LLNL	×10	Low T	The importance of α-hydroperoxy radical decomposition is probably overstated.
C_7H_{14}-2	LLNL	×12	Low T	
C_7H_{14}-3	LLNL	×19	Low T	
C_6H_{12}-1	Pitsch	30%	β scission	There is not enough competing routes for secondary heptyl radical β scission. For example, no SXC_7H_{15} => $NC_3H_7 + C_4H_8$-1. Thus the reaction toward C_6H_{12}-1 is overfed.
C_6H_{12}-1	Utah	51%	β scission	The decomposition 3-heptyl radical toward $CH_3 + C_6H_{12}$-1 should be less active than the one toward $NC_3H_7 + C_4H_8$-1 since the activation energy of the first reaction is higher.
C_4H_8-1	Utah	-38%	β scission	
C_6H_{12}-1	Utah	51%	Isomerization	C7H15-3 formation gains 50% from isomerization
C_5H_{10}-1	LLNL	85%	H abstraction	The formation rate of symmetric 4-heptyl radical is probably overestimated.
C_5H_{10}-1	LLNL	85%	Isomerization	C7H15-4 formation gains from C7H15-1 isomerization
C_5H_{10}-1	LLNL	85%	β scission	The rate maybe too fast coupled with hydrogen abstraction and isomerization gains.

of abstraction fluxes since its abstraction reactions by OH and H take place at two different temperature regions.

Unimolecular decomposition reaction dominates very high temperature region. However, at that high temperature there is not much fuel left (<1%) suggested by carbon atomic distribution analysis. Thus the contribution from unimolecular decomposition toward total fuel consumption process is limited.

Olefin formation relies heavily on β scission of alkyl radical except for the largest or smallest olefins. Heptene formation is suggested mainly by dehydrogenation in Utah-Gas2 or by decomposition of α-hydroperoxy heptyl radical in LLNL mechanism. Formation of some smaller olefins also favors hydrogen addition and combination reactions. Larger olefins are consumed mainly by direct decomposition and sometimes by a minor route of hydrogen abstraction followed by decomposition. Hydrogen abstraction reaction takes the lead in smaller olefin decomposition and in some occasions, addition of a radical onto olefin followed by decomposition also consumes a portion of fuel. Isomerization between heptyl radicals also influences formation of olefins since isomerization may change concentration of some olefins as much as 50%.

Flux analysis coupled with atomic distribution technique is a very useful tool. With knowledge of relative importance of competing reaction classes, mechanisms can be tailored to each specific application. Insignificant contributions are eliminated or lumped into a few reactions to facilitate faster numerical combustion and make the model more applicable for a variety of simulation needs. The philosophy of reduction also finds its application in building larger paraffin combustion models. Based on the idea of chemical similarity between paraffins, the major reaction classes of heptane numerical combustion should suggest a universal fuel consumption pattern for even longer paraffins. Therefore, a complete model with every avenue of chemistry is not a must to catch the true nature of combustion phenomena. Some kinetic adjustments of major reaction classes in heptane flame should be adequate to build accurate but also cost-effective reaction models for larger paraffins. These observations help to shape the fundamental philosophy

that a new simple, effective and also accurate aviation fuel model is based on.

The extension of major reaction classes in heptane flame into larger paraffin fuel combustion modeling can be done only if the numerical performance of the base model lives to the expectations of simulation requirements. When numerical performance is not quite satisfactory or even misleading, the base model needs to be corrected before its philosophy can be spread. Flux analysis is also a good tool to improve numerical performance of an existing model. There are many occasions in this paper that possible reasons for numerical deviation are discussed from a point view of reaction fluxes. Table 5 summarizes these discussions. Most of these discussions involve with olefins since they are the most direct product from fuel consumption. Numerical deviation of other species including some smallest olefins such as ethylene and propene has more reactions involved and thus more complicated for diagnosis. It is not the focus of this paper to discuss numerical deviation of most species except those critical to fuel consumption process.

Also attention should be taken in interpreting the results and conclusions of this study since it is limited by the experimental setting of a premixed laminar flame. The conclusion of relative importance of different reaction classes may not be valid for other combustion environments. For example, for a counter diffusion flame no radical pool is forming to facilitate hydrogen abstraction reaction and no oxygen is available either to initiate low temperature chemistry when the fuel stream flows toward the oxygen stream. However the heat from the combustion makes the fuel hot enough to break down the carbon backbone by unimolecular decomposition. A significant portion of fuel was reported consumed in that way[15].

Bibliography

1. Edwards, T.; Maurice, L. Q. J. of Propulsion & Power 2001, 17(2), 461-466.
2. Wood, C. P.; McDonell, V. G.; Smith, R. A.; Samuelson, G. S. AIAA Journal of Propulsion and Power, 1989, 5(4), 399-405.
3. Sobel, D. R.; Spadaccini, L. J. ASME Journal of Engineering for Gas Turbine and Power, 1997, 119(2), 344-351.
4. Doute, C.; Delfau, J. L.; Akrich, R.; Vovelle, C. Combustion Science and Technology, 1995, 106(4-6), 327-344.
5. Dagaut, P.; Reuillon, M.; Cathonnet, M. Combustion and Flame, 1995, 101, 132-140.
6. Simon, Y.; Scacchi, G.; Baronnet, F. Can. J. Chem. 1996, 74, 1391-1402.
7. Minitte, R.; Carlier, M.; Ribaucour, M.; Therssen, E.; Sochet, L. R. Proc. Combust. Inst., 1996, 26, 747-753.
8. Seiser, R.; Pitsch, H.; Seshadri, K.; Pitz, W. J.; Curran, H. J. Proc. Combust. Inst., 2000, 28, 2029-2037.
9. Colket, M. B. III; Spadaccini, L. J. J. Prop. and Power, 2001, 17, 315-323.
10. Burcat, A.; Farmer, R. C.; Matula, R. A.; Proc. 13th Int. Symp. On Shock Tubes and Shock Waves, 1981, 826-833.
11. El Bakali, A.; Delfau, J. L.; Vovelle, C. Combustion Science and Technology, 1998, 140, 69-91.
12. Doute, C.; Delfau, J. L.; Akrich, R.; Vovelle, C. Combustion Science and Technology, 1997, 124, 249-276.
13. Personal Communication.
14. El Bakali, A.; Delfau, J. L.; Vovelle, C. Combustion and Flame, 1999, 118, 381-398.
15. Bollig, M.; Pitsch, H. Proc. Combust. Inst., 1996, 729-737.
16. Doute, C.; Delfau, J. L.; Vovelle, C. Combustion Science and Technology, 1999, 147, 61-109.
17. Ranzi, E.; Faravelli, T.; Gaffuri, P.; Sogaro, A.; Danna, A.; Ciajolo, A. Combustion and Flame, 1997, 108, 24-42.
18. Violi, A.; Yan, S.; Eddings, E. G.; Sarofim, A. F.; Granata, S.; Faravelli, T.; Ranzi, E. Combustion Science and Technology, 2002, 174, 399-417.
19. Curran, H. J.; Gaffuri, P.; Pitz, W. J.; Westbrook, C. K. Combustion and Flame, 1998, 114, 149-177.
20. Davis, S. G.; Law, C. K.; Proc. Combust. Inst., 1998, 27, 521-527.
21. Held, T. J.; Marchese, A. J.; Dryer, F. L. Combustion Science and Technology, 1997, 123, 107-146.
22. Davidson, D. F.; Horning, D. C.; Hanson, R. K.; Hitch, B. 22nd Int. Symp. Shock Waves, 1999, paper 360.
23. Davidson, D. F.; Herbon, J. T.; Horning, D. C.; Hanson, R. K. Int. J. Chem. Kinetics, 2000, 32, 589-614.
24. Ranzi, E.; Gaffuri, P.; Faravelli, T.; Dagaut, P. Combustion and Flame, 1995, 103, 91-106.
25. Seiser, H.; Pitsch, H.; Seshadri, K.; Pitz, W.J.; Curran, H. J. Proceedings of the Combustion Institute, 2000, 2029-2037.
26. Personal Communication.
27. Miller, J. A.; Melius, C. F. Combustion and Flame, 1992, 91, p21.
28. Tsang, W. Journal of Physics and Chemistry Reference Data, 1988, 17, p887.
29. Tsang, W. Journal of Physics and Chemistry Reference Data, 1991, 20, p221.
30. Pitz, W. J.; Westbrook, C. K.; Leppard, W. K. SAE Transactions, SAE Paper No. 912315, 1991.
31. Emdee, J.; Brezinsky, K.; Glassman, I Journal of Physics and Chemistry, 1992, 96, p2151.
32. Marinov, N. M.; Malte, P. C. International Journal of Chemical Kinetics, 1995, 27, p957.

33. Marinov, N. M.; Westbrook, C. K.; Pitz, W. J. 8th International Symposium on Transport Processes, 1998.
34. Wang, H.; Frenklach, M.; Journal of Physical and Chemistry, 1994, 2, p11465.
35. Hwang, S. M.; Gardiner, W. C. Jr.; Frenklach, M.; Hidaka, Y. Combustion and Flame, 1986, 67, p65.
36. Miller, J. A.; Mitchell, R. E.; Smooke, M. D.; Kee, R. J. 19th Symposium (International) on Combustion, 1982, 19, p.181.
37. Westbrook, C. K.; Combustion and Flames, 1982, 46, p.191.
38. Pitsch, H.; Peters, N.; Seshadri, K. Twenty-Sixth Symposium (International) on Combustion, 1996, 26, 763-771.
39. Kee, R. J.; Grear, J. F.; Smooke, M. D.; Miller, J. A. Sandia Report #SAND 85-824, 1985.
40. Kee, R. J.; Rupley, F. M.; Miller, J. A. Sandia Report #SAND 87-8215B, 1993.
41. Muller C.; Michel V.; Scacchi G.; Côme G.M. J. Chim. Phys., 1995, 92, 1154-1178.
42. Kee, R. J.; Dixon-Lewis, G.; Warnatz, J.; Coltrin, M. E.; Miller, J A. Sandia Report #SAND 86-8246, 1986.
43. Bittner, J. D.; Howard, J. B. 18th Symposium (International) on Combustion, 1981, 18, p.1105.
44. Hartlieb, A. T.; Atakan, B.; Kohse-Höinghaus, K. Combustion and Flame, 2000, 121, 610-624.
45. Kerr, J. A.; Stocker, D. W. In CRC Handbook of Chemistry and Physics, 81st ed.; Lide, D. R., Ed.; 2000-2001, Chapter 9, 64-66.
46. Solomons, T. W. G. Fundamentals of Organic Chemistry, 3d edition, John Wiley & Sons, 1990, Section 5.13A.
47. Bozzelli, J. W.; Chen, C.; Sheng, C.; Dean, A. M. Preprints of Symposia - American Chemical Society, Division of Fuel Chemistry, 2002, 47(1), 219-222.
48. Sheng, C. Y.; Bozzelli, J. W.; Dean, A. M.; Chang, A. Y. Journal of Physical Chemistry A, 2002, 106(32), 7276-7293.

Appendix 1. Numerical Combustion Database of Pitsch Mechanism

HAB (cm)	T (K)	Fuel Consumption (mole/cm^3 s, %)			Isomerization (mole/cm^3 s, %)	
		PXC_7H_{15}	SXC_7H_{15}	PXC_4H_9+ NC_3H_7	1° → 2°	2° → 1°
Φ	**1.9**	**1.9**	**1.9**	**1.9**	**1.9**	**1.9**
0.000	450.0	3.16×10^{-12} 14.5%	1.86×10^{-11} 85.5%	NULL		
0.025	552.4	5.33×10^{-12} 16.6%	2.68×10^{-11} 83.4%	NULL		1.05×10^{-11} 32.7%
0.050	654.8	9.95×10^{-11} 18.2%	4.47×10^{-10} 81.8%	NULL		1.7×10^{-10} 31.1%
0.075	757.2	2.34×10^{-9} 21.3%	8.65×10^{-9} 78.7%	NULL		2.4×10^{-9} 21.8%
0.100	859.6	3.00×10^{-8} 23.9%	9.54×10^{-8} 76.1%	NULL		1.02×10^{-8} 8.2%
0.125	962.0	2.68×10^{-7} 25.9%	7.64×10^{-7} 73.8%	4.08×10^{-9} 0.4%		1.1×10^{-8} 1.1%
0.150	1064.4	2.27×10^{-6} 28.5%	5.53×10^{-6} 69.4%	1.69×10^{-7} 2.1%	2.4×10^{-7} 1.3%	
0.175	1166.8	1.49×10^{-5} 30.8%	3.08×10^{-5} 63.6%	2.72×10^{-6} 5.6%	1.15×10^{-6} 2.4%	
0.200	1269.2	5.21×10^{-5} 32.5%	9.43×10^{-5} 58.8%	1.39×10^{-5} 8.7%	3.81×10^{-6} 2.4%	
0.225	1371.6	2.83×10^{-5} 33.7%	4.48×10^{-5} 53.4%	1.09×10^{-5} 13.0%	2.15×10^{-6} 2.6%	
0.250	1474.0	8.01×10^{-7} 29.0%	1.13×10^{-6} 40.7%	8.37×10^{-7} 30.3%	5.8×10^{-8} 2.1%	
0.275	1552.5	2.66×10^{-9} 18.7%	3.50×10^{-9} 24.7%	8.03×10^{-9} 56.6%	1.78×10^{-10} 1.3%	
0.300	1585.0	5.85×10^{-12} 12.7%	7.47×10^{-12} 16.2%	3.27×10^{-11} 71.1%	3.84×10^{-13} 0.8%	
0.325	1605.0	6.07×10^{-15} 8.8%	7.62×10^{-15} 11.0%	5.57×10^{-14} 80.3%	3.98×10^{-16} 0.6%	
0.350	1625.0	5.02×10^{-17} 5.9%	6.22×10^{-17} 7.3%	7.40×10^{-16} 86.8%	3.21×10^{-18} 0.4%	
0.375	1632.5	3.80×10^{-19} 4.5%	4.68×10^{-19} 5.6%	7.58×10^{-18} 89.9%	2.38×10^{-20} 0.3%	
0.400	1640.0	2.70×10^{-21} 3.5%	3.31×10^{-21} 4.3%	7.15×10^{-20} 92.3%	1.69×10^{-22} 0.2%	
0.500	1620.0	1.69×10^{-27} 3.0%	2.09×10^{-27} 3.8%	5.16×10^{-26} 93.2%	1.08×10^{-28} 0.2%	

HAB (cm)	β scission (mole/cm^3 s, %)			Early Buildup (%)	
	$PXC_7H_{15} \rightarrow C_2H_4 + PXC_5H_{11}$	$SXC_7H_{15} \rightarrow C_3H_6 + PXC_4H_9$	$SXC_7H_{15} \rightarrow CH_3 + PXC_6H_{12}$	1°	2°
Φ	**1.9**	**1.9**	**1.9**	**1.9**	**1.9**
0.000	NULL	NULL	NULL		
0.025	4.23×10^{-12} 13.2%	4.29×10^{-12} 13.4%	1.47×10^{-13} 0.5%	39.2	36.8
0.050	2.63×10^{-10} 48.2%	2.59×10^{-10} 47.4%	1.74×10^{-11} 3.2%	1.1	0.1
0.075	4.73×10^{-9} 43.0%	5.66×10^{-9} 51.5%	6.19×10^{-10} 5.6%	0.1	-0.2
0.100	3.98×10^{-8} 31.8%	7.38×10^{-8} 59.0%	1.17×10^{-8} 9.4%	0.3	-0.5
0.125	2.78×10^{-7} 26.7%	6.21×10^{-7} 59.7%	1.32×10^{-7} 12.7%	0.3	0.3
0.150	2.17×10^{-6} 27.2%	4.44×10^{-6} 55.7%	1.20×10^{-6} 15.1%	0.0	-0.1
0.175	1.39×10^{-5} 28.7%	2.40×10^{-5} 49.5%	7.88×10^{-6} 16.2%	-0.3	0.3
0.200	4.82×10^{-5} 30.1%	7.08×10^{-5} 44.3%	2.74×10^{-5} 17.1%	0.0	-0.2
0.225	2.62×10^{-5} 31.2%	3.25×10^{-5} 38.7%	1.44×10^{-5} 17.1%	-0.1	0.2
0.250	7.43×10^{-7} 26.9%	7.89×10^{-7} 28.6%	3.95×10^{-7} 14.3%	0.0	-0.1
0.275	2.48×10^{-9} 17.5%	2.38×10^{-9} 16.8%	1.29×10^{-9} 9.1%	-0.1	0.1
0.300	5.47×10^{-12} 11.9%	5.03×10^{-12} 10.9%	2.82×10^{-12} 6.1%	0.0	0.0
0.325	5.68×10^{-15} 8.2%	5.10×10^{-15} 7.3%	2.91×10^{-15} 4.2%	0.0	0.1
0.350	4.70×10^{-17} 5.5%	4.13×10^{-17} 4.8%	2.91×10^{-15} 2.8%	0.0	0.1
0.375	3.56×10^{-19} 4.2%	3.10×10^{-19} 3.7%	1.82×10^{-19} 2.2%	0.0	0.0
0.400	2.53×10^{-21} 3.3%	2.19×10^{-21} 2.8%	1.29×10^{-21} 1.7%	0.0	0.0
0.500	1.55×10^{-27} 2.8%	1.36×10^{-27} 2.5%	7.86×10^{-28} 1.4%	0.0	0.1

HAB (cm)	T (K)	Carbon Atom Distribution (%)					
		C_7H_{16}	CO	CO_2	CH_4	C_2H_2	C_3H_4
Φ	**1.9**	**1.9**	**1.9**	**1.9**	**1.9**	**1.9**	**1.9**
0.000	450.0	92.74	4.30	0.58	0.38	0.30	0.16
0.025	552.4	89.42	6.07	0.89	0.52	0.45	0.27
0.050	654.8	85.16	8.24	1.29	0.69	0.65	0.42
0.075	757.2	79.77	10.89	1.82	0.89	0.90	0.63
0.100	859.6	72.88	14.16	2.51	1.13	1.22	0.94
0.125	962.0	63.73	18.35	3.44	1.43	1.65	1.38
0.150	1064.4	51.05	24.06	4.75	1.84	2.26	2.05
0.175	1167.0	33.26	32.32	6.70	2.40	3.18	3.16
0.200	1269.0	12.20	44.35	9.61	3.07	4.69	4.99
0.225	1372.0	1.00	56.59	12.99	3.25	6.76	6.99
0.250	1474.0	0.01	62.53	15.64	2.75	7.74	7.37
	C_2H_4	C_3H_6	C_4H_8	C_6H_{12}	C_3H_5	CH_2O	total
Φ	**1.9**	**1.9**	**1.9**	**1.9**	**1.9**	**1.9**	**1.9**
0.000	1.08	0.13	0.10	0.02	0.07	0.11	99.97
0.025	1.64	0.22	0.17	0.04	0.11	0.17	99.97
0.050	2.37	0.36	0.28	0.07	0.18	0.25	99.96
0.075	3.31	0.56	0.44	0.12	0.26	0.34	99.93
0.100	4.52	0.85	0.66	0.20	0.37	0.47	99.91
0.125	6.13	1.27	1.00	0.33	0.51	0.63	99.85
0.150	8.32	1.87	1.49	0.53	0.73	0.85	99.80
0.175	11.05	2.57	2.07	0.70	1.12	1.16	99.69
0.200	12.27	2.58	2.03	0.47	1.85	1.42	99.53
0.225	7.18	1.01	0.66	0.05	2.02	1.00	99.50
0.250	1.88	0.15	0.08	0.00	1.24	0.28	99.67

Appendix 4. Low Temperature Chemistry of LLNL Reduced Mechanism

X, Y are the position of radical site

C_7H_{15}-X (alkyl radical)

C_7H_{15}-X + O_2	→ $C_7H_{15}O_2$-X	
C_7H_{15}-X + HO_2	→ $C_7H_{15}O$-X + OH	(X≠4)
C_7H_{15}-X + CH_3O_2	→ $C_7H_{15}O$-X + CH_3O	(X≠4)
C_7H_{15}-X + $C_7H_{15}O_2$-Y	→ $C_7H_{15}O$-X + $C_7H_{15}O$-Y	(X≠4)

$C_7H_{15}O_2$-X (peroxy alkyl radical)

$C_7H_{15}O_2$-X + HO_2	→ $C_7H_{15}O_2H$-X + O_2	(X≠4)
$C_7H_{15}O_2$-X + H_2O_2	→ $C_7H_{15}O_2H$-X + HO_2	(X≠4)
$C_7H_{15}O_2$-X + NC_7H_{16}	→ $C_7H_{15}O_2H$-X + C7H15-Y	(X≠4)
$C_7H_{15}O_2$-X + CH_3O_2	→ $C_7H_{15}O$-X + CH_3O + O_2	(X≠4)
$C_7H_{15}O_2$-X + $C_7H_{15}O_2$-Y	→ $C_7H_{15}O$-X + $C_7H_{15}O$-Y + O_2	(X≠4, Y≠4)
$C_7H_{15}O_2$-X + C_7H_{15}-Y	→ $C_7H_{15}O$-X + $C_7H_{15}O$-Y	(X≠4, Y≠4)
$C_7H_{15}O_2$-X	→ $C_7H_{14}OOHX$-Y	
	(Y≠X, 3≥Y-X≥-3, (X,Y)≠(2,1), (4,1), (4,7))	

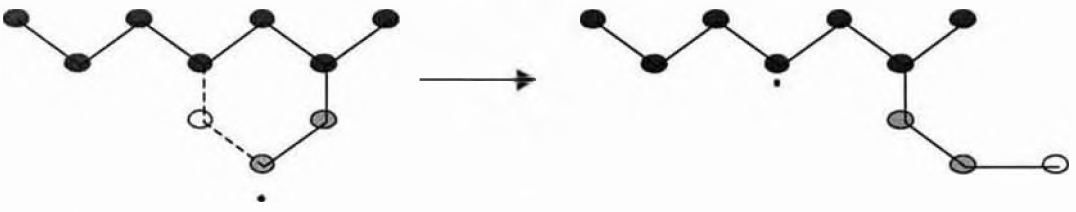

$C_7H_{15}O_2H$-X (hydroperoxy alkyl radical)

$C_7H_{15}O_2H$-X	→ $C_7H_{15}O$-X + OH	(X≠4)

$C_7H_{15}O$-X (alkanoyl radical)

$C_7H_{15}O$-X	→ C_{7-X} alkyl radical + C_X aldehyde (X≠4)

$C_7H_{14}OOHX$-Y (α-hydroperoxy alkyl radical)

$C_7H_{14}OOHX$-Y + O_2	→ $C_7H_{14}OOHX$-YO_2	(X≠4, (X,Y)≠(1,2), (1,4))
$C_7H_{14}OOHX$-Y	→ C_7H_{14}-Z + HO_2	(if |X-Y|=1, Z=min(X,Y))
	→ C_{9-Y} olefin + C_{Y-2} olefin + HO_2	(if Y-X=3, (X,Y)≠(3,6))
	→ C_{9-Y} olefin + C_{Y-2} aldehyde + OH	(if Y-X=2)
	→ C_{Y+1} olefin + C_{6-Y} aldehyde + OH	(if Y-X=2)

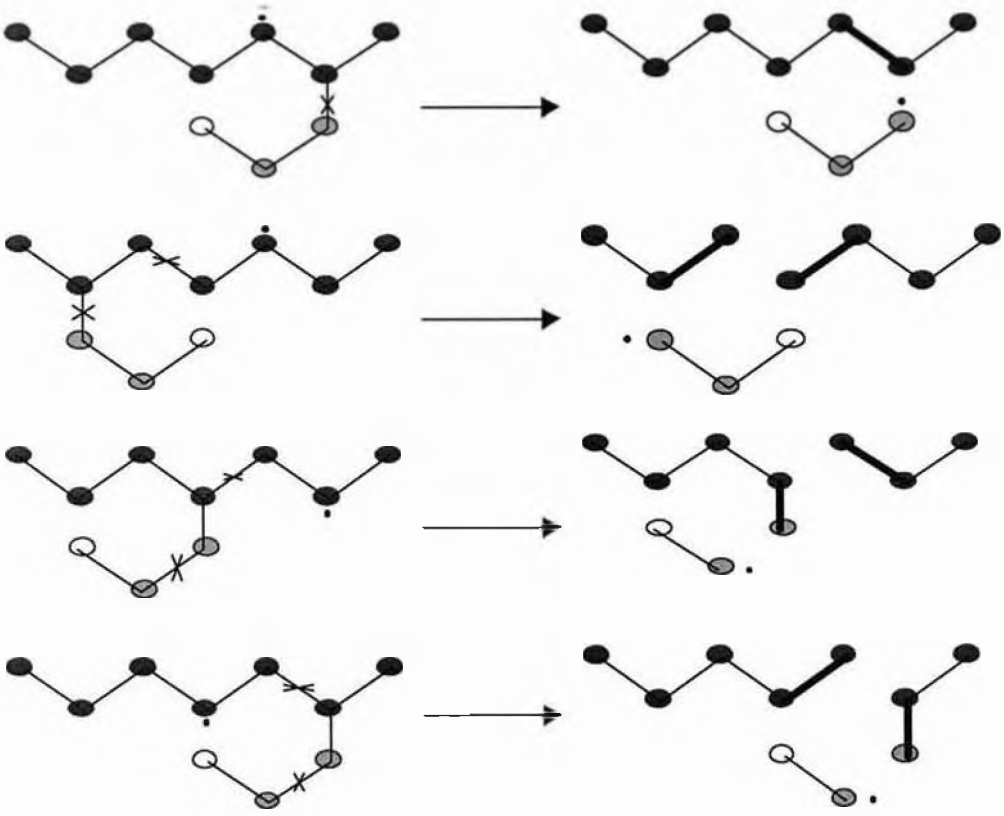

$C_7H_{14}OOHX\text{-}Y \rightarrow C_{6\text{-}Y}$ alkyl radical + $C_{Y\text{-}1}$ hydroperoxy olefin (if Y-X=2, (X,Y)≠(3,5))

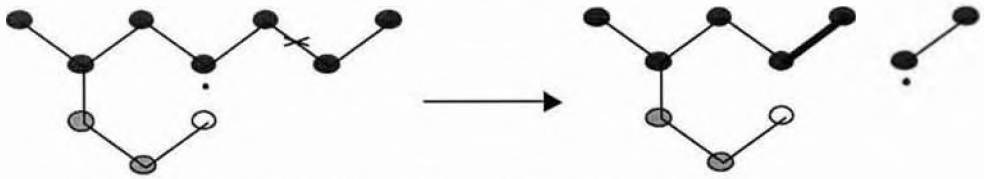

$C_7H_{14}OOHX\text{-}Y \rightarrow C_7H_{14}OX\text{-}Y + OH$ (if |X-Y|≠1)

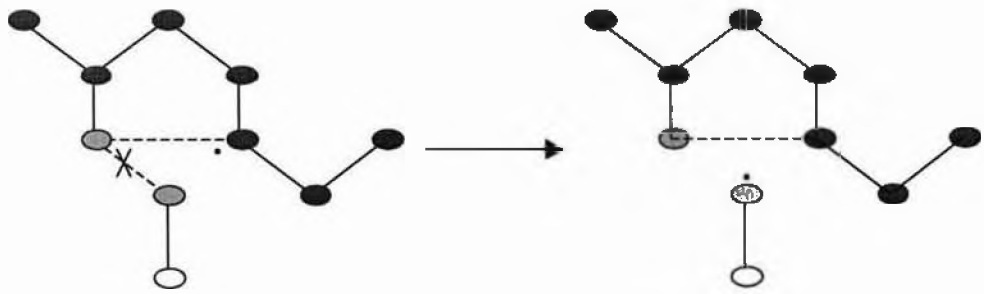

$C_7H_{14}OX\text{-}Y$

$C_7H_{14}OX\text{-}Y + OH \rightarrow C_{9\text{-}Y}$ olefin + $C_{Y\text{-}2}$ alkyl carbonyl + H_2O (if Y-X=2)

$C_7H_{14}OX\text{-}Y + HO_2 \rightarrow C_{9\text{-}Y}$ olefin + $C_{Y\text{-}2}$ alkyl carbonyl + H_2O_2 (if Y-X=2)

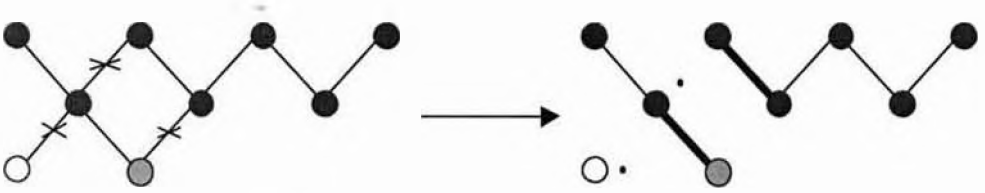

$C_7H_{14}OX\text{-}Y + OH \rightarrow C_{X-1}$ olefin + C_{6-X} alkyl carbonyl + H_2O (if Y-X=2)
$C_7H_{14}OX\text{-}Y + HO_2 \rightarrow C_{X-1}$ olefin + C_{6-X} alkyl carbonyl + H_2O_2 (if Y-X=2)

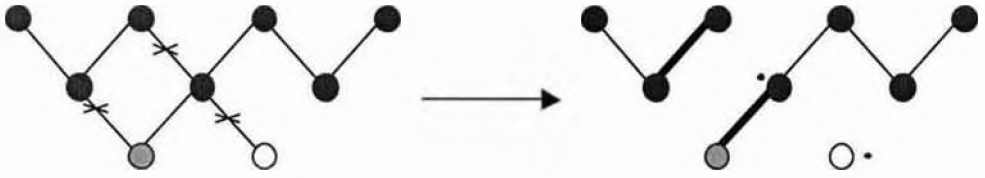

$C_7H_{14}OX\text{-}Y + OH \rightarrow C_{9-Y}$ olefin + C_{Y-2} ketonyl alkyl + H_2O (if Y-X=3)
$C_7H_{14}OX\text{-}Y + HO_2 \rightarrow C_{9-Y}$ olefin + C_{Y-2} ketonyl alkyl + H_2O_2 (if Y-X=3)

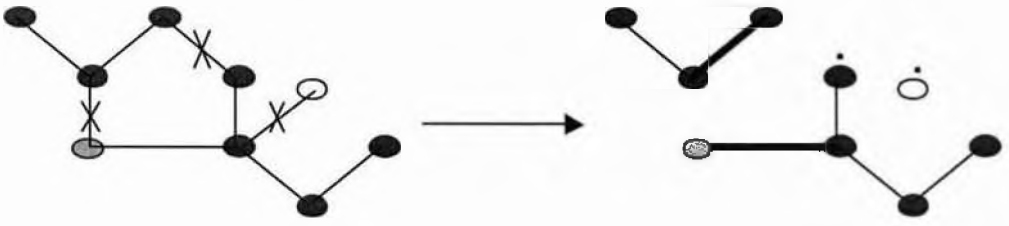

$C_7H_{14}OX\text{-}Y + OH \rightarrow C_{X-1}$ olefin + C_{6-X} ketonyl alkyl + H_2O (if Y-X=3)
$C_7H_{14}OX\text{-}Y + HO_2 \rightarrow C_{X-1}$ olefin + C_{6-X} ketonyl alkyl + H_2O_2 (if Y-X=3)

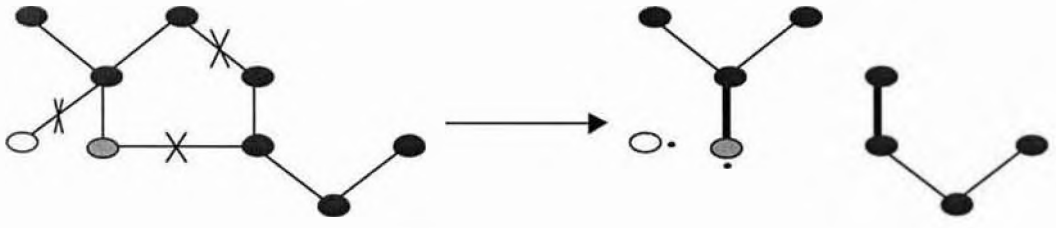

$C_7H_{14}O3\text{-}5 + OH \rightarrow C_4H_7 + C_2H_5CHO + H_2O$
$C_7H_{14}O3\text{-}5 + HO_2 \rightarrow C_4H_7 + C_2H_5CHO + H_2O_2$

Appendix 2. Numerical Combustion Database for Utah-Gas2

HAB (cm)	T (K)	Fuel Consumption (mole/cm^3 s, %)						Early Buildup (%)			
		C_7H_{15}-1	C_7H_{15}-2	C_7H_{15}-3	C_7H_{15}-4	C_2H_5+ C_5H_{11}-1	NC_3H_7+C_4H_9-1	1	2	3	4
Φ	**1.9**	**1.9**	**1.9**	**1.9**	**1.9**	**1.9**	**1.9**	**1.9**	**1.9**	**1.9**	**1.9**
0.000	450.0	1.21×10^{-11} 12.9%	3.24×10^{-11} 34.4%	3.24×10^{-11} 34.4%	1.72×10^{-11} 18.3%	-NULL	-NULL	6.0	21.7	20.6	11.5
0.025	552.4	1.85×10^{-11} 14.8%	4.20×10^{-11} 33.7%	4.20×10^{-11} 33.7%	2.22×10^{-11} 17.8%	-NULL	2.33×10^{-22} 0.0%	0.0	-0.1	-0.2	-0.2
0.050	654.8	2.62×10^{-10} 16.6%	5.19×10^{-10} 33.0%	5.19×10^{-10} 33.0%	2.74×10^{-10} 17.4%	1.88×10^{-17} 0.0%	1.98×10^{-17} 0.0%	-0.1	-0.1	0.1	-0.1
0.075	757.2	2.69×10^{-9} 17.8%	4.92×10^{-9} 32.5%	4.92×10^{-9} 32.5%	2.61×10^{-9} 17.3%	7.92×10^{-14} 0.0%	7.47×10^{-14} 0.0%	-0.1	0.1	0.0	-0.1
0.100	859.6	3.00×10^{-8} 18.7%	5.15×10^{-8} 32.1%	5.15×10^{-8} 32.1%	2.73×10^{-8} 17.0%	4.29×10^{-11} 0.0%	3.74×10^{-11} 0.0%	0.0	-0.2	0.2	0.0
0.125	962.0	3.37×10^{-7} 20.0%	5.28×10^{-7} 31.3%	5.28×10^{-7} 31.3%	2.81×10^{-7} 16.7%	5.57×10^{-9} 0.3%	4.56×10^{-9} 0.3%	0	0.0	-0.3	0.1
0.150	1064.4	3.51×10^{-6} 21.9%	4.76×10^{-6} 29.7%	4.76×10^{-6} 29.7%	2.55×10^{-6} 15.9%	2.39×10^{-7} 1.5%	1.86×10^{-7} 1.2%	0.1	0.0	-0.1	0.0
0.175	1166.8	1.87×10^{-5} 22.8%	2.22×10^{-5} 27.1%	2.22×10^{-5} 27.1%	1.22×10^{-5} 14.9%	3.72×10^{-6} 4.6%	2.78×10^{-6} 3.4%	0.0	-0.1	0.1	0.1
0.200	1269.2	3.30×10^{-5} 21.4%	3.56×10^{-5} 23.1%	3.56×10^{-5} 23.1%	2.01×10^{-5} 13.0%	1.73×10^{-5} 11.2%	1.25×10^{-5} 8.1%	-0.2	0.0	0.1	0.1
0.225	1371.6	9.64×10^{-6} 16.4%	9.42×10^{-6} 16.0%	9.42×10^{-6} 16.0%	5.41×10^{-6} 9.2%	1.47×10^{-5} 25.0%	1.03×10^{-5} 17.5%	-0.1	0.1	0.0	0.1
0.250	1474.0	1.75×10^{-7} 8.5%	1.56×10^{-7} 7.6%	1.56×10^{-7} 7.6%	8.79×10^{-8} 4.3%	8.81×10^{-7} 42.8%	6.02×10^{-7} 29.3%	0.1	0.0	-0.1	0.0
0.275	1552.5	8.29×10^{-11} 4.0%	6.99×10^{-11} 3.4%	6.99×10^{-11} 3.4%	3.81×10^{-11} 1.8%	1.09×10^{-9} 52.4%	7.29×10^{-10} 35.1%	0.0	0.0	0.0	0.0
0.300	1585.0	9.25×10^{-15} 2.7%	7.59×10^{-15} 2.2%	7.59×10^{-15} 2.2%	4.03×10^{-15} 1.2%	1.91×10^{-13} 55.1%	1.27×10^{-13} 36.7%	0.0	0.0	0.0	0.1

HAB (cm)	β scission (mole/cm^3 s, %)					Isomerization (mole/cm^3 s, %)			
	C_7H_{15}-1 → C_5H_{11}-1 + C_2H_4	C_7H_{15}-2 → C_4H_9-1 + C_3H_6	C_7H_{15}-3 → NC_3H_7 + C_4H_8-1	C_7H_{15}-4 → C_2H_5 + C_5H_{10}-1	C_7H_{15}-3 → CH_3 + C_6H_{12}-1	1 → 2	1 → 3	2 → 3	4 → 1
0.000	6.52×10^{-19} 0.0%	8.66×10^{-18} 0.0%	2.74×10^{-18} 0.0%	7.99×10^{-18} 0.0%	-NULL	4.29×10^{-16} 0.0%	1.31×10^{-12} 1.4%	1.7×10^{-15} 0.0%	1.92×10^{-16} 0.0%
0.025	5.38×10^{-16} 0.0%	5.64×10^{-15} 0.0%	2.10×10^{-15} 0.0%	5.14×10^{-15} 0.0%	-NULL	-8×10^{-16} -0.0%	7.3×10^{-12} 5.8%	1.34×10^{-13} 0.1%	9.14×10^{-14} 0.1%
0.050	3.96×10^{-13} 0.0%	2.60×10^{-12} 0.2%	1.20×10^{-12} 0.1%	2.20×10^{-12} 0.1%	2.68×10^{-13} 0.0%	-5×10^{-13} -0.0%	1.3×10^{-10} 8.3%	7.4×10^{-12} 0.5%	1.47×10^{-11} 0.9%
0.075	8.03×10^{-11} 0.5%	3.47×10^{-10} 2.3%	1.90×10^{-10} 1.3%	2.27×10^{-10} 1.5%	7.41×10^{-11} 0.5%	9×10^{-12} 0.1%	1.7×10^{-9} 11.2%	2×10^{-11} 0.1%	5.54×10^{-10} 3.7%
0.100	6.55×10^{-9} 4.1%	2.10×10^{-8} 13.1%	1.26×10^{-8} 7.9%	1.01×10^{-8} 6.3%	6.77×10^{-9} 4.2%	8×10^{-10} 0.5%	2×10^{-8} 12.5%	-2×10^{-9} -1.2%	7×10^{-9} 4.4%
0.125	1.73×10^{-7} 10.3%	4.44×10^{-7} 26.4%	2.81×10^{-7} 16.7%	1.92×10^{-7} 11.4%	1.93×10^{-7} 11.5%	1.3×10^{-8} 0.8%	1×10^{-7} 5.9%	-3×10^{-8} -1.8%	5.3×10^{-8} 3.1%
0.150	2.20×10^{-6} 13.7%	4.71×10^{-6} 29.4%	3.09×10^{-6} 19.3%	2.04×10^{-6} 12.7%	2.58×10^{-6} 16.1%	1.1×10^{-7} 0.7%	1.5×10^{-6} 9.4%	-1.6×10^{-7} -1.0%	4.3×10^{-7} 2.7%
0.175	1.21×10^{-5} 14.8%	2.23×10^{-5} 27.3%	1.49×10^{-5} 18.2%	1.00×10^{-5} 12.2%	1.46×10^{-5} 17.9%	4.2×10^{-7} 0.5%	8×10^{-6} 9.8%	-1×10^{-7} -0.1%	2.05×10^{-6} 2.5%
0.200	2.17×10^{-5} 14.1%	3.53×10^{-5} 22.9%	2.35×10^{-5} 15.3%	1.67×10^{-5} 10.8%	2.64×10^{-5} 17.1%	6×10^{-7} 0.4%	1.4×10^{-5} 9.1%	7×10^{-7} 0.5%	3.3×10^{-6} 2.1%
0.225	6.36×10^{-6} 10.8%	9.23×10^{-6} 15.7%	6.04×10^{-6} 10.3%	4.55×10^{-6} 7.7%	7.64×10^{-6} 13.0%	1.5×10^{-7} 0.3%	4×10^{-6} 6.8%	3.1×10^{-7} 0.5%	8.5×10^{-7} 1.4%
0.250	1.16×10^{-7} 5.6%	1.52×10^{-7} 7.4%	9.64×10^{-8} 4.7%	7.58×10^{-8} 3.7%	1.35×10^{-7} 6.6%	2.5×10^{-9} 0.1%	6.8×10^{-8} 3.3%	6.8×10^{-9} 0.3%	1.21×10^{-8} 0.6%
0.275	5.57×10^{-11} 2.7%	6.77×10^{-11} 3.3%	4.16×10^{-11} 2.0%	3.35×10^{-11} 1.6%	6.23×10^{-11} 3.0%	1.2×10^{-12} 0.1%	3×10^{-11} 1.4%	3.5×10^{-12} 0.2%	4.5×10^{-12} 0.2%
0.300	6.41×10^{-15} 1.9%	7.40×10^{-15} 2.1%	4.38×10^{-15} 1.3%	3.60×10^{-15} 1.0%	6.68×10^{-15} 1.9%	1.4×10^{-16} 0.0%	3.2×10^{-15} 0.9%	3.3×10^{-16} 0.1%	4.4×10^{-16} 0.1%

HAB (cm)	T (K)	β scission (mole/cm^3 s, %)					
		C_7H_{15}-1 → H + C_7H_{14}-1	C_7H_{15}-2 → H + C_7H_{14}-1	C_7H_{15}-2 → H + C_7H_{14}-2	C_7H_{15}-3 → H + C_7H_{14}-2	C_7H_{15}-3 → H + C_7H_{14}-3	C_7H_{15}-4 → H + C_7H_{14}-3
Φ	**1.9**	**1.9**	**1.9**	**1.9**	**1.9**	**1.9**	**1.9**
0.000	450.0	5.18×10^{-12} 5.5%	3.28×10^{-12} 3.5%	8.66×10^{-12} 9.2%	7.14×10^{-12} 7.6%	7.14×10^{-12} 7.6%	6.42×10^{-12} 6.8%
0.025	552.4	1.13×10^{-11} 9.1%	1.20×10^{-11} 9.6%	3.01×10^{-11} 24.1%	2.48×10^{-11} 19.9%	2.48×10^{-11} 19.9%	2.23×10^{-11} 17.9%
0.050	654.8	1.46×10^{-10} 9.3%	1.49×10^{-10} 9.5%	3.61×10^{-10} 22.9%	3.28×10^{-10} 20.8%	3.28×10^{-10} 20.8%	2.59×10^{-10} 16.5%
0.075	757.2	1.48×10^{-9} 9.8%	1.36×10^{-9} 9.0%	3.20×10^{-9} 21.1%	3.18×10^{-9} 21.0%	3.18×10^{-9} 21.0%	1.84×10^{-9} 12.2%
0.100	859.6	1.17×10^{-8} 7.3%	1.01×10^{-8} 6.3%	2.34×10^{-8} 14.6%	2.39×10^{-8} 14.9%	2.39×10^{-8} 14.9%	1.01×10^{-8} 6.3%
0.125	962.0	4.63×10^{-8} 2.8%	3.87×10^{-8} 2.3%	8.82×10^{-8} 5.2%	9.05×10^{-8} 5.4%	9.05×10^{-8} 5.4%	3.48×10^{-8} 2.1%
0.150	1064.4	1.19×10^{-7} 0.7%	9.66×10^{-8} 0.6%	2.17×10^{-7} 1.4%	2.22×10^{-7} 1.4%	2.22×10^{-7} 1.4%	8.72×10^{-8} 0.5%
0.175	1166.8	1.61×10^{-7} 0.2%	1.27×10^{-7} 0.2%	2.83×10^{-7} 0.3%	2.85×10^{-7} 0.3%	2.85×10^{-7} 0.3%	1.19×10^{-7} 0.1%
0.200	1269.2	7.97×10^{-8} 0.1%	6.16×10^{-8} 0.0%	1.36×10^{-7} 0.1%	1.33×10^{-7} 0.1%	1.33×10^{-7} 0.1%	6.09×10^{-8} 0.0%
0.300	1585.0	4.15×10^{-19} 0.0%	2.93×10^{-19} 0.0%	6.34×10^{-19} 0.0%	5.45×10^{-19} 0.0%	5.45×10^{-19} 0.0%	3.00×10^{-19} 0.0%

HAB (cm)	T (K)	Carbon Atom Distribution (%)							
		C_7H_{16}	CO	CO_2	CH_4	C_2H_6	C_2H_2	C_2H_4	C_3H_6
0.000	450.0	92.33	3.23	0.43	0.74	0.07	0.44	2.17	0.24
0.025	552.4	88.91	4.55	0.65	1.01	0.12	0.65	3.12	0.38
0.050	654.8	84.65	6.15	0.95	1.33	0.17	0.91	4.29	0.58
0.075	757.2	79.36	8.07	1.33	1.70	0.25	1.23	5.71	0.84
0.100	859.6	72.61	10.44	1.83	2.15	0.35	1.63	7.47	1.19
0.125	962.0	63.53	13.54	2.52	2.71	0.49	2.17	9.80	1.70
0.150	1064.4	50.54	17.96	3.54	3.50	0.70	2.95	13.05	2.43
0.175	1166.8	31.53	24.98	5.19	4.67	1.00	4.23	17.62	3.38
0.200	1269.2	10.51	35.39	7.74	5.99	1.21	6.22	21.32	3.73
0.225	1371.6	0.91	45.74	10.53	6.44	0.94	8.38	18.57	2.34
0.250	1474.0	0.01	53.01	12.81	5.96	0.51	10.08	12.14	0.89
		C_4H_8-1	C_5H_{10}-1	C_6H_{12}-1	AC_3H_4	13-C_4H_6	CH_2O	CH_2CO	total
0.000	450.0	0.06	0.02	0.02	0.02	0.04	0.04	0.08	99.93
0.025	552.4	0.10	0.04	0.04	0.03	0.07	0.06	0.13	99.86
0.050	654.8	0.16	0.08	0.07	0.04	0.11	0.09	0.20	99.78
0.075	757.2	0.25	0.14	0.12	0.07	0.17	0.12	0.28	99.64
0.100	859.6	0.38	0.23	0.21	0.09	0.26	0.17	0.41	99.42
0.125	962.0	0.57	0.39	0.37	0.14	0.40	0.22	0.58	99.13
0.150	1064.4	0.85	0.62	0.63	0.20	0.62	0.30	0.83	98.72
0.175	1166.8	1.08	0.84	0.79	0.31	0.93	0.39	1.24	98.18
0.200	1269.2	0.75	0.59	0.37	0.46	1.09	0.40	1.77	97.54
0.225	1371.6	0.13	0.10	0.02	0.45	0.63	0.25	2.05	97.48
0.250	1474.0	0.01	0.00	0.00	0.25	0.19	0.12	1.86	97.84

Appendix 3. Numerical Combustion Database for LLNL Reduced Mechanism

HAB (cm)	T (K)	Fuel Consumption (mole/cm^3 s, %)						
		C_7H_{15}-1	C_7H_{15}-2	C_7H_{15}-3	C_7H_{15}-4	CH_3+C_6H_{13}-1	C_2H_5+C_5H_{11}-1	NC_3H_7+PC_4H_9
Φ	**1.9**	**1.9**	**1.9**	**1.9**	**1.9**	**1.9**	**1.9**	**1.9**
0.000	450.0	7.77×10^{-11} 7.6%	3.77×10^{-10} 36.9%	3.77×10^{-10} 36.9%	1.89×10^{-10} 18.5%	-NULL	-NULL	-NULL
0.050	532.1	3.85×10^{-9} 10.9%	1.26×10^{-8} 35.7%	1.26×10^{-8} 35.7%	6.32×10^{-9} 17.8%	-NULL	-NULL	-NULL
0.100	657.3	9.01×10^{-7} 15.5%	1.97×10^{-6} 33.8%	1.97×10^{-6} 33.8%	9.83×10^{-7} 16.9%	-NULL	-NULL	-NULL
0.150	811.2	8.48×10^{-6} 15.6%	1.84×10^{-5} 33.8%	1.84×10^{-5} 33.8%	9.16×10^{-6} 16.9%	-NULL	-NULL	-NULL
0.175	888.1	8.26×10^{-6} 14.8%	1.90×10^{-5} 34.1%	1.90×10^{-5} 34.1%	9.51×10^{-6} 17.0%	-NULL	-NULL	-NULL
0.200	965.0	8.02×10^{-6} 14.3%	1.93×10^{-5} 34.3%	1.93×10^{-5} 34.3%	9.62×10^{-6} 17.1%	-NULL	-NULL	3.04×10^{-10} 0.0%
0.209	1131.4	1.76×10^{-5} 14.4%	4.16×10^{-5} 34.1%	4.16×10^{-5} 34.1%	2.09×10^{-5} 17.1%	1.23×10^{-8} 0.0%	1.44×10^{-7} 0.1%	1.17×10^{-7} 0.1%
0.216	1242.3	2.21×10^{-5} 15.1%	4.87×10^{-5} 33.3%	4.87×10^{-5} 33.3%	2.43×10^{-5} 16.6%	1.18×10^{-7} 0.1%	1.33×10^{-6} 0.9%	1.08×10^{-6} 0.7%
0.219	1297.8	2.00×10^{-5} 15.2%	4.25×10^{-5} 32.3%	4.25×10^{-5} 32.3%	2.13×10^{-5} 16.1%	2.58×10^{-7} 0.2%	2.87×10^{-6} 2.2%	2.34×10^{-6} 1.8%
0.225	1337.5	9.39×10^{-6} 15.1%	1.95×10^{-5} 31.4%	1.95×10^{-5} 31.4%	9.76×10^{-6} 15.7%	1.88×10^{-7} 0.3%	2.06×10^{-6} 3.3%	1.68×10^{-6} 2.7%
0.250	1420.0	7.61×10^{-8} 14.4%	1.52×10^{-7} 28.8%	1.52×10^{-7} 28.8%	7.61×10^{-8} 14.4%	3.57×10^{-9} 0.7%	3.81×10^{-8} 7.2%	3.11×10^{-8} 5.9%
0.275	1498.8	4.60×10^{-10} 12.7%	8.85×10^{-10} 24.3%	8.85×10^{-10} 24.3%	4.43×10^{-10} 12.2%	4.87×10^{-11} 1.3%	5.05×10^{-10} 13.9%	4.13×10^{-10} 11.4%
0.300	1565.0	9.92×10^{-13} 10.1%	1.85×10^{-12} 18.9%	1.85×10^{-12} 18.9%	9.24×10^{-13} 9.4%	2.12×10^{-13} 2.2%	2.18×10^{-12} 22.3%	1.78×10^{-12} 18.2%

HAB (cm)	β scission (mole/cm^3 s, %)					Isomerization (mole/cm^3 s, %)			
	C_7H_{15}-1 → C_5H_{11}-1 + C_2H_4	C_7H_{15}-2 → PC_4H_9 + C_3H_6	C_7H_{15}-3 → NC_3H_7 + C_4H_8-1	C_7H_{15}-3 → CH_3 + C_6H_{12}-1	C_7H_{15}-4 → C_2H_5 + C_5H_{10}-1	1 → 2	1 → 3	1 → 4	2 → 3
Φ	**1.9**	**1.9**	**1.9**	**1.9**	**1.9**	**1.9**	**1.9**	**1.9**	**1.9**
0.000	-4.89×10^{-13} -0.1%	1.75×10^{-18} 0.0%	NULL	NULL	1.13×10^{-18} 0.0%	4.17×10^{-24} 0.0%	5.64×10^{-23} 0.0%	1.39×10^{-17} 0.0%	10^{-25} 0.0%
0.025	-3.01×10^{-12} -0.1%	1.34×10^{-16} 0.0%	2.66×10^{-15} 0.0%	5.08×10^{-17} 0.0%	1.05×10^{-16} 0.0%	1.03×10^{-21} 0.0%	8.26×10^{-21} 0.0%	5.22×10^{-16} 0.0%	1×10^{-24} 0.0%
0.050	-1.42×10^{-11} -0.0%	1.38×10^{-14} 0.0%	1.67×10^{-13} 0.0%	4.80×10^{-15} 0.0%	1.11×10^{-14} 0.00%	3.15×10^{-19} 0.0%	1.61×10^{-18} 0.0%	3.20×10^{-14} 0.0%	10^{-20} 0.0%
0.075	-5.27×10^{-11} -0.0%	1.78×10^{-12} 0.0%	1.32×10^{-11} 0.0%	5.57×10^{-13} 0.0%	1.50×10^{-12} 0.0%	1.08×10^{-16} 0.0%	3.53×10^{-16} 0.0%	2.21×10^{-12} 0.0%	5×10^{-19} 0.0%
0.100	2.37×10^{-10} 0.0%	1.41×10^{-9} 0.0%	5.48×10^{-9} 0.1%	3.90×10^{-10} 0.0%	1.19×10^{-9} 0.0%	2.13×10^{-13} 0.0%	3.89×10^{-13} 0.0%	5.43×10^{-10} 0.0%	7×10^{-15} 0.0%
0.125	8.99×10^{-8} 0.2%	4.13×10^{-7} 0.8%	9.20×10^{-7} 1.8%	9.8×10^{-8} 0.2%	3.58×10^{-7} 0.7%	1.06×10^{-10} 0.0%	1.24×10^{-10} 0.0%	5.14×10^{-8} 0.1%	1.25×10^{-11} 0.0%
0.150	1.30×10^{-6} 2.4%	6.67×10^{-6} 12.3%	7.87×10^{-6} 14.5%	1.14×10^{-6} 2.1%	4.98×10^{-6} 9.2%	3.05×10^{-9} 0.0%	2.70×10^{-9} 0.0%	4.10×10^{-7} 0.8%	1.14×10^{-9} 0.0%
0.175	4.67×10^{-6} 8.4%	1.66×10^{-5} 29.7%	1.43×10^{-5} 25.6%	2.68×10^{-6} 4.8%	9.79×10^{-6} 17.5%	2.41×10^{-8} 0.0%	1.49×10^{-8} 0.0%	1.07×10^{-6} 1.9%	6.10×10^{-9} 0.0%
0.200	6.17×10^{-6} 11.0%	1.86×10^{-5} 33.1%	1.52×10^{-5} 27.1%	3.51×10^{-6} 6.2%	1.04×10^{-5} 18.5%	5.91×10^{-8} 0.1%	2.65×10^{-8} 0.0%	1.02×10^{-6} 1.8%	8.30×10^{-9} 0.0%
0.225	7.64×10^{-6} 12.3%	1.98×10^{-5} 31.9%	1.30×10^{-5} 20.9%	5.71×10^{-6} 9.2%	1.02×10^{-5} 16.4%	5.60×10^{-7} 0.9%	7.81×10^{-8} 0.1%	4.40×10^{-7} 0.7%	-7.4×10^{-8} -0.1%
0.250	5.99×10^{-8} 11.3%	1.54×10^{-7} 29.1%	9.66×10^{-8} 18.2%	4.62×10^{-8} 8.7%	7.82×10^{-8} 14.8%	6.07×10^{-9} 1.1%	6.9×10^{-10} 0.1%	2.99×10^{-9} 0.6%	-1.00×10^{-9} -0.2%
0.275	3.44×10^{-10} 9.5%	8.86×10^{-10} 24.3%	5.60×10^{-10} 15.4%	2.34×10^{-10} 6.4%	4.44×10^{-10} 12.2%	4.62×10^{-11} 1.3%	4.10×10^{-12} 0.1%	1.53×10^{-11} 0.4%	-1.08×10^{-11} -0.3%
0.300	7.88×10^{-13} 8.1%	2.49×10^{-12} 25.4%	9.06×10^{-12} 92.6%	-9.74×10^{-12} -99.5%	9.24×10^{-13} 9.4%	1.14×10^{-13} 1.2%	-7.97×10^{-14} -0.8%	3.22×10^{-14} 0.3%	-7.19×10^{-13} -7.3%

HAB (cm)	β scission (mole/cm^3 s, %)						Early Buildup (%)			
	C_7H_{15}-1 → H + C_7H_{14}-1	C_7H_{15}-2 → H + C_7H_{14}-1	C_7H_{15}-2 → H + C_7H_{14}-2	C_7H_{15}-3 → H + C_7H_{14}-2	C_7H_{15}-3 → H + C_7H_{14}-3	C_7H_{15}-4 → H + C_7H_{14}-3	R1	R2	R3	R4
Φ	**1.9**	**1.9**	**1.9**	**1.9**	**1.9**	**1.9**	**1.9**	**1.9**	**1.9**	**1.9**
0.000	-NULL	-NULL	-NULL	NULL	NULL	-NULL	0.8	4.2	4.2	2.1
0.025	-2.29×10^{-13} -0.0%	-1.31×10^{-12} -0.0%	-4.84×10^{-13} -0.0%	-4.84×10^{-13} -0.0%	-5.70×10^{-13} -0.0%	-5.70×10^{-13} -0.0%	-0.0	0.1	0.1	0.0
0.050	-3.40×10^{-12} -0.0%	-1.70×10^{-11} -0.0%	-7.19×10^{-12} -0.0%	-7.19×10^{-12} -0.0%	-8.46×10^{-12} -0.0%	-8.46×10^{-12} -0.0%	-0.0	-0.1	0.1	0.0
0.075	-4.20×10^{-11} -0.0%	-1.83×10^{-10} -0.1%	-8.89×10^{-11} -0.0%	-8.89×10^{-11} -0.0%	-1.05×10^{-10} -0.0%	-1.05×10^{-10} -0.0%	0.0	0.1	0.1	-0.1
0.100	-6.76×10^{-10} -0.0%	-2.49×10^{-9} -0.0%	-1.45×10^{-9} -0.0%	-1.45×10^{-9} -0.0%	-1.70×10^{-9} -0.0%	-1.70×10^{-9} -0.0%	0.1	-0.1	-0.2	-0.1
0.125	-1.07×10^{-8} -0.0%	-3.65×10^{-8} -0.1%	-2.51×10^{-8} -0.0%	-2.52×10^{-8} -0.0%	-2.90×10^{-8} -0.1%	-2.89×10^{-8} -0.1%	0.0	-0.4	0.1	0.1
0.150	-1.79×10^{-8} -0.0%	-9.15×10^{-8} -0.2%	-6.18×10^{-8} -0.1%	-7.05×10^{-8} -0.1%	-7.59×10^{-8} -0.1%	-7.17×10^{-8} -0.1%	-0.1	-0.6	1.4	-0.1
0.175	4.62×10^{-8} 0.1%	-9.75×10^{-8} -0.2%	-4.54×10^{-8} -0.1%	-7.92×10^{-8} -0.1%	-7.94×10^{-8} -0.1%	-8.08×10^{-8} -0.1%	-0.0	-0.1	0.1	-0.0
0.200	1.14×10^{-7} 0.2%	-1.09×10^{-7} -0.2%	-3.6×10^{-8} -0.1%	-7.1×10^{-8} -0.1%	-6.5×10^{-8} -0.1%	-9.38×10^{-8} -0.2%	0.2	0.6	0.3	0.3
0.225	6.70×10^{-7} 1.1%	1.71×10^{-7} 0.3%	1.42×10^{-7} 0.4%	3.59×10^{-7} 0.6%	4.39×10^{-7} 0.7%	3.4×10^{-8} 0.1%	-0.0	-0.1	0.0	-0.0
0.250	6.52×10^{-9} 1.2%	2.23×10^{-9} 0.4%	2.85×10^{-9} 0.5%	4.18×10^{-9} 0.8%	5.01×10^{-9} 0.9%	8.9×10^{-10} 0.2%	-0.0	0.1	0.0	0.0
0.275	5.11×10^{-11} 1.4%	2.92×10^{-11} 0.8%	2.71×10^{-11} 0.8%	3.95×10^{-11} 1.1%	4.51×10^{-11} 1.2%	1.33×10^{-11} 0.4%	-0.0	-0.0	-0.0	0.0
0.300	1.39×10^{-13} 1.4%	1.09×10^{-13} 1.1%	8.79×10^{-14} 0.9%	8.16×10^{-13} 8.3%	9.18×10^{-13} 9.4%	3.25×10^{-13} 0.3%	-0.0	-0.0	-0.0	-0.0

HAB (cm)	T (K)	Oxidation (mole/cm^3 s, %)						
		C_7H_{15}-1 → $C_7H_{15}O_2$-1	C_7H_{15}-2 → $C_7H_{15}O_2$-2	C_7H_{15}-3 → $C_7H_{15}O_2$-3	C_7H_{15}-4 → $C_7H_{15}O_2$-4	C_7H_{15}-1 → $C_7H_{15}O$-1	C_7H_{15}-2 → $C_7H_{15}O$-2	C_7H_{15}-3 → $C_7H_{15}O$-3
Φ	**1.9**	**1.9**	**1.9**	**1.9**	**1.9**	**1.9**	**1.9**	**1.5**
0.000	450.0	7.02×10^{-11} 6.9%	3.35×10^{-10} 32.8%	3.35×10^{-10} 32.8%	1.68×10^{-10} 16.4%	NULL	NULL	NULL
0.025	491.1	3.56×10^{-10} 8.8%	1.48×10^{-9} 36.4%	1.48×10^{-9} 36.5%	7.41×10^{-10} 18.3%	NULL	NULL	NULL
0.050	532.1	3.86×10^{-9} 10.9%	1.27×10^{-8} 35.8%	1.26×10^{-8} 35.6%	6.32×10^{-9} 17.8%	2.78×10^{-12} 0.0%	5.62×10^{-12} 0.0%	5.61×10^{-12} 0.0%
0.075	580.4	4.43×10^{-8} 13.1%	1.18×10^{-7} 34.7%	1.17×10^{-7} 34.7%	5.89×10^{-8} 17.4%	8.01×10^{-11} 0.0%	1.47×10^{-10} 0.0%	1.45×10^{-10} 0.0%
0.100	657.3	8.91×10^{-7} 15.3%	1.96×10^{-6} 33.7%	1.96×10^{-6} 33.7%	9.90×10^{-7} 17.0%	5.68×10^{-9} 0.1%	1.29×10^{-8} 0.2%	1.22×10^{-8} 0.2%
0.125	734.2	8.10×10^{-6} 15.7%	1.65×10^{-5} 31.9%	1.57×10^{-5} 30.4%	8.30×10^{-6} 16.1%	2.17×10^{-7} 0.4%	6.78×10^{-7} 1.3%	5.80×10^{-7} 1.1%
0.150	811.2	6.50×10^{-6} 12.0%	1.10×10^{-5} 20.2%	8×10^{-6} 14.7%	4.7×10^{-6} 8.7%	3.32×10^{-7} 0.6%	1.16×10^{-6} 2.1%	7.54×10^{-7} 1.4%
0.175	888.1	2.3×10^{-6} 4.1%	2.30×10^{-6} 4.1%	2.0×10^{-6} 3.6%	9×10^{-7} 1.6%	1.41×10^{-7} 0.3%	3.36×10^{-7} 0.6%	2.15×10^{-7} 0.4%
0.200	965.0	5.2×10^{-7} 0.9%	5×10^{-7} 0.9%	5×10^{-7} 0.9%	1.8×10^{-7} 0.3%	2.78×10^{-8} 0.0%	5.58×10^{-8} 0.1%	4.27×10^{-8} 0.1%
0.225	1337.5	1.2×10^{-9} 0.0%	1×10^{-9} 0.0%	1×10^{-9} 0.0%	2×10^{-10} 0.0%	2.91×10^{-10} 0.0%	4.67×10^{-10} 0.0%	5.77×10^{-10} 0.0%
0.250	1420.0	3×10^{-12} 0.0%	1×10^{-12} 0.0%	2×10^{-12} 0.0%	5×10^{-13} 0.0%	6.40×10^{-13} 0.0%	1.00×10^{-12} 0.0%	1.29×10^{-12} 0.0%
0.275	1498.8	4×10^{-15} 0.0%	2×10^{-15} 0.0%	4×10^{-15} 0.0%	1×10^{-15} 0.0%	1.13×10^{-13} 0.0%	1.76×10^{-15} 0.0%	2.46×10^{-15} 0.0%
0.300	1565.0	3×10^{-18} 0.0%	2×10^{-18} 0.0%	3×10^{-17} 0.0%	1×10^{-18} 0.0%	9.05×10^{-19} 0.0%	1.69×10^{-18} 0.0%	1.45×10^{-17} 0.0%

HAB (cm)	T (K)	Carbon Atom Distribution (%)							
		C_7H_{16}	CO	CO_2	CH_4	C_2H_6	C_3H_8	C_2H_2	C_7H_{13}
0.000	450.0	95.43	2.25	0.19	0.32	0.04	0.01	0.18	0.01
0.025	491.1	92.73	3.36	0.32	0.46	0.06	0.02	0.28	0.01
0.050	532.1	88.59	4.86	0.51	0.64	0.10	0.04	0.43	0.04
0.075	580.4	82.16	6.86	0.80	0.88	0.17	0.07	0.63	0.09
0.100	657.3	71.88	9.50	1.21	1.18	0.26	0.12	0.91	0.21
0.125	734.2	56.65	13.11	1.82	1.58	0.40	0.20	1.31	0.45
0.150	811.2	41.11	18.11	2.74	2.14	0.62	0.35	1.91	0.66
0.175	888.1	26.71	25.21	4.15	2.91	0.95	0.57	2.83	0.59
0.200	965.0	11.33	35.93	6.44	3.98	1.31	0.71	4.35	0.21
0.225	1337.5	0.48	48.85	9.46	4.96	1.18	0.29	6.49	0.00
0.250	1420.0	0.00	56.34	11.79	4.81	0.68	0.05	8.27	0.00
0.275	1498.8	0.00	60.34	13.62	4.22	0.36	0.01	9.78	0.00
0.300	1565.0	0.00	62.29	15.01	3.70	0.20	0.00	11.01	0.00
	CH_2O	CH_3CHO	C_2H_5CHO	C_3H_7CHO	C_2H_3CHO	CH_3OH	CH_2CO	CH_3COCH_3	$C_3H_7COCH_2$
0.000	0.14	0.12	0.04	0.02	0.01	0.06	0.06	0.02	0.02
0.025	0.23	0.21	0.08	0.05	0.03	0.10	0.11	0.04	0.04
0.050	0.36	0.36	0.15	0.09	0.05	0.16	0.19	0.07	0.09
0.075	0.54	0.60	0.28	0.19	0.10	0.25	0.32	0.13	0.19
0.100	0.81	0.95	0.50	0.37	0.18	0.37	0.50	0.24	0.39
0.125	1.17	1.45	0.83	0.65	0.33	0.54	0.76	0.40	0.70
0.150	1.53	1.86	0.94	0.70	0.53	0.70	0.90	0.60	0.64
0.175	1.68	2.00	0.79	0.52	0.74	0.74	0.93	0.72	0.26
0.200	1.39	1.70	0.48	0.29	0.84	0.63	0.88	0.56	0.03
0.225	0.62	0.86	0.14	0.08	0.58	0.41	0.71	0.18	0.00
0.250	0.22	0.25	0.01	0.01	0.21	0.23	0.50	0.02	0.00
0.275	0.09	0.04	0.00	0.00	0.06	0.13	0.34	0.00	0.00
0.300	0.05	0.00	0.00	0.00	0.02	0.08	0.24	0.00	0.00

HAB (cm)	T (K)	Carbon Atom Distribution (%)							
		C_2H_4	C_3H_6	C_4H_8-1	C_5H_{10}-1	C_6H_{12}-1	C_7H_{14}-1	C_7H_{14}-2	C_7H_{14}-3
0.000	450.0	0.75	0.13	0.05	0.02	0.00	0.00	0.01	0.01
0.025	491.1	1.16	0.22	0.10	0.04	0.01	0.01	0.01	0.02
0.050	532.1	1.72	0.37	0.18	0.08	0.02	0.02	0.04	0.04
0.075	580.4	2.48	0.62	0.32	0.16	0.04	0.04	0.09	0.10
0.100	657.3	3.51	1.00	0.57	0.33	0.09	0.10	0.21	0.24
0.125	734.2	4.92	1.61	1.00	0.67	0.18	0.21	0.47	0.54
0.150	811.2	6.85	2.46	1.57	1.22	0.35	0.29	0.67	0.72
0.175	888.1	9.32	3.23	1.89	1.60	0.52	0.26	0.56	0.58
0.200	965.0	12.14	3.62	1.61	1.38	0.53	0.16	0.31	0.31
0.225	1337.5	13.53	2.63	0.46	0.25	0.12	0.03	0.03	0.03
0.250	1420.0	10.32	0.97	0.04	0.01	0.00	0.00	0.00	0.00
0.275	1498.8	6.96	0.39	0.00	0.00	0.00	0.00	0.00	0.00
0.300	1565.0	4.54	0.19	0.00	0.00	0.00	0.00	0.00	0.00
	AC_3H_5	AC_3H_4	1,3-C_4H_6	$C_7H_{14}O$1-3	$C_7H_{14}O$1-4	$C_7H_{14}O$2-4	$C_7H_{14}O$2-5	$C_7H_{14}O$3-5	Total
0.000	0.00	0.00	0.00	0.01	0.01	0.01	0.03	0.00	99.93
0.025	0.00	0.00	0.01	0.02	0.03	0.03	0.07	0.01	99.85
0.050	0.00	0.01	0.01	0.05	0.07	0.08	0.20	0.04	99.64
0.075	0.00	0.01	0.02	0.12	0.18	0.19	0.50	0.09	99.20
0.100	0.00	0.02	0.04	0.31	0.43	0.48	1.22	0.23	98.33
0.125	0.00	0.03	0.07	0.72	0.90	1.12	2.53	0.52	97.82
0.150	0.00	0.05	0.13	1.12	1.22	1.73	3.31	0.77	98.49
0.175	0.01	0.08	0.27	1.18	1.22	1.74	3.18	0.77	98.70
0.200	0.03	0.16	0.57	1.05	1.07	1.52	2.77	0.67	98.96
0.225	0.18	0.28	0.86	0.82	0.83	1.18	2.15	0.52	99.21
0.250	0.07	0.20	0.45	0.58	0.59	0.84	1.53	0.37	99.37
0.275	0.02	0.12	0.20	0.41	0.41	0.59	1.07	0.26	99.45
0.300	0.01	0.09	0.09	0.29	0.30	0.42	0.77	0.19	99.49